ELUCIDATING THE GENOMIC SIGNATURES OF SELECTION USING THEORETICAL AND EMPIRICAL APPROACHES

A Thesis

by

SARAH PERRY FLANAGAN

Submitted to the Office of Graduate and Professional Studies of
Texas A&M University
in partial fulfillment of the requirements for the degree of

DOCTOR OF PHILOSOPHY

Chair of Committee,	Adam G. Jones
Committee Members,	Lisa Campbell
	Mariana Mateos
	Gil Rosenthal
Head of Department,	Tom McKnight

August 2016

Major Subject: Biology

ABSTRACT

Selection acts on phenotypes, but it is important to understand how its effects on the genome result in evolutionary change. Population genomics has provided several methods for detecting the form of selection acting on populations (e.g. positive or balancing), but current techniques are limited in their ability to identify the type of selection acting on traits (e.g. natural or sexual). Selection components analysis detects the types of selection acting in a population by comparing allele frequencies at different life history stages. In my dissertation, I used both population genomics analyses and selection components analysis to identify signatures of selection in natural populations.

I first conducted a traditional population genomics study to determine the population structure of multiple populations throughout the Gulf of Mexico and Atlantic Ocean in Gulf pipefish (*Syngnathus scovelli*). I also identified genome-wide loci that were differentiated between populations due to local adaptation. Although the results suggest that population divergence is driven by a variety of factors in *S. scovelli*, including neutral processes and selection on multiple traits, this population genetics approach could not differentiate among sexual or natural selective processes.

Next, I developed an individual-based simulation model to test the power of a selection components analysis approach with genome-wide data that mimicked next-generation sequencing datasets. The model showed that quantitative trait loci can be identified with relatively high power if selection was strong, sample sizes were large, and there were few loci underlying the trait.

Finally, I implemented the genome-wide selection components analysis in one population of Gulf pipefish and identified loci significantly associated with sexual selection and differential viability selection between males and females. Together, these studies allowed to me identify several signatures of selection at the genomic level in pipefish, which provides a better understanding of the relationship between selection and the genome. The genomic signatures of selection identified here can be integrated with other studies for a better understanding of broad-scale evolutionary patterns at the genomic level.

DEDICATION

This thesis is dedicated to my grandmother Elizabeth Flanagan, who helped pave the way for women in science, and to my grandfather Charles Peck who helped me look through my first microscope.

ACKNOWLEDGEMENTS

I would like to thank my PhD advisor, Dr. Adam Jones, whose advice and guidance made this thesis possible. My committee members, Dr. Campbell, Dr. Mateos, and Dr. Rosenthal also provided invaluable guidance and support throughout the course of this research. Thanks to all of the undergraduates and graduate students in the Jones lab these past five years for all of their help in the lab.

This research would not have been possible without funding from the National Science Foundation, including my Graduate Research Fellowship and my Doctoral Dissertation Improvement Grant. Additionally, I would like to thank Texas A&M for funding during my first year through a Merit Fellowship.

Thanks also go to my friends and colleagues and the department faculty and staff for making my time at Texas A&M University a great experience. My Texas family helped keep me sane throughout my PhD and I credit a great deal of success to you.

Finally, thanks to my family, in particular my mother, father, sister, and brother for their encouragement and support.

TABLE OF CONTENTS

Page

LIST OF FIGURES

Page

LIST OF TABLES

Page

CHAPTER I

INTRODUCTION

For evolution to occur, selection must act on traits with a genetic basis (Futuyma 1998). Therefore, selection must have a lasting impact on the genome and may be key to understanding how evolution occurs. Understanding the impacts of selection on the genome can lead to insights in many aspects of biology, including medicine (Carlson et al. 2004), agriculture (Morris et al. 2013), conservation biology (Ekblom and Galindo 2011; Narum et al. 2013a; Dierickx et al. 2015), and evolutionary biology (Nielsen 2005).

Population genetics theory provides a set of predictions regarding how selection is expected to affect the genome (e.g., Wright 1931, 1943; Hartl and Clark 2007). Of course, selection is not a monomorphic process and can manifest itself in a variety of ways. Balancing selection favors a mix of alleles and so is evident as an increase in heterozygosity around the locus under selection. Directional selection favors one allele over the others, and results in selective sweeps, in which one allele goes to fixation in a population (Hartl and Clark 2007; Hohenlohe et al. 2010b). Signatures of these types of selection can be detected genome-wide using summary statistics, such as F_{ST}, to compare allele frequencies between populations.

Recent advances in genetic sequencing technologies have allowed researchers to rapidly and relatively cheaply collect huge amounts of genomic sequence data in species

without pre-existing genomic resources (Davey and Blaxter 2010; Davey et al. 2011; Narum et al. 2013a). These data reveal patterns of introgression (e.g., Liao et al. 2012; Chiang et al. 2013; Hohenlohe et al. 2013; Morris et al. 2013; Combosch and Vollmer 2015), genetic incompatibilities (e.g., Schumer et al. 2014), migration (e.g., Harvey and Brumfield 2015; Monnahan et al. 2015), incipient speciation, and population structure (e.g., Asgharian et al. 2015; Boehm et al. 2015; Candy et al. 2015; Blanco-Bercial and Bucklin 2016) that have previously been unknown. These findings have resulted in insights about how species interact and how evolution is occurring in many systems.

Detecting the genomic signature of selection is commonly accomplished in three ways. First, population genomics approaches detect population-level selection episodes by identifying loci with summary statistics (e.g., F_{ST}) with values more extreme than a null or background distribution (Hohenlohe et al. 2010b). Second, genome-wide association studies can detect selection in a population by comparing many individuals with a particular phenotype to many individuals without that genotype (Carlson et al. 2004). Finally, quantitative trait loci mapping investigates family groups for regions with unexpectedly high numbers of shared alleles in individuals with the phenotype of interest, and is an effective means of identifying loci that contribute to a given trait, but requires a good deal of husbandry effort to generate second-generation crosses.

Most population genomics studies rely on comparisons between geographically distinct populations to assess the impacts of selection. However, a complementary approach is genome-wide selection components analysis, in which allele frequencies are compared between groups within a population (Christiansen and Frydenberg 1973).

Because different types of selection (e.g. viability selection, sexual selection) occur at different stages of the life cycle, loci that are outliers in specific comparisons are putative candidate loci under selection (Monnahan et al. 2015). A genome-wide selection components analysis approach is likely to succeed in a species in which one parent can be collected with its offspring (Christiansen and Frydenberg 1973) and in species where selection is known to be strong, such as the Gulf pipefish (Jones et al. 2001; Paczolt and Jones 2010; Rose et al. 2013; Flanagan et al. 2014).

In this thesis, I investigated the genomic signature of selection using a combination of approaches. First, I examined the extent to which neutral and selective processes contribute to population differentiation in twelve geographically distinct populations of a pipefish species. Next, I tested a genome-wide selection components analysis approach using a simulation model. Finally, I used the genome-wide selection components analysis to evaluate the contributions of sexual and viability selection to variation in the genome in a single population of pipefish.

CHAPTER II

POPULATION GENOMICS REVEALS MULTIPLE DRIVERS OF POPULATION DIFFERENTIATION IN A SEX-ROLE-REVERSED PIPEFISH

Overview

A major goal of molecular ecology is to identify the causes of genetic and phenotypic differentiation among populations. Population genomics is suitably poised to tackle these key questions by diagnosing the evolutionary mechanisms driving divergence in nature. Here, we set out to investigate the evolutionary processes underlying population differentiation in the Gulf pipefish, *Syngnathus scovelli*. We sampled approximately 50 fish from each of 12 populations distributed from the Gulf Coast of Texas to the Atlantic Coast of Florida and performed restriction-site-associated DNA sequencing (RAD-seq) to identify SNPs throughout the genome. After imposing quality and stringency filters, we selected a panel of 6,348 SNPs present in all 12 populations, 1,753 of which snowed no evidence of linkage disequilibrium. We identified a genome-wide pattern of isolation by distance, in addition to a more substantial genetic break separating populations in the Gulf of Mexico from those in the Atlantic. We also used several divergence outlier approaches and tests for genotype-environment correlation to identify 400 SNPs putatively involved in local adaptation. Patterns of phenotypic differentiation and variation diverged from the overall genomic pattern, suggesting that selection, phenotypic plasticity or demographic factors may be shaping phenotypes in distinct populations. Overall, our results suggest that population

divergence is driven by a variety of factors in *S. scovelli*, including neutral processes and selection on multiple traits.

Introduction

Pinpointing the causes of variation in genotypes and phenotypes is a major goal in molecular ecology, with clear implications for evolutionary biology and conservation genetics (Narum et al. 2013a). Recent advances in DNA sequencing technology have led to improved insights into the processes underlying genetic differentiation. However, the relative contributions of the mechanisms driving variation and differentiation among populations are still unclear for most species.

Major evolutionary factors shaping the genome include mutation, selection, gene flow, and genetic drift, which work together to drive population differentiation at the genetic level (Hartl and Clark 2007). Mutation, gene flow, and genetic drift are expected to behave similarly at all loci throughout the genome, whereas selection is expected to target one or several loci. Selection will have different effects on the genome depending on the type of selection and the number of loci it affects. Directional selection can occur in the form of either a hard selective sweep or a soft selective sweep, depending on whether selection acts on standing genetic variation or a novel mutation, and will ultimately result in fixation of a single allele in a population. Balancing selection, on the other hand, maintains polymorphism and can be more difficult to detect than directional selection (Hohenlohe et al. 2010b). When phenotypes under selection are encoded by many genes, the effect of selection on each locus is expected to be reduced, particularly if the genetic effects on the phenotype are additive.

Next-generation sequencing methods, including reduced-representation sequencing approaches, have permitted the identification of thousands of SNPs throughout the genome at relatively low cost in species without any preexisting genomic resources (Davey and Blaxter 2010; Davey et al. 2011; Narum et al. 2013a), providing unprecedented opportunities for researchers to understand how evolutionary forces drive genetic changes across the entire genome. Such genome-wide studies frequently make use of summary statistics, such as F_{ST}, the allele frequency spectrum, and Tajima's D, all of which potentially show distinct patterns for selected loci relative to the background distribution observed for neutral loci (i.e., the selected loci will be outliers; reviewed in Hohenlohe et al. (2010b).

A complementary understanding of the effects of selection on the genome can be gained by examining associations between genotypes and environmental variables (e.g. Günther and Coop 2013), especially if the associations also control for population structure (Lotterhos and Whitlock 2014). These genetic-environment association studies can test hypotheses regarding the importance of specific environmental variables in determining genetic differentiation and thus represent a potentially powerful way to complement and extend selection analyses based on F_{ST} outlier approaches (Fraser et al. 2015; Guo et al. 2015).

Another potentially powerful approach to investigate selection in natural populations is to examine phenotypic differentiation in light of the population genetic structure revealed by molecular markers. Recent studies using both restriction-site-associated DNA sequencing (RAD-seq) and microsatellites have demonstrated

preliminary evidence for selection on traits by comparing neutral genomic variation to phenotypic differentiation (e.g. Oneal and Knowles 2013; Barley et al. 2015; Ozerov et al. 2015). These studies compare a metric of phenotypic differentiation (P_{ST}) to a metric of neutral genetic variation (F_{ST}) to identify whether phenotypic variation follows the same pattern as the neutral genetic variation. If the patterns differ, then selection can be implicated as playing a role in phenotypic divergence (Leinonen et al. 2006). A second phenotype-based approach does not use genetic variation, but rather characterizes the matrix of phenotypic variances and covariances (**P**-matrix) and compares the direction and magnitude of variation between populations. If the populations differ in unexpected ways, then additional work on the role of selection in producing these patterns could be warranted.

Here, we set out to investigate population structure and signatures of selection in the Gulf pipefish, *Syngnathus scovelli.* Gulf pipefish are an excellent species in which to study the factors shaping differentiation and population divergence for several reasons. First, Gulf pipefish occur along the Atlantic coast of Florida and the Gulf of Mexico (Dawson 1982) on both sides of a region in which many marine species show a major Atlantic-Gulf phylogeographic discontinuity (Avise 1992), so population structure may exist simply due to geographic barriers to dispersal. The vicinity of the Atlantic-Gulf break contains a patchy distribution of shallow seagrass beds, which is the primary habitat of this cryptic species (Diaz-Ruiz et al. 2000). Additionally, *S. scovelli* exhibit male pregnancy and give birth to non-pelagic juveniles (Jones and Avise 1997), so their capacity for dispersal may be more limited compared to other marine species, which

often have pelagic larvae or strong-swimming adults. This limited dispersal ability supports a hypothesis that neutral processes (genetic drift, mutation, and migration) leads to an isolation-by-distance pattern, since individuals will not be travelling to and from distant populations. However, *S. scovelli* do not show site fidelity (Masonjones et al. 2010) and exhibit yearly fluctuations in population density (Bolland and Boettcher 2005; Masonjones et al. 2010). Additionally, a microsatellite-based population structure analysis revealed only weak differentiation among populations in the northern Gulf of Mexico (Partridge et al. 2012). Therefore, the relative importance of neutral processes such as migration and drift versus selective pressures leading to local adaptation in the Gulf pipefish remains to be established.

Local adaptation may also play a role in driving population differentiation, and is plausible in Gulf pipefish, given their limited dispersal abilities. Local adaptation occurs when different populations of a species, among which gene flow is restricted, experience directional selection on the same trait or traits but in different directions. This process has been observed in numerous species due to a variety of environmental factors. Examples include local adaptation to freshwater environments in threespine sticklebacks (Jones et al. 2012), clinal patterns of local adaptation likely relating to temperature in *Arabidopsis thaliana* (Fournier-Level et al. 2011), and adaptation to insecticide resistance in the mosquito *Culex pipiens* (Asgharian et al. 2015). Several environmental factors, such as temperature, salinity, and seagrass cover, may contribute to local adaptation in Gulf pipefish. Temperature and salinity have been shown to be important factors for other marine fish species (Dionne et al. 2007; Jones et al. 2012; Berg et al.

2015; Picq et al. 2016). Gulf pipefish rely on crypsis to avoid predation so the composition of the seagrass beds (e.g. seagrass density, species composition) might also exert variable selective pressures.

Geographic variation in sexual selection may also drive population differentiation in Gulf pipefish. Other species of pipefish have been shown to experience different sexual selection pressures than Gulf pipefish and several of these species have well-documented variation in mating systems among populations (Mobley and Jones 2007; Mobley and Jones 2009; Monteiro and Lyons 2012). Consequently, spatially varying sexual selection pressures could represent an additional cause of phenotypic or genetic divergence among populations. Gulf pipefish are sex-role reversed in the sense that females experience stronger sexual selection than do males (Jones et al. 2001; Rose et al. 2013; Flanagan et al. 2014). Female *S. scovelli* have bright iridescent bands that run dorso-ventrally along their trunk. These bands appear to be direct targets of sexual selection and are correlated with body size, resulting in indirect selection for larger female body size (Flanagan et al. 2014).

In this study, we characterize population differentiation in Gulf pipefish, using both a RAD-seq population genomic approach and direct measurements of phenotypic variation. We use these data to analyze patterns of population structure and to investigate the relative roles of migration, genetic drift, local adaptation, and sexual selection in driving Gulf pipefish genetic and phenotypic divergence across the Gulf of Mexico and Atlantic coast of the United States.

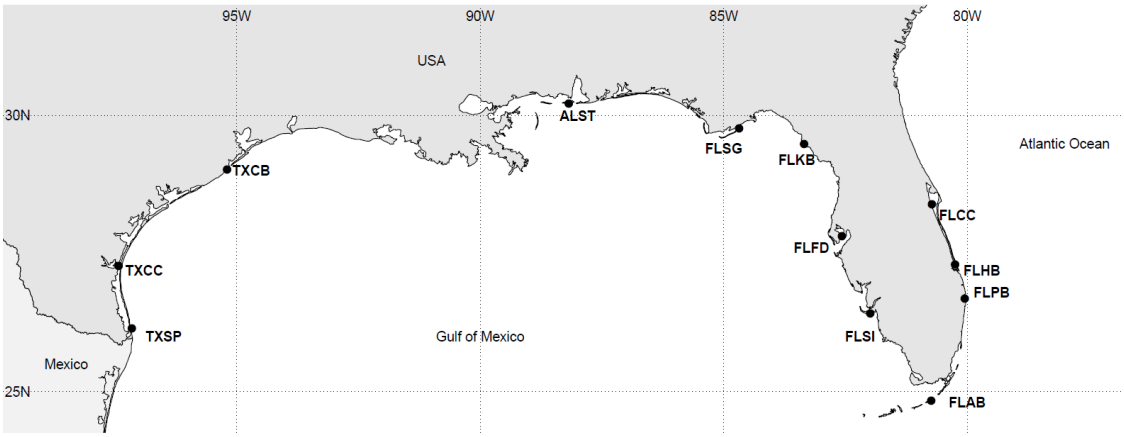

Figure 1. A map of the locations of the 12 collecting sites. The first two letters of each site name refer to the state where the sample was collected (TX = Texas; AL = Alabama; FL = Florida).

Methods

Sample collection

Samples were collected at eight sites in the Gulf of Mexico and four sites along the Atlantic coast of Florida (Figure 1) in July and August 2012, except the South Padre Island site which was collected in June 2014. The map in Figure 1 was created in R (R Core Team 2013) using packages maps (Becker et al. 2014b), mapdata (Becker et al. 2014a), and gplots (Warnes et al. 2015). Pipefish were collected by pulling a seine net through seagrass beds. We collected an average of 25 males and 25 females at each site (Table 1). Once fish were collected, each fish was photographed while alive before being sacrificed and preserved for DNA analysis. Samples were kept frozen on dry ice until they could be stored in -80 °C freezers. All fish were collected under valid permits from the states of Texas, Alabama, and Florida. At each sampling site we measured the surface temperature of the water, estimated salinity with a refractometer, and estimated

seagrass coverage on a scale of 1 to 5. A seagrass estimate of 1 referred to very patchy seagrass coverage, whereas a patch with an estimate of 5 was fully covered with no bare patches. The estimates were made after having collected the fish and referenced the portions of the seagrass bed that we had sampled (a patch of roughly $20m^2$).

The program ImageJ (Rasband 1997-2012) was used to quantify several phenotypic traits from the photographs of pipefish. The traits of interest included tail length, snout-vent length (SVL), body depth, snout length, head length not including the snout length, and snout depth. Additionally, we used the program tpsDig2 (Rohlf 2005) to measure two female traits known to be under sexual selection, namely band area and band number (Flanagan et al. 2014).

Table 1. Summary statistics for each population. The number of individuals of each sex class is the number that were sequenced and included in the analyses. The number of RAD loci and the number of SNPs are the same for all populations because the filtering steps required that all SNPs used in the analyses be present in all twelve populations. Below are summary statistics with their standard errors for all 166,383 sites and for the 1753 pruned SNPs. Populations differed in the percent of all sites that were polymorphic (%Poly), the average major allele frequency (P), observed heterozygosity (H_{obs}), and nucleotide diversity (π). The variance in the statistics are in parentheses. These summary statistics were calculated by populations in Stacks (Catchen et al. 2013).

	N Pregnant Males	*N* Non-Pregnant Males	*N* Females	*N* Juveniles	% Poly	All Sites P	Pruned SNPs P	All Sites H_{obs}	Pruned SNPs H_{obs}	All Sites π	Pruned SNPs π
ALST	24	0	23	0	0.9646	0.9988 (0.0002)	0.8881 (0.0112)	0.0019 (0.0006)	0.1811 (0.0216)	0.0019 (0.0005)	0.1786 (0.0189)
FLAB	5	18	19	0	0.9394	0.9987 (0.0003)	0.8807 (0.0128)	0.0019 (0.0006)	0.1845 (0.0226)	0.002 (0.0006)	0.1872 (0.0209)
FLCC	7	12	22	0	0.5277	0.9992 (0.0002)	0.9275 (0.0118)	0.0011 (0.0004)	0.1055 (0.0227)	0.0012 (0.0004)	0.1126 (0.0229)
FLFD	22	0	18	0	0.9628	0.9988 (0.0002)	0.886 (0.0097)	0.0017 (0.0004)	0.1659 (0.0154)	0.002 (0.0005)	0.1854 (0.0169)
FLHB	11	2	28	0	0.6052	0.9991 (0.0002)	0.917 (0.0136)	0.0014 (0.0005)	0.1314 (0.0304)	0.0013 (0.0004)	0.1268 (0.0253)
FLKB	21	0	21	0	0.9791	0.9986 (0.0003)	0.87 (0.0098)	0.0022 (0.0007)	0.2095 (0.0193)	0.002 2 (0.0006)	0.2091 (0.0172)
FLPB	18	1	19	5	0.6737	0.9991 (0.0002)	0.9171 (0.0124)	0.0014 (0.0005)	0.1329 (0.0287)	0.0014 (0.0004)	0.1289 (0.0236)
FLSG	20	0	24	5	0.9839	0.9987 (0.0003)	0.8722 (0.0097)	0.0021 (0.0006)	0.2037 (0.0179)	0.0022 (0.0006)	0.206 (0.0167)
FLSI	23	0	22	0	0.967	0.9987 (0.0003)	0.8779 (0.01)	0.002 (0.0006)	0.1928 (0.0186)	0.0021 (0.0006)	0.1969 (0.0173)
TXCB	21	1	14	0	0.7603	0.999	0.9059	0.0016	0.1484	0.0016	0.1483

Table 1. Continued

	N Pregnant Males	*N* Non-Pregnant Males	*N* Females	*N* Juveniles	% Poly	All Sites P	Pruned SNPs P	All Sites H_{obs}	Pruned SNPs H_{obs}	All Sites π	Pruned SNPs π
						(0.0002)	(0.0123)	(0.0005)	(0.0243)	(0.0005)	(0.0223)
TXCC	15	2	19	0	0.7837	0.999 (0.0002)	0.9083 (0.0108)	0.0016 (0.0005)	0.1495 (0.0232)	0.0015 (0.0004)	0.1471 (0.0206)
TXSP	39	0	20	0	0.8	0.9991 (0.0002)	0.9168 (0.0096)	0.0014 (0.0004)	0.1359 (0.0207)	0.0014 (0.0004)	0.1347 (0.0118)

RAD-seq library preparation

PureGene DNA extraction kits (QIAGEN) were used to extract DNA from preserved pipefish specimens. The quality of DNA samples was assessed using a Nanodrop spectrophotometer, a Qubit 2.0 Fluorometer (Life Technologies), and by visual examination of extracted DNA on a 1% agarose gel. Only high-quality samples with high molecular weights were used in the RAD-seq libraries.

Preparation of RAD-seq libraries followed previously published protocols (Peterson et al. 2012), with slight modifications. Instead of the double-indexing used in Peterson et al. (2012), we used the 96 unique 6-basepair barcodes from the single-digest RAD protocols (Miller et al. 2007; Baird et al. 2008). These adapters ligate to the restriction sites from several restriction enzymes, including *PstI* and *MboI*, the enzymes we used. Briefly, we digested 1μg of high-quality DNA per sample with 100 units of *PstI*-HF (New England Biolabs) and 25 units of *MboI* (New England Biolabs) at 37°C for 3 hours. After purification with AMPure XP beads (Agilent), 250ng of each DNA sample was ligated to a unique adapter with T4 ligase (Epicentre) at 23 °C for 30 minutes followed by a heat shock at 65 °C for 10 min and a slow cool-down to room temperature. Samples were purified using AMPure XP beads (Agilent) and pooled to form one library of 96 individual samples. The library was then run on a 1% agarose gel with SafeView DNA stain (ABMGood) and size-selected for 250-500bp fragments. The Zymo Gel Purification kit was used to obtain the DNA, and then four separate PCRs using Phusion polymerase (New England Biolabs) were run with 12 cycles each (cycle conditions: 98°C for 30s; 12 cycles of 98°C for 10s, 60°C for 30s, 72°C for 10s; 72°C

for 5min). Finally, the four individual PCRs were pooled, purified with AMPure XP beads (Agilent), and quantified with a Qubit 2.0 Fluorometer (Life Technologies). Libraries were sent to the University of Oregon Genomics Core Facility for Single-End sequencing on an Illumina Hi-Seq 2000 machine.

Generating a catalog of RAD loci

Raw reads were filtered for quality and separated by barcode using the process_radtags function of Stacks v. 1.29 (Catchen et al. 2011; Catchen et al. 2013b). The filtered reads were mapped to a draft *S. scovelli* genome assembly (pers. comm. William Cresko) using bowtie2.0 (Langmead and Salzberg 2012) with the default 'sensitive' parameters (--sensitive), ensuring that only reads mapping to the genomic pipefish sequence were retained. The ref_map.pl program in Stacks v1.20 (Catchen et al. 2011; Catchen et al. 2013b) was used to group the mapped reads into a catalog of RAD loci, and individual sequences were genotyped by comparing each individual's RAD loci to the catalog. The minimum depth of coverage required to report a stack in the building of a catalog was three, and two mismatches were allowed between loci when assembling the catalog of RAD loci. Stacks uses a multinomial-based likelihood model to call SNPs, which incorporates a bounded error rate and calculates the likelihood of the two most frequently observed nucleotides at each SNP location (Catchen et al. 2013b).

Calling the genotypes of each individual resulted in RAD loci, which are 100-bp sequences aligned to scaffolds of the draft genome. Not all RAD loci were polymorphic, but those that were had at least one SNP, and each SNP had at least two alleles in the dataset.

Filtering

We used the populations program in Stacks v. 1.29 (Catchen et al. 2013b) to calculate population genetics statistics and to filter the dataset to contain only SNPs found in all twelve populations, in at least 75% of all individuals, and with a minor allele frequency greater than 0.05. This set of SNPs will be referred to as the "non-pruned SNPs" in the rest of the manuscript. These loci were further pruned using a custom program to keep only a random SNP from each RAD locus. The SNPs were then required to be at least 1kb apart in either direction. Finally, PLINK v. 1.07 (Purcell et al. 2007) was used to remove SNPs deviating from Hardy-Weinberg equilibrium frequencies. This filtering process retained only non-linked SNPs in Hardy-Weinberg equilibrium ("pruned SNPs" throughout the manuscript), which comply with the assumptions of the tests used to evaluate population structure. The populations module of Stacks was run a second time on only the pruned SNPs to generate files in the correct formats for further analyses and to calculate summary statistics such as observed and expected heterozygosity and nucleotide diversity.

Isolation by distance

Population differentiation can occur simply due to short-range dispersal causing populations to become isolated from each other because they are geographically distant (Wright 1931, 1943). To test whether patterns in genomic differentiation in this dataset were driven by this random isolation by distance effect, we tested for a correlation between measures of genetic differentiation and geographic distance. To conduct this analysis, pairwise F_{ST} values were recalculated for pruned SNPs using the populations

module in Stacks (Catchen et al. 2013b). Distance between sites was estimated from the shortest line between points while remaining in marine waters, estimated with the path tool in Google Earth. We compared average pairwise F_{ST} values output from the populations module of Stacks (Catchen et al. 2013b) and geographic distances between sites using a Mantel test in R (R Core Team 2013), with package ade4 (Dray and Dufour 2007). The pairwise F_{ST} values were also re-calculated for each of the pruned SNPs with a custom script in R as

$$F_{\mathrm{ST}} = \frac{(H_T - H_S)}{H_T}$$

where H_T is the heterozygosity among populations and H_S is the average heterozygosity within populations (Hartl and Clark 2007). These pairwise F_{ST} values were then compared to geographic distances as above to differentiate between pruned SNPs that follow the isolation-by-distance pattern and those that do not.

Estimating migration

Any pattern of isolation by distance and the random differentiation resulting from can be affected by migration rate, as long-range dispersal will greatly reduce random population differentiation (Wright 1943). Therefore, we used the program MIGRATE-N to estimate migration rates and estimate population sizes. The Bayesian model was used with the default settings and 10,000 burn-in chains. We ran the program on a subset of 485 of the pruned SNPs, which were randomly chosen using PLINK v. 1.07 (Purcell et al. 2007). An estimated number of migrants per generation (Nm) was calculated from the overall mean values estimated by MIGRATE-N of θ ($4N_e\mu$) and M (m/μ). The number of migrants joining population i from population j was calculated as (θ_i*$\mathrm{M}_{j\rightarrow i}$)/4. The

results of the migrate analysis were visualized on a map plotted in R using the packages maps (Becker et al. 2014b), gplots (Warnes et al. 2015), and mapdata (Becker et al. 2014a), with arrows scaled to the mutation-scaled migration rate (M) and points scaled to the estimated value of $4N_e\mu$.

Analysis of population structure

Populations may be subdivided for reasons other than isolation by distance, and alternative patterns of population differentiation can be characterized by analyses of population structure. We used STRUCTURE (Pritchard et al. 2000; Falush et al. 2003, 2007), which implements a Bayesian framework for posterior inference, to infer population structure. STRUCTURE was run with both admixture and no admixture models, each with 10,000 burn-in steps followed by 10,000 Markov Chain Monte Carlo (MCMC) steps. For both models, we first ran STRUCTURE for $K = 1$ through $K = 12$, and then for an additional 10 replicates at the values of K most likely to be accurate, as determined by a drop-off in Pr(K) in Structure Harvester (Earl and vonHoldt 2012).

An alternative approach to admixture models is to use principal components analysis to identify population differentiation. This approach is particularly effective in cases of isolation by distance (Engelhardt and Stephens 2010). To implement a principal components analysis of population structure within the pruned SNPs we used adegenet 2.0.0 (Jombart 2008; Jombart and Ahmed 2011). The first step in using adegenet was to run the package-specific principal components analysis, glPca, retaining five factors. The clusters in the dataset were visualized by graphing the PCA results, as well as by running a discriminant analysis of principal components. This analysis identified the

clusters within the dataset without any input regarding the expected number of populations. Finally, we used an approach that shares components of admixture-based models and principal components, PCAdapt (Duforet-Frebourg et al. 2014). PCAdapt uses a Bayesian hierarchical factor model that approximates individual genotypes using two lower-rank matrices, one of which contains population structure using *K* latent factors and the other of which measures the extent to which individual SNPs are related to population structure and infers parameters with a MCMC algorithm (Duforet-Frebourg et al. 2014). PCAdapt was run on the pruned SNPs with default parameters (200 burn-in MCMC steps followed by an additional 200 MCMC steps for parameter estimation) with $K = 1$ through $K = 12$. The best *K* was determined by examining the mean squared error and PCAdapt was re-run with 10 replicates of the best *K*; consistency was evaluated with the R scripts in the PCAdapt package.

Local adaptation

Populations that occupy different geographic locations, such as those we sampled in this study, may experience different selective pressures, which could drive differences in allele frequencies (Wright 1943). A common approach to comparing allele frequencies among populations is to use F_{ST} outlier tests, many of which assume specific demographic histories, such as the island model (Beaumont and Nichols 1996). Lotterhos and Whitlock (2014) compared tests that assume specific population demographic models and other approaches that use covariance or coancestry to infer population structure. In situations involving isolation by distance or range expansion, their study shows that the best programs were those that did not assume a specific

demographic history (Lotterhos and Whitlock 2014). In addition, a recent simulation-based study from our lab shows that mathematical constraints on the relationship between expected heterozygosity and F_{ST} severely limits the generality of outlier approaches, especially in populations composed of a small number of demes (Flanagan & Jones, *in review*).

Given these considerations, we used three approaches to identify loci putatively under selection. First, we used Bayesian approach to identify loci putatively affected by adaptation, implemented in PCAdapt (Duforet-Frebourg et al. 2014). We ran PCAdapt on the non-pruned SNPs 10 times at the best K (K = 4, see Results). Any SNPs that were found to be putatively under selection in all 10 runs were used as the set of outlier SNPs from the PCAdapt analysis.

Our second approach to identify outlier loci involved a threshold determined by the distribution of F_{ST} for the pruned SNPs. We identified outliers in two ways: first, we calculated global F_{ST} values using in-house C++ code (available on github), using the following equation:

$$F_{\mathrm{ST}} = 1 - \frac{\sum_{i=1}^{k} H_{wi}}{kH_b},$$

where k is the number of sampling locations, H_w is the expected heterozygosity within each population, and H_b is the overall expected heterozygosity calculated among all populations (Nei 1986). Expected heterozygosity was calculated from allele frequencies, p, as $1 - \sum_{i=1}^{a} p_i^2$ for each locus with a alleles. We calculated F_{ST} values for the non-pruned SNPs. The 99% quantile was calculated in R (R Core Team 2013) to create a

99% cutoff. All SNPs with F_{ST} values above this 99% cutoff were considered as outliers in this analysis.

Finally, we utilized the neutral parameterization in Bayenv2.0 to account for population structure in identifying outlier loci related to population differentiation. We estimated a covariance matrix of allele frequencies among populations by running Bayenv2.0 (Coop et al. 2010; Günther and Coop 2013) with the pruned SNPs 10 separate times, each with 100,000 MCMC iterations. The matrices from each run were highly correlated, so we took a representative matrix from the 100,000th iteration from one of the 10 runs. This matrix was then used as a null distribution to calculate the statistic X^TX, which describes population differentiation and is analogous to F_{ST}.

Isolation by ecology

The above approaches can identify local adaptation, but may be confounded by population structure (Lotterhos and Whitlock 2015) and are not easily interpreted in light of biological processes driving local adaptation. A recent study comparing the power of a variety of programs implementing genetic-environment associations showed that the Bayes Factors from Bayenv2.0 (Coop et al. 2010; Günther and Coop 2013) had relatively high power at detecting selected loci (Lotterhos and Whitlock 2015). Therefore, we used Bayenv2.0 (Coop et al. 2010; Günther and Coop 2013) to conduct a genetic-environment association test and identify loci putatively experiencing local adaptation due to specific environmental factors.

When fish were collected, we measured the salinity and surface temperature and estimated the seagrass density of the site (scale of 1-5). Seawater temperature and

salinity data were also downloaded from the World Ocean Database (Ocean Climate Laboratory 1984) for the years 2004-2014. Measurements collected ±0.5° north or south of the actual latitude of the collection site and ±0.5° east or west of the actual longitude were averaged over the ten years and the average temperature, variance in temperature, and salinity measurements were also included in the analysis. All environmental variables were standardized to a mean of zero and a standard deviation of one.

To conduct the genetic-environment association analysis, we first calculated the covariance matrix of pruned loci to generate a genetic covariance matrix. The pruned SNPs were then compared individually to the standardized environmental variables in Bayenv2.0 (Coop et al. 2010; Günther and Coop 2013) to identify significant allele frequency patterns associated with variation in environmental variables. The resulting output statistics were Bayes Factors associated with each locus for each environmental variable.

Selection on phenotypes

If selection is acting on morphological characters, differentiation in those traits is not expected to have the same pattern as the primarily neutral genetic variation characterized by the pruned SNPs (Leinonen et al. 2006). To assess whether divergence of measured traits (tail length, SVL, body depth, snout length, snout depth, and head length in both sexes, as well as band area and band number in females) was associated with genetic divergence, we calculated P_{ST}, the degree of phenotypic divergence between populations. P_{ST} is analogous to Q_{ST} (Leinonen et al. 2006), which describes the divergence in quantitative trait loci. Q_{ST} has been used to test whether neutral phenotypic

evolution leads to observed differentiation in quantitative traits by comparing it to F_{ST} or similar measures of differentiation of pruned loci (Spitze 1993; Whitlock and Guillaume 2009). Although P_{ST} has been used as an approximation of Q_{ST} by some researchers, the approximation depends on the heritability of the quantitative traits (Brommer 2011). Here, we do not suggest that P_{ST} is reflective of Q_{ST}. Rather, we use P_{ST} simply as a measure of phenotypic differentiation among populations because we have no way of measuring heritabilities from our samples. We calculated P_{ST} following Spitze (1993) and Barley et al. (2015):

$$\frac{\sigma_B^2}{\sigma_B^2+2\sigma_W^2},$$

where σ_B^2 is the variance between populations and σ_W^2 is the within-population variance. These variances were estimated from a linear mixed model implemented in the R package nlme (Pinheiro et al. 2016). Pairwise P_{ST} values were calculated for each trait separately for males and females. We present results from non-standardized trait values because standardizing trait values can mask important biological variation (Houle et al. 2011), but mean-standardizing the traits yields qualitatively similar results. Mantel tests were conducted per trait in R (R Core Team 2013) with package ade4 (Dray and Dufour 2007) to compare the mean pairwise P_{ST} matrices to the mean pairwise F_{ST} matrix estimated from the pruned SNPs in Stacks. We also compared the P_{ST} matrices to a pairwise F_{ST} matrix for each individual SNP, as calculated above for the individual SNP isolation by distance test, using a Mantel test to identify loci that follow the same pattern as the traits.

Additionally, we conducted principal components analyses using the R package vegan (Oksanen et al. 2013) to capture overall trait variation. Three principal components analyses were run: one on female band area and female band number (these traits are not found in males); one on female body size traits, including snout and head measurements; one on male body size traits, including snout and head measurements. The scores for each individual for PC1 were retained and pairwise P_{ST} values were calculated from the PC1 scores. These P_{ST} values were compared to the pruned SNP F_{ST} matrix from Stacks and the distance matrix using Mantel tests.

*Phenotypic differentiation: comparing **P**-matrices*

To examine the **P**-matrices of the different populations, we considered male and female trait values separately. Females had an additional two traits, band area and band number, that are sexually selected (Flanagan et al. 2014). The calculation of **P**-matrices was done on a matrix of all of the unstandardized traits, but male and female traits were treated separately. We chose to use the unstandardized trait values because standardizing the traits would change the variance structure induced by among-population differences in means.

We took two approaches to comparing **P**-matrices between populations. First, we followed the Krzanowski (1979) common subspace method (Aguirre et al. 2014). This method creates a subspace matrix, **H**, which describes the trait subspace most similar across populations. **H** is calculated as:

$$\mathbf{H} = \sum_{t=1}^{p} \mathbf{A}_t \mathbf{A}_t^T$$

where p is the number of populations and $\mathbf{A}_i$ contains a subset of the eigenvectors of $\mathbf{P}_i$. We used the first three eigenvectors of each **P**. An eigenanalysis of **H** reveals which eigenvectors best represent the data contained in the original **P**-matrices; eigenvectors with an associated eigenvalue equal to p can be exactly reconstructed by a linear combination of the subset of eigenvectors of any population's **P**-matrix. If an eigenvalue is less than p, that eigenvector cannot be exactly reconstructed by at least one population. We evaluated how close eigenvectors of **H** are to each population's **P**-matrix by calculating the angle (δ) between each eigenvector of **H** ($\boldsymbol{h}_i$) and each population's subspace: $\delta = \cos^{-1}\{(\boldsymbol{h}_i^T \mathbf{A}_t \mathbf{A}_t^T \boldsymbol{h}_i)^{0.5}\}$, as described in Aguirre et al. (2014).

The second approach is the tensor approach (Hine et al. 2009), outlined by Aguirre et al. (2014). This method calculates a fourth-order covariance tensor, **Σ**, which represents the variances and covariances of multiple covariance matrices: $\sum_{ijkl} cov(\mathbf{P}_{ij}, \mathbf{P}_{kl})$. This covariance tensor is analogous to the **P**-matrix, except it describes variation among multiple **P**-matrices as opposed to variation among multiple traits. The eigentensors ($\mathrm{E_i}$) and eigenvalues ($\boldsymbol{e}_i$) of **Σ** are analogous to the eigenvectors and eigenvalues of **P**, so to understand the direction and magnitude of the variation among **P**-matrices it is important to explore the eigentensors and eigenvalues of **Σ**. The number of eigentensors was determined as $\frac{n(n+1)}{2}$, where n is the number of traits in the analysis. To calculate the eigentensors and eigenvalues of **Σ**, we created a symmetrical, square **S** matrix with $\frac{n(n+1)}{2}$ rows and $\frac{n(n+1)}{2}$ columns. This **S** matrix had four quadrants: the upper left contained the (co)variances of variances in the **P**-matrix; the lower right

contained the covariances of the **P**-matrix covariances, the upper right contained the covariances of the variances and covariances of the **P**-matrix, and the lower left also contained the covariances of the covariances and variances of the **P**-matrix. The eigenvectors of **S** were scaled and rearranged to form the eigentensors of **Σ**. We focused our attention on the eigentensors of **Σ** that were non-zero, and we were able to identify those E_i that describe trait combinations with the most variation among **P**-matrices. We calculated the coordinates of each **P**-matrix in the space of the relevant eigentensors to examine the contribution of each population to the variation in the eigentensor. Finally, we projected the eigenvectors of the relevant E_i on each population's **P**-matrix, to identify which eigenvector describes the most variation within each eigentensor. We used R scripts from Aguirre et al. (2014), modified to calculate and analyze **S** for the male and female **P**-matrices separately.

Results

A total of 166,383 RAD loci were identified by Stacks, and individuals had an average coverage of 10x. The filtering steps resulted in 6348 SNPs, representing 3829 RAD loci. Of those, 1753 were retained after pruning for physical linkage. The populations for the most part had similar observed heterozygosities (H_{obs}), major nucleotide frequencies (P), and nucleotide diversity (π; Table 1).

Table 2. Mean pairwise F_{ST} values between populations. These values were generated by Stacks v.1.39 (Catchen et al. 2011; Catchen et al. 2013b) for all SNPs found in 75% of individuals in all 12 populations (non-pruned SNPs).

	FLKB	FLPB	TXSP	ALST	FLAB	FLCC	FLFD	FLHB	FLSG	FLSI	TXCB	TXCC
FLKB		0.0473	0.0401	0.0245	0.0223	0.0500	0.0121	0.0497	0.0072	0.0112	0.0369	0.0367
FLPB			0.0457	0.0451	0.0419	0.0088	0.0429	0.0072	0.0455	0.0442	0.0504	0.0494
TXSP				0.0265	0.0443	0.0466	0.0381	0.0475	0.0380	0.0396	0.0141	0.0071
ALST					0.0329	0.0469	0.0253	0.0471	0.0227	0.0260	0.0238	0.0249
FLAB						0.0477	0.0197	0.0464	0.0224	0.0185	0.0420	0.0425
FLCC							0.0464	0.0080	0.0481	0.0471	0.0542	0.0526
FLFD								0.0457	0.0127	0.0080	0.0370	0.0366
FLHB									0.0478	0.0472	0.0535	0.0520
FLSG										0.0121	0.0348	0.0349
FLSI											0.0371	0.0369
TXCB												0.0142
TXCC												

Neutral processes: isolation by distance

Random population differentiation is driven in part by isolation by distance. Pairwise F_{ST} values averaged over the 6348 SNPs (Table 2) showed significant isolation by distance (Mantel test, *obs* = 0.680, $p = 0.01$), as did pairwise F_{ST} values averaged over only the 1753 pruned SNPs (Mantel test, *obs* = 0.687, $p = 0.01$). Of the 1753 pruned SNPs, 315 loci showed significant association by distance (Mantel test, $p \leq 0.05$).

Migration rates

The migration rates estimated by MIGRATE support the notion that *S. scovelli* dispersal is limited across the observed genetic break between the Atlantic populations and the Gulf populations. The lowest migration between neighboring populations, scaled for the mutation rate (*Nm* = 0.031) was observed between a Gulf-like population (FLAB) and an Atlantic coast population (FLPB). The largest number of migrants per generation between neighboring populations (*Nm* = 0.271) was observed between two Gulf of Mexico populations (FLFD to FLKB). The average number of migrants per generation between neighboring populations was 0.14. The estimates of θ ($4N_e\mu$) did not vary greatly among populations, ranging from 0.00324 to 0.00655, with an average of 0.004 ± 0.001 sd (Appendix II).

Analysis of population structure

The analyses of population structure revealed that isolation by distance appears to be the primary driver of random population differentiation. The various population structure software packages showed similar patterns, suggesting that the twelve sampling locations actually cluster into three to five distinct populations. Both the admixture and

no admixture model runs of STRUCTURE found that $K = 5$ maximized ΔK and had the highest likelihood when analyzed in Structure Harvester (Evanno et al. 2005; Earl and vonHoldt 2012) (Figure 2). The PCA-based analyses found slightly different results from STRUCTURE; adegenet found $K = 3$ to be the best number of populations, and PCAdapt found $K = 4$ to be ideal (Figure 2). These similar yet disparate results are likely explained by the pattern of isolation by distance that we identified above, especially since an underlying pattern of isolation by distance can cause spurious signals of hierarchical population structure (Meirmans 2012).

Local adaptation

Diverging selection pressures appear to affect allele frequencies of 2.2% of the 6,348 SNPs in this dataset. We used several approaches to identify loci putatively under selection. One approach took advantage of PCAdapt, which uses a Bayes Factor approach to identify loci putatively affected by selection. We ran PCAdapt on the non-pruned SNPs 10 times with $K = 4$ (the number of populations diagnosed by PCAdapt) and pulled out putatively selected loci that were found in all 10 runs. A total of 66 SNPs in 54 RAD loci fell into this category, and these RAD loci were distributed on 50 of the draft genome's scaffolds. A total of five scaffolds contained more than one RAD locus identified as significant by PCAdapt.

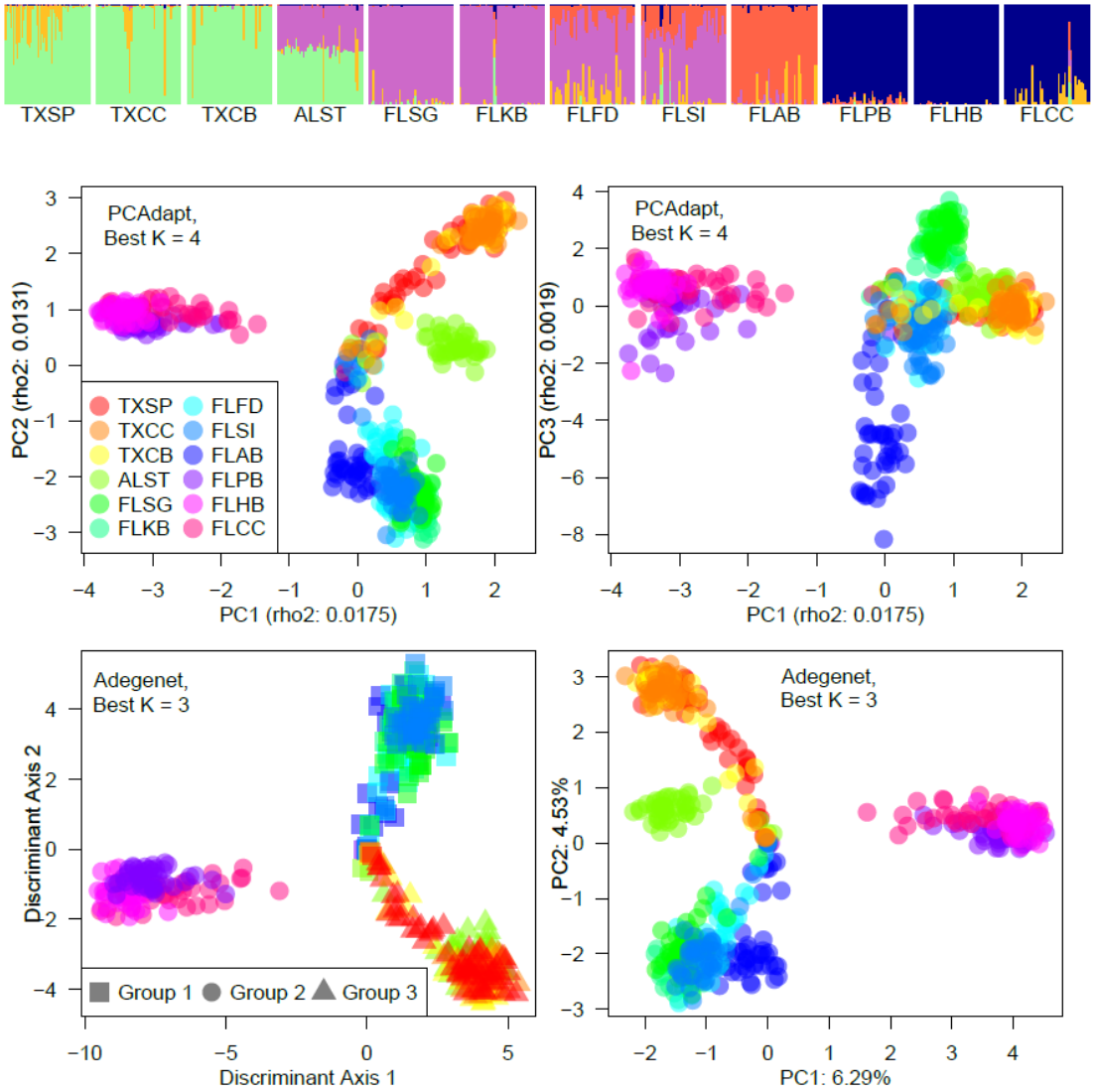

Figure 2. Analysis of population structure. The top panel displays the admixture model analyses of population structure from STRUCTURE (Falush et al. 2003, 2007) with 5 populations (*K* = 5). The middle two are the output from PCAdapt (Duforet-Frebourg et al. 2014), which had an optimal number of populations of four. The bottom two panels are the output from adegenet, a principal components analysis-based approach to identifying population structure (Jombart 2008; Jombart & Ahmed 2011), which identified three distinct populations. The bottom left panel depicts the results of the adegenet discriminant function analysis.

Another approach to identify outlier loci was based on a threshold determined by a 99% quantile. Using global F_{ST} values calculated for the subset SNP set, we found 18 SNPs on 17 scaffolds that exceeded the 99% confidence intervals.

Bayenv2.0 (Günther and Coop 2013) was run to identify signatures of population differentiation in the pruned SNPs. The analysis produced a skewed distribution of X^TX differentiation values. We imposed an arbitrary cutoff of the upper 5% to identify candidate SNPs, which resulted in 88 SNPs (each representing one RAD locus), distributed on 80 scaffolds.

We compared the RAD loci identified as candidate loci by PCAdapt, the F_{ST} outlier approach, and Bayenv2.0 (Figure 3). PCAdapt identified fewer SNPs that were shared with the other analyses; PCAdapt shared only four SNPs with the X^TX analysis and one locus with the F_{ST} analysis. The F_{ST} and X^TX analyses shared a total of 18 SNPs, including one shared by all analyses (Appendix III, Supplemental File 1). Only one locus was found in all three analyses, RAD locus 37615 on scaffold 823. The 5kb region surrounding this RAD locus was compared to the non-redundant protein database with blastx, and the gene *H ACA ribonucleoprotein complex non-core subunit NAF1* was determined to be located near this shared SNP ($E = 1.8 \times 10^{-11}$).

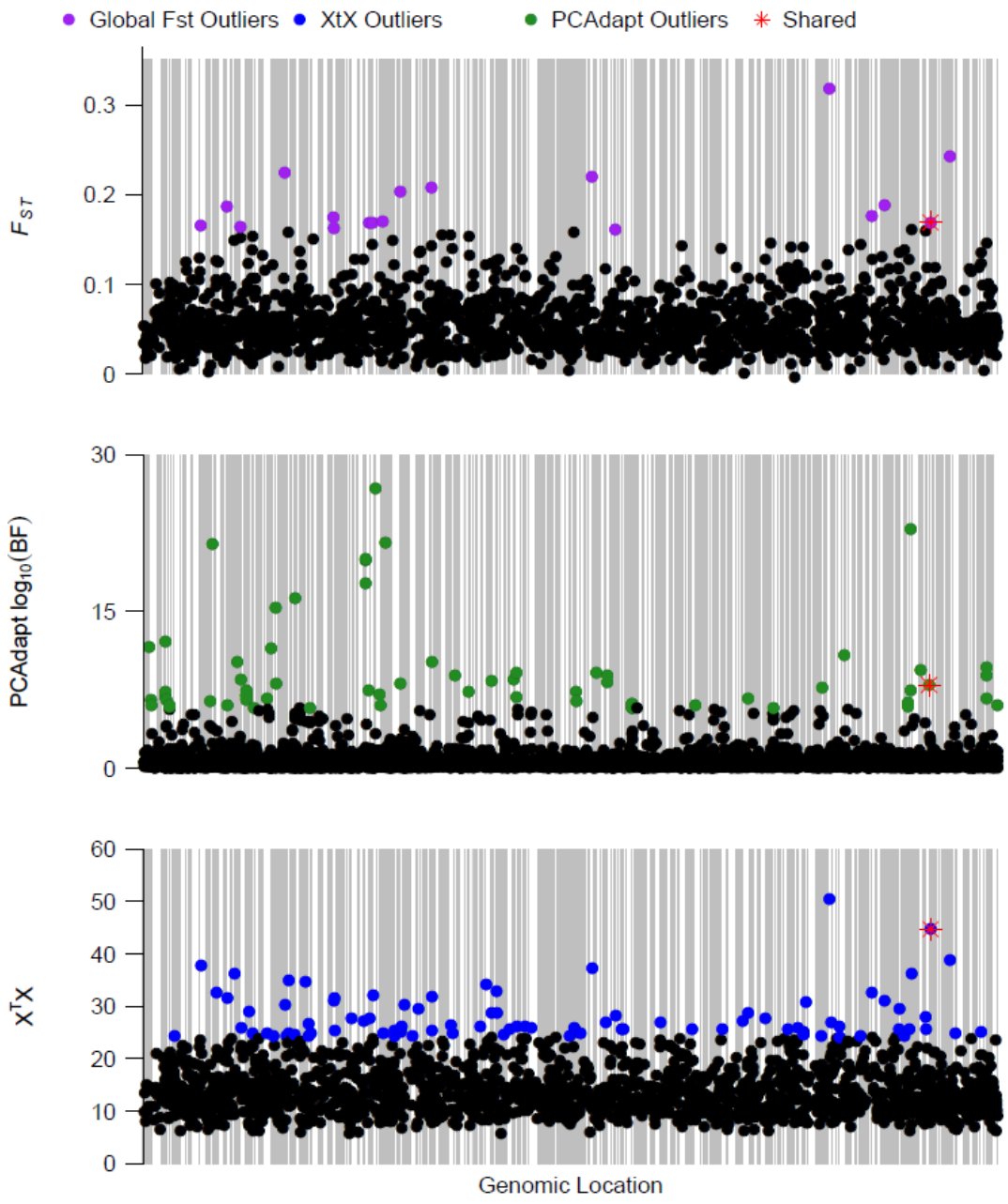

Figure 3. Identification of local adaptation outlier loci. Alternating grey and white bars in the background indicate scaffolds in the draft genome. Each panel shows non-significant SNPs in that analysis as solid black circles and the significant SNPs as colored filled circles (purple = F_{ST} , green = PCAdapt, blue = X^TX,). The red stars show the SNP at the RAD locus that was significant in all three analyses. The F_{ST} and X^TX analyses included only the 1753 pruned SNPs but the PCAdapt analysis included all 6453 non-pruned SNPs.

Isolation by ecology

Some of the selection causing the genetic differentiation may be due to temperature, salinity, seagrass cover, or other factors associated with these variables. We used Bayenv2.0 to identify associations between the pruned SNPs and six environmental variables (Table 3). Although Bayenv2.0 also calculates Spearman Rank correlation coefficients (Günther and Coop 2013), the Spearman Rank correlation has lower power than the Bayes Factors (Lotterhos and Whitlock 2015), so we restricted our attention to Bayes Factors. We selected the loci with the top 5% of the distribution of Bayes Factors for each environmental variable (88 SNPs). These SNPs are candidates for being associated with environmental variables. Four outlier SNPs were shared between the mean temperature and the variance in temperature analyses, but no SNPs were shared among both of those and the collection temperature analysis. The collection salinity analysis shared 13 outlier SNPs with the mean salinity analysis. The seagrass analysis shared four SNPs with both the mean temperature and mean salinity analyses and a different four SNPs with the collection temperature and collection salinity outliers. Seagrass had no overlapping outlier SNPs with the variance in temperature outliers.

Table 3. Environmental variables for each population. The 10-year averages were taken from measurements taken within ±0.5° of latitude and longitude in each direction (north, south, east, and west) from the collection location in the World Oceans Database (Ocean Climate Laboratory 1984). All measurements were taken at a depth of ≤ 10m and were averaged over 2004-2014. The collection temperatures, salinity, and seagrass index were taken at the sample location at the time of collection. The seagrass index is on a scale of 1-5 with 1 being very patchy and 5 being completely covered.

	ALST	FLAB	FLCC	FLFD	FLHB	FLKB	FLPB	FLSI	FLSG	TXCB	TXCC	TXSP
10-year Average Temperature (°C)	26.57	28.67	22.13	29.82	23.70	28.82	29.36	30.63	28.53	28.76	28.14	27.25
10-year Variance in Temperature (°C)	7.24	2.56	7.64	0.61	7.62	18.07	4.99	1.42	8.43	2.26	0.97	1.20
10-year Average Salinity (ppt)	22.86	36.34	36.29	35.36	36.28	33.01	36.17	36.2	33.89	30.88	35.38	35.07
Collection Temperature (°C)	28.5	33.0	33.0	33.0	32.0	30.5	30.0	30.0	30.5	28.0	33.0	29.0
Collection Salinity (ppt)	25	36	21	21	25	20	20	30	26	35	48	32
Seagrass Index	2	4	3	4	3	2	3	4	3	2	2	3

Because isolation by ecology could be related to local adaptation, we compared SNPs identified as outliers in the Bayenv analyses with those in the local adaptation analyses. The locus shared by all three local adaptation analyses was also found in the outliers associated with temperature variance and in the outliers associated with the salinity at the time of collection. Each of the genotype-environment outlier sets shared 10-21 outliers with at least one local adaptation analysis. A total of 383 SNPs were associated with at least one environmental factor. The 5kb regions surrounding these SNPs were compared to the non-redundant database using blastx and annotated by Blast2GO. A number of biological processes were associated with most of the environmental variables, such as regulation of biological processes, metabolic processes, and developmental processes (Appendix IV). All outlier SNPs are listed in Supplemental File 1.

Table 4. Means and standard deviations (sd) of male and female traits for each population. Sample sizes for each population are listed in Table 1. Band area refers to the mean band area per band.

Population	Sex	SVL ± sd (mm)		Tail Length ± sd (mm)		Body Depth ± sd (mm)		Head Length ± sd (mm)		Snout Length ± sd (mm)		Snout Depth ± sd (mm)		Band Area ± sd (mm^2)		Band Number ± sd (count)	
ALST	Females	40.00	1.58	48.94	3.13	4.77	0.50	6.60	0.37	6.37	0.49	1.72	0.18	0.33	0.08	15.87	1.55
	Males	31.20	3.77	40.64	4.66	3.03	0.43	5.54	0.88	4.73	0.83	1.41	0.20	NA	NA	NA	NA
FLAB	Females	50.71	4.19	64.46	6.54	6.81	0.78	8.67	0.91	6.85	0.68	2.16	0.27	1.02	0.45	15.74	1.52
	Males	45.36	3.89	61.12	5.52	5.96	0.52	8.23	0.91	5.92	0.54	2.03	0.29	NA	NA	NA	NA
FLCC	Females	39.81	4.29	48.85	4.91	4.07	0.59	7.17	0.98	6.10	0.73	1.79	0.23	0.21	0.08	15.09	1.51
	Males	31.97	3.46	40.47	5.04	2.82	0.53	5.89	0.63	4.99	0.64	1.45	0.21	NA	NA	NA	NA
FLFD	Females	55.41	7.94	65.67	6.10	7.17	1.01	8.88	0.80	8.39	0.92	2.41	0.32	0.65	0.25	16.06	1.43
	Males	46.57	4.65	60.81	5.04	5.70	0.78	7.93	0.73	6.83	0.64	2.14	0.22	NA	NA	NA	NA
FLHB	Females	39.75	3.65	50.18	4.27	4.65	0.78	6.96	0.77	5.96	0.59	1.73	0.21	0.31	0.08	15.29	2.19
	Males	30.90	3.28	40.84	4.87	3.00	0.41	5.50	0.56	4.54	0.42	1.38	0.23	NA	NA	NA	NA
FLKB	Females	43.82	3.11	53.97	4.78	5.13	0.59	7.89	0.94	6.56	0.52	1.95	0.18	0.35	0.12	15.76	1.26
	Males	35.08	3.44	46.54	6.31	3.64	0.63	6.30	0.77	5.34	0.50	1.56	0.24	NA	NA	NA	NA
FLPB	Females	38.31	6.95	51.52	5.25	4.33	0.65	6.84	0.52	5.80	0.56	1.68	0.22	0.35	0.12	15.42	1.87
	Males	32.24	3.09	45.10	4.49	3.15	0.54	5.75	0.58	4.56	0.55	1.37	0.27	NA	NA	NA	NA
FLSG	Females	40.93	3.86	49.82	4.16	4.64	0.79	7.44	0.99	6.82	0.68	1.80	0.19	0.43	0.22	16.10	2.10
	Males	34.05	3.72	44.92	4.56	3.11	0.57	6.41	0.75	5.45	0.77	1.51	0.20	NA	NA	NA	NA
FLSI	Females	44.83	2.10	56.53	3.28	5.51	0.48	7.93	0.76	6.57	0.53	1.87	0.15	0.34	0.09	15.77	1.57
	Males	35.49	2.89	49.40	3.61	3.88	0.46	6.36	0.62	5.10	0.63	1.55	0.17	NA	NA	NA	NA
TXCB	Females	35.67	3.42	44.17	6.45	4.03	0.46	6.40	0.42	5.39	0.74	1.52	0.20	0.27	0.06	16.79	1.42
	Males	27.95	4.59	39.23	7.50	2.49	0.58	5.10	0.73	4.12	0.83	1.25	0.21	NA	NA	NA	NA
TXCC	Females	34.59	2.58	43.81	3.37	3.79	0.48	6.09	0.40	5.10	0.65	1.48	0.17	0.21	0.09	16.89	1.49
	Males	26.62	3.12	36.21	2.96	2.28	0.34	4.90	0.52	3.80	0.36	1.10	0.14	NA	NA	NA	NA

Table 4. Continued

Population	Sex	SVL ± sd (mm)		Tail Length ± sd (mm)		Body Depth ± sd (mm)		Head Length ± sd (mm)		Snout Length ± sd (mm)		Snout Depth ± sd (mm)		Band Area ± sd (mm^2)		Band Number ± sd (count)	
TXSP	Females	40.48	3.17	48.19	4.28	3.91	0.62	7.30	0.61	5.36	0.45	1.78	0.18	0.47	0.15	18.96	2.38
	Males	32.78	4.33	42.91	6.39	3.55	0.56	6.27	0.76	4.26	0.48	1.50	0.25	NA	NA	NA	NA

Selection on phenotypes

Patterns in among-population phenotypic variation did not align closely with the patterns of random differentiation due to isolation by distance observed in the genotypes. In all populations, females were larger than males, but both sexes varied in size among populations (Table 4). A principal components analysis of the body-size traits (SVL, tail length, head length, snout length, snout depth, and body depth) found that the first two axes of variation account for most of the variation in both males (99.52%) and females (98.92%). For both males and females, populations group along PC1 and intra-population variation is captured by PC2 (Figure 4). Tail length and SVL had the highest loadings in PC1 for both males (-10.73 and -7.82, respectively) and females (-9.31 and -7.82, respectively). SVL and tail length also had the highest loadings in PC2 in males (2.11 and -1.60, respectively) and for females (-2.67 and 2.29, respectively). A PCA of female band traits showed that most of the variation in band traits is also among populations, along the PC1 axis. However, variation within the Florida Keys population (FLAB) had a large amount of variation in PC2 (Figure 4). In the female bands PCA, band number had the highest loading on PC1 (5.593) and band area had the highest loading on PC2 (-0.75).

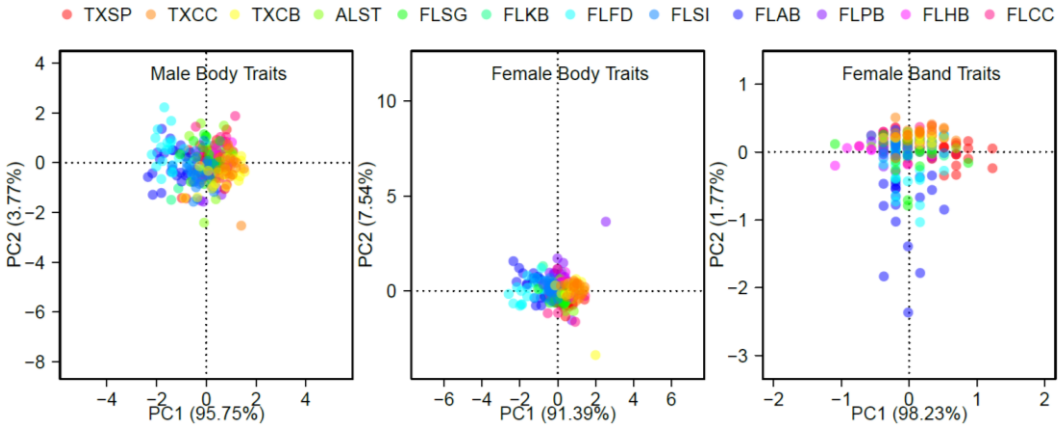

Figure 4. Principal components analysis of the phenotypic traits for males and females. The panel labeled "Male Body Traits" shows the first two principal component axes for male SVL, tail length, head length, snout length, snout depth, and body depth, which account for 99.52% of the total variation. The trait with the largest loading in PC1 is tail length (-10.73) and for PC2 is SVL (2.11), and PC1 separates the FLFD and FLAB populations from the other populations. The panel labeled "Female Body Traits" shows the first two principal component axes, which account for 98.93% of the total variation, for female SVL, tail length, head length, snout length, snout depth, and body length. Females show a similar pattern to males. The panel labeled "Female Band Traits" shows the results of a principal components analysis of just female band number and mean band area. Most of the variation among populations is in the direction of PC1, but FLAB has a large amount of variation in PC2.

To test the hypothesis that genotypic and phenotypic differentiation follow the same patterns, we calculated P_{ST}, a measure analogous to F_{ST} but based on phenotypic variation (P_{ST} matrices are presented in S2). We found no association between mean pairwise F_{ST} and the body trait P_{ST} values when calculated between the twelve sampling locations for the pruned and the non-pruned SNPs (Mantel tests, $p > 0.05$). Band number, however, was significantly associated with pairwise F_{ST} (Mantel test, *obs*. = 0.2975, $p = 0.0137$). We compared each P_{ST} matrix with pairwise F_{ST} matrices calculated for each pruned SNP, which revealed SNPs significantly correlated with P_{ST}

matrices (Mantel tests, $p \leq 0.05$): 951 SNPs were significantly associated with SVL, 671 with tail length, 1076 with body depth, 505 with snout length, 1266 with snout depth, 690 with head length, and 244 with at least one of the band traits (Supplemental File 2).

When pairwise P_{ST} was calculated from the first principal component scores, female body measurements and male measurements, we also found no significant associations with F_{ST} (Mantel tests, $p = 0.3602$ and $p = 0.5926$, respectively; Fig. 5), although the principal component-based P_{ST} for band traits was significantly correlated with average pairwise F_{ST} (Mantel test, *obs*. = 0.2973, $p = 0.0123$). Comparisons of population divergence for each trait or for PCA scores of the traits were similarly unrelated to the distance matrix (i.e. there was no signal of isolation by distance in terms of trait variation, Mantel tests, all tests $p > 0.05$), except for the band traits. The P_{ST} values calculated from the female band measurements showed a significant pattern of isolation by distance (Mantel test, *obs*. = 0.6775, $p = 0.0001$), although the pattern may not be strictly linear (Figure 5).

Figure 5. Comparison of phenotypic and genetic differentiation. This figure shows a plot of pairwise F_{ST} values for the pruned SNPs and pairwise P_{ST} values as a function of distance. The P_{ST} values plotted are calculated from principal components analysis of the body variables (tail length, standard length, body depth, snout length, snout depth, and head length) for males and females separately ("Male PCA P_{ST}" and "Female PCA P_{ST}", respectively). Also plotted are P_{ST} values calculated from just female band measurements (mean band area and band number; "Female Bands PCA P_{ST}"). This plot demonstrates that P_{ST} values follow a very different pattern from F_{ST} values. The F_{ST} values are divided into two noticeably separate lines due to the increased divergence of the Florida Atlantic populations relative to the other locales. Mean pairwise F_{ST} values were significantly correlated with geographic distance (Mantel test, $p = 0.01$), but body P_{ST} values were not. Female band P_{ST} values were associated with distance and F_{ST}, although the pattern does not appear to be strictly linear. These different patterns suggest that selection is playing a role in phenotypic differentiation.

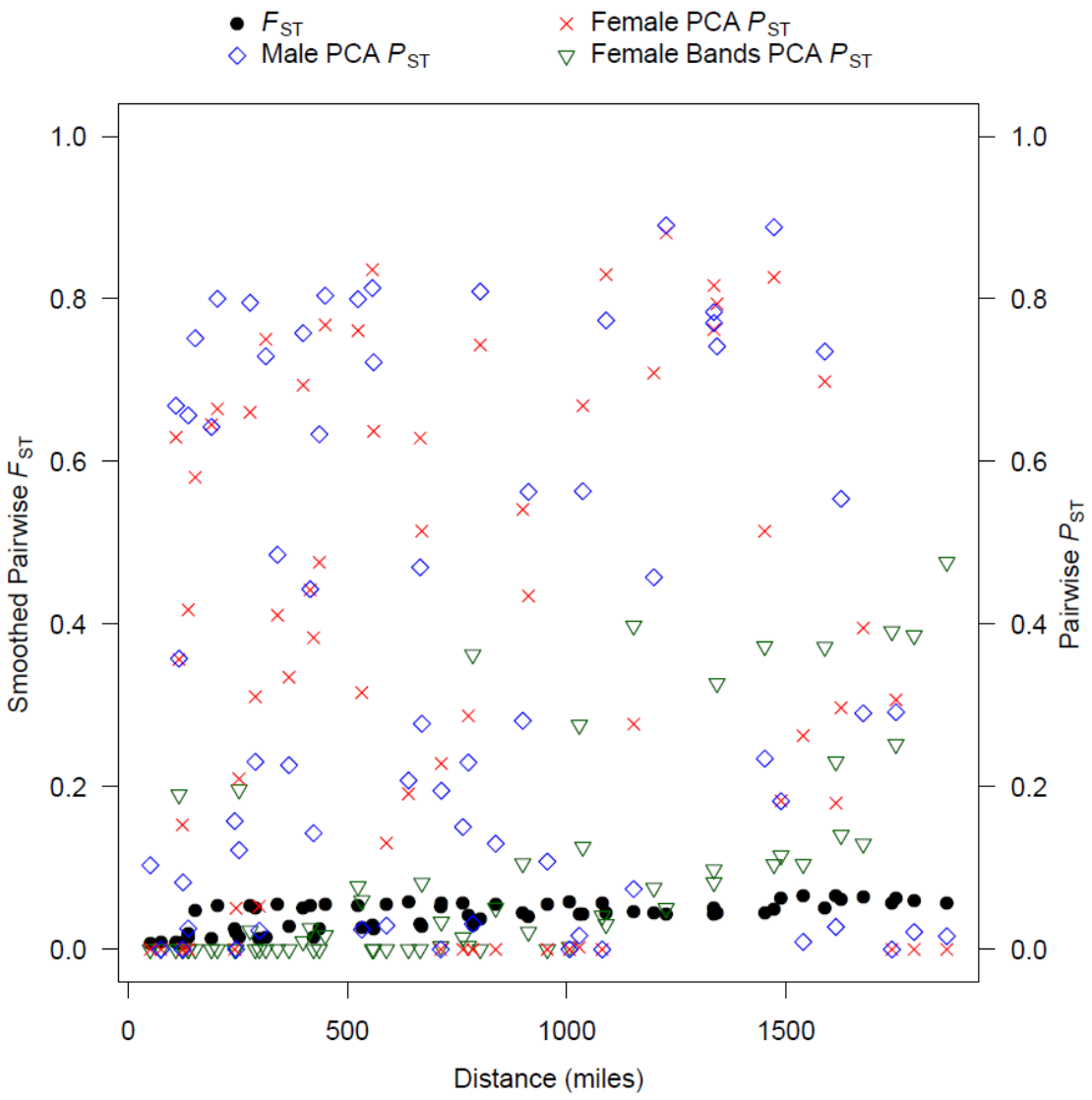
F_{ST}
Male PCA P_{ST}
Female PCA P_{ST}
Female Bands PCA P_{ST}
Smoothed Pairwise F_{ST}
Pairwise P_{ST}
1.0
0.8
0.6
0.4
0.2
0.0
0
500
1000
1500
Distance (miles)

Comparing phenotypic variation among populations

Patterns of phenotypic differentiation are primarily driven by body size and female band number. The **P**-matrices of males and females did not contain the same variables (Appendices V, VI) and so were treated separately in the analyses. The eigenvectors and their associated eigenvalues of male and female **P**-matrices are presented in Appendices VII and VIII. The common subspace method of matrix comparison revealed that our populations have shared subspaces for the first three eigenvectors of the shared subspace matrix for both males and females, although the third eigenvector is not as shared in males as in females (Supplemental File 3). These eigenvectors are primarily related to SVL and tail length ($\boldsymbol{h}_1$ and $\boldsymbol{h}_2$), as well as band number in females ($\boldsymbol{h}_3$) and head length in males ($\boldsymbol{h}_3$) (Supplemental File 3). The angles between each of these three eigenvectors of **H** and the **P**-matrices of each population show that, in both males and females, the populations do not show much variation for the first two eigenvectors. These two eigenvectors are primarily associated with body size. The third eigenvector, however, reveals more variation among populations. In females, the population from Keaton Beach, Florida (FLKB) and the population from Palm Beach (FLPB) are more divergent from the common subspace than the other populations (Figure 6A), suggesting that females from those populations may have a different distribution of band number. In males, the third eigenvector of **H** is not as representative of the populations as the other eigenvectors (i.e., the populations tend to differ from one another), which is why the angles are much larger (Figure 6B). The populations that differ the most from the common subspace are Corpus Christi, TX

(TXCC), Tampa Bay, FL (FLFD), Sanibel Island, FL (FLSI), and Cape Canaveral, FL (FLCC).

The analysis of the phenotypic covariance tensor found that the first three eigentensors comprised most of the distribution of α_i, which describes the variance among the **P**-matrices for the aspect of the covariance structure estimated by E_i (Supplemental File 3). In other words, there are three different combinations of traits that contribute to the majority of the variation in phenotypes among populations. Examining the contribution of each population to the variation of each E_i, one or two populations drive most of the variation for each E_i in females. The pattern for males, however, shows a general pattern of variability, in which no individual population stands out as being a particularly strong contributor to the variation in **P** (Supplemental File 3). The first eigenvector ($\boldsymbol{e}_{11}$,$\boldsymbol{e}_{21}$, and $\boldsymbol{e}_{31}$) of each eigentensor accounted for most of the variance in each eigentensor for both males (99%, 61%, 86%) and females (67%, 53%, and 58%). In males and females, $\boldsymbol{e}_{11}$ and $\boldsymbol{e}_{21}$ are mainly explained by SVL and tail length. In females, $\boldsymbol{e}_{31}$ represents band number, whereas in males $\boldsymbol{e}_{31}$ mainly comprises variation in head length, snout length, and body depth (Supplemental File 3). We projected $\boldsymbol{e}_{11}$, $\boldsymbol{e}_{21}$, and $\boldsymbol{e}_{31}$ onto each population's **P**-matrix to estimate phenotypic variance in the direction of each $\boldsymbol{e}_{ij}$. This analysis revealed that females from four populations tend to have high variances in the three eigenvectors: Galveston, TX (TXCB), Tampa Bay, FL (FLFD), the Florida Keys (FLAB), and Palm Beach, FL (FLPB) (Figure 6C). Males show smaller differences among populations, although males from Galveston, TX (TXCB) showed a particularly

high contribution to variance in $\boldsymbol{e}_{31}$ (Figure 6D), which represents variance in traits other than body size.

All told, the two approaches to comparing **P**-matrices among populations reveal that the major axis of phenotypic variance, relating to body size, seems to be fairly well shared among populations, but that the second or third axes of phenotypic variance, relating to female band traits and male head size, are more variable among populations.

Discussion

In this study, we found evidence that isolation by distance, local adaptation, and phenotypic variation are all contributing to population differentiation the Gulf pipefish. Genetic structure among populations was driven by random differentiation due to isolation by distance, which resulted in 3-5 unique population clusters. However, we also found a signature of local adaptation in approximately 100 SNPs. Several of these SNPs are also associated with temperature, salinity, and seagrass variables, suggesting that one or more of these factors may be driving local adaptation. Additionally, the pattern of phenotypic differentiation is discordant with the random differentiation observed at genomic markers, suggesting that selection, phenotypic plasticity or differences in demography could be contributing to phenotypic variation across the range of the Gulf pipefish.

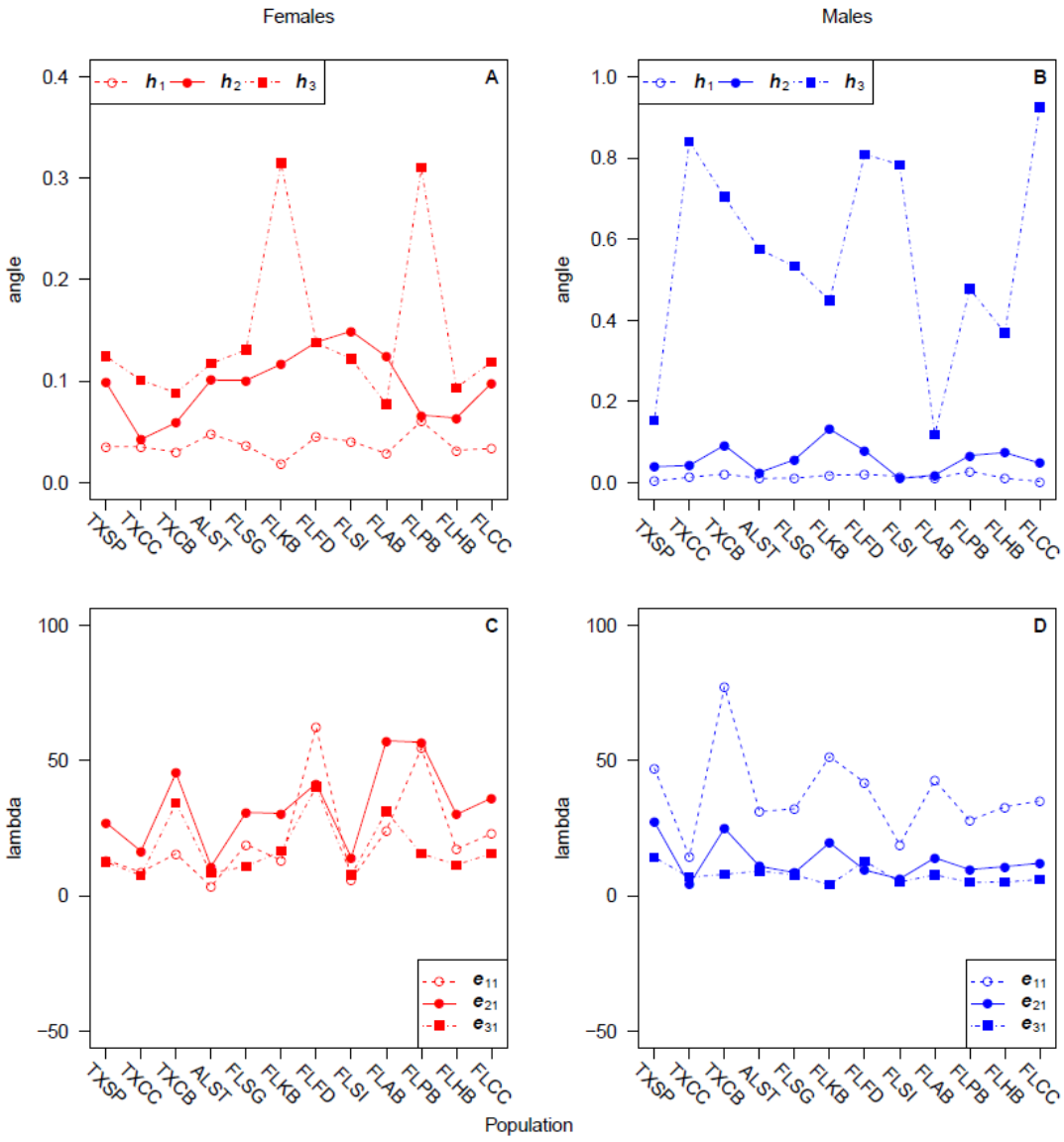

Figure 6. The results of two P-matrix analyses. Panels (A) and (B) show the results of the Krzanowski (1979) common subspace method. These panels show the angles between the eigenvectors (h_i) of the common subspace matrix and each of the population's P-matrices. Panel (A) shows the results of the female analysis and Panel (B) shows the results of the male analysis. Panels (C) and (D) show the results of the eigentensor analysis. Lamba is the eigenvalue associated with the eigenvectors of the eigentensors, and represents the phenotypic variance in the direction of e_{11}, e_{21}, and e_{31}. Panel (C) shows the results of the female analysis and Panel (D) shows the results of the male analysis. We have included connecting lines to improve visualization of the patterns of each eigenvector, and do not suggest that values between points can be interpolated.

Although the overall population structure seemed be shaped by isolation by distance and migration primarily between neighboring populations, we did observe a stronger genetic break between the populations on the Atlantic coast of Florida and the populations in the Florida Keys and Gulf of Mexico (Table 2, Figure 2). This genetic gap is the underlying cause of the two parallel groups of F_{ST} values in Figure 5. This pattern, a break between populations on the Atlantic coast and the Gulf of Mexico, has been observed in many species and is likely due to shared histories of glaciation and paleoclimate (Avise 1992). In other syngnathid species, such as *Syngnathus floridae* (Mobley et al. 2010), a similar break has been documented for microsatellite markers but not mitochondrial markers. A recent study of the lined seahorse, *Hippocampus erectus*, also using RAD-seq, found substantial differentiation between northern Atlantic sites and the southern populations (both Atlantic and Gulf of Mexico populations), with a unique set of genotypes in the Florida Keys (Boehm et al. 2015). A study using microsatellites in *S. scovelli* initially identified a pattern of isolation by distance, but the pattern was driven entirely by three sampling sites in one low-salinity bay (Mobile Bay, AL), indicating that population structure was most likely driven by differences in habitat (Partridge et al. 2012). Partridge et al. (2012) sampled only along a small portion of the northern edge of the Gulf of Mexico, so our sampling is more complete and better able to detect range-wide patterns of isolation by distance.

We also identified numerous SNPs that showed significant differentiation between populations in three different outlier analyses testing for local adaptation. One SNP was significant in all three tests, and was also found to be significant in associations

with variance in temperature and seagrass coverage. The RAD locus that was significant in all analyses was located within a few thousand base pairs of an open reading frame that shows homology to a known gene, *H/ACA ribonucleoprotein complex, non-core subunit NAF1*. This locus was also associated with variance in temperature and salinity, suggesting that local adaptation may be a result of divergent temperature and salinity regimes among populations. Indeed, of the 383 SNPs associated with at least one of the six environmental factors, 58 were also found in the panel of local adaptation outliers. Therefore, it is likely that local adaptation is driven at least in part by temperature, salinity, and seagrass cover, or other factors associated with those variables.

If temperature and salinity are driving local adaptation, as our population genomic data suggest, such a result is consistent with our current understanding of pipefish natural history and ecology. For instance, studies involving pipefish show that temperature affects potential reproductive rates (Ahnesjo 1995, 2008), the strength of sexual selection (Monteiro and Lyons 2012), immune defense (Landis et al. 2012a), and susceptibility to infection (Landis et al. 2012b). Therefore, in addition to physiology-related genes, genes related to reproductive behavior and immune response are likely candidates for adaptation to water temperature in pipefish. In our Blast2GO annotation of the 5kb regions surrounding the SNPs associated with one or more of the temperature variables, we identified some regions involved in immune processes, growth, and behavior, among other biological processes (Appendix IV). Studies in other species, dating all the way back to the allozyme era (Mitton and Koehn 1975), have identified temperature-associated loci that are involved in similarly diverse functions. Examples

include heatshock proteins associated with thermal stress differences in desert and montane populations of the redband trout (Narum et al. 2013b), as well as immune and stress-response genes differentiated between individuals reared at two different temperatures in brown trout (Meier et al. 2014). In Atlantic salmon, temperature and precipitation characteristics of populations were associated with neutral genetic and adaptive divergence, with the latter likely related to growth and immune-related functions (Vincent et al. 2013). Understanding the genetic basis of adaptation to important environmental variables like temperature will not only aid in our understanding of selective pressures but can also play a role in prioritizing populations for conservation (Everett and Seeb 2014).

Salinity is also an important variable in the context of local adaptation for coastal marine species, and Gulf pipefish are of special interest on this front because they are euryhaline. Isolated freshwater populations of *S. scovelli* have been identified (Bolland and Boettcher 2005) and a microsatellite-based study of one of these populations showed it to be differentiated from nearby saltwater populations (Partridge et al. 2012). Furthermore, the salinity of estuarine seagrass beds, a common Gulf pipefish habitat, fluctuates seasonally (Bolland and Boettcher 2005; Masonjones et al. 2010), so the populations we sampled may accommodate spatial and temporal changes in salinity through a combination of local adaptation and phenotypic plasticity, a topic that was beyond the scope of the present study. A genome-wide SNP study including freshwater populations would be a more precise approach to understand additional signatures of

adaptation related to salinity in this species, especially since the patterns of selection due to salinity are likely more complex than those captured in this study.

The finding that mean F_{ST} values were not correlated with body trait P_{ST} values suggests that selection may be driving phenotypic differentiation (Leinonen et al. 2006). Band-related P_{ST} values did follow a pattern similar to F_{ST} values. However, their pattern is not as clearly linear as the F_{ST} values, so the traits are likely differentiating due to a number of factors, especially when the **P**-matrix results are taken into account. Populations displaying phenotypic variation in the same direction in phenotypic space (e.g. FLFD and TXSP in Figure 4, FLKB and FLPB in Figure 6A) did not belong to the same genotypic grouping (Figure 2), suggesting that other processes, beyond the neutral process of isolation by distance, affects the phenotypes. Body size (SVL and tail length) made the largest contribution to the variance among populations (Figure 4, 5, 6, Supplemental File 3). When we analyzed SNPs significantly associated with phenotypic variance, these SNPs did not exhibit an isolation by distance pattern, suggesting either that the phenotypic differences between populations are not entirely plastic differences (i.e., there is an associated genetic signal) or that some loci show a spurious pattern of F_{ST} that coincidentally matches the P_{ST} pattern.. Additionally, each of the sets of SNPs showing a significant relationship between P_{ST} and F_{ST} had a subset of SNPs also found in the local adaptation or environmental association analyses (Supplemental File 1, Supplemental File 2). These results suggest that phenotypic differences may be at least in part shaped by local adaptation due to temperature, salinity, or seagrass cover, although this sort of comparative study cannot provide definitive evidence that selection

plays a role. In addition to selection, phenotypic plasticity and differences in age structure could result in divergence in phenotype among populations, so additional work will be necessary to tease out the precise source of the values of P_{ST} observed here.

Sexual selection may also be leading to phenotypic differentiation. Both a principal components analysis and an eigenanalysis of the common subspace of the **P**-matrix revealed that variation in female band number shape differs among populations (Figures 4, 6). Variation in band area mainly contributes to within-population variation (Figure 4), but two populations (FLKB and FLPB) diverge from the common phenotypic subspace due to variance associated with band number (Figure 6, Supplemental File 3). Since band number is known to be a target of sexual selection (Flanagan et al. 2014), population differentiation with regard to band traits may be a result of different sexual selection pressures in different populations. Sexual selection has been shown to vary in strength geographically for other pipefish species (Mobley and Jones 2007; Mobley and Jones 2009; Monteiro and Lyons 2012). In-depth studies of mating systems across the geographic range of *S. scovelli* will be required to verify whether populations are experiencing different selective pressures.

The results we have presented here must be interpreted with a note of caution. While the RAD-seq approach can be useful for the identification of candidate loci involved in adaptation (Davey and Blaxter 2010; Hohenlohe et al. 2010b; Davey et al. 2011; Narum et al. 2013a), RAD-seq also brings with it sources of inherent bias and errors. These issues arise from a diverse array of technical challenges, including a possible dearth of apparent heterozygotes due to low sequencing depth (Buerkle and

Gompert 2013), allele dropout due to polymorphic restriction sites (Arnold et al. 2013; Gautier et al. 2013), erroneous SNPs due to PCR error or sequencing error, and PCR bias (Davey et al. 2013; Puritz et al. 2014; Mastretta-Yanes et al. 2015). Consequently, validation of putatively selected loci will be an essential step in the population-genomic search for genetic signatures of adaptation [see Rausher (2015) for a discussion of when identifying genes is particularly useful in evolutionary biology]. Here, we identified hundreds of putative candidate loci associated with local adaptation, environmental factors, and phenotypic differentiation, but additional work will be necessary to validate these loci. The low level of overlap between complementary outlier analyses suggests that many of the putative candidate loci are spurious. However, we did identify some RAD loci that were shared among multiple outlier tests. Validation of candidate loci via genetic manipulation is currently impossible in pipefish but other approaches may be possible. For instance, if these regions of the genome are identified in complementary analyses, such as genome-wide comparisons of freshwater and saltwater populations or a genome-wide selection components analysis to partition the changes in allele frequencies due to episodes of selection within a generation (Christiansen and Frydenberg 1973; Flanagan and Jones 2015; Monnahan et al. 2015), it would be highly unlikely that those outliers are spurious. More conclusively, quantitative trait locus mapping involving crosses between differentiated populations may provide an excellent approach to obtain additional evidence that a candidate SNP is indeed involved in phenotypic divergence and selection.

In summary, we compared populations of Gulf pipefish at both the genetic and phenotypic levels. We used a combination of approaches to identify a genome-wide pattern of isolation by distance, with some loci putatively involved in local adaptation and selection due to environmental factors. Selection also appears to be at least partly responsible for shaping phenotypic differentiation, likely due to an aspect of the environment that we were unable to measure or varying patterns of sexual selection. This study provides an example of how multiple approaches utilizing next-generation sequencing technologies in a non-model organism can help paint a more complete picture of the evolutionary mechanisms affecting genetic and phenotypic divergence among populations within a widely distributed species.

CHAPTER III

IDENTIFYING SIGNATURES OF SEXUAL SELECTION USING GENOMEWIDE SELECTION COMPONENTS ANALYSIS[*]

Overview

Sexual selection must affect the genome for it to have an evolutionary impact, yet signatures of selection remain elusive. Here we use an individual-based model to investigate the utility of genome-wide selection components analysis, which compares allele frequencies of individuals at different life history stages within a single population to detect selection without requiring a priori knowledge of traits under selection. We modeled a diploid, sexually reproducing population and introduced strong mate choice on a quantitative trait to simulate sexual selection. Genome-wide allele frequencies in adults and offspring were compared using weighted F_{ST} values. The average number of outlier peaks (i.e., those with significantly large F_{ST} values) with a quantitative trait locus in close proximity ("real" peaks) represented correct diagnoses of loci under selection, whereas peaks above the F_{ST} significance threshold without a quantitative trait locus reflected spurious peaks. We found that, even with moderate sample sizes, signatures of strong sexual selection were detectable, but larger sample sizes improved detection rates. The model was better able to detect selection with more neutral markers, and when quantitative trait loci and neutral markers were distributed across multiple chromosomes.

[*] Reprinted with permission from Identifying signatures of sexual selection using genomewide selection components analysis, by Sarah P. Flanagan and Adam G. Jones. 2015. *Ecology and Evolution* 5: 2722-2744. Copyright [2015], by Flanagan et al.

Although environmental variation decreased detection rates, the identification of real peaks nevertheless remained feasible. We also found that detection rates can be improved by sampling multiple populations experiencing similar selection regimes. In short, genome-wide selection components analysis is a challenging but feasible approach for the identification of regions of the genome under selection.

Introduction

One of the most important questions in evolutionary biology is how selection, which by definition acts on phenotypes, causes heritable changes (Nielsen 2005). Recent advances in DNA sequencing technologies have provided many new opportunities to explore how genomes are affected by selection, but no method currently exists to detect the signature of individual episodes of selection within the time frame of a single generation on a genome-wide scale. Yet, we know that total selection can be decomposed into several components of selection that affect individuals at various stages during the life cycle (Christiansen and Frydenberg 1973) and that these episodes can provide important insights into mating systems (Emlen and Oring 1977), or ecological factors acting as agents of selection (Loehle and Pechmann 1988). Episodes of selection can also help evaluate threats and conservation issues (Stockwell et al. 2003). Additionally, much of the quantitative genetics theory commonly used in empirical studies focuses on individual episodes of selection (Arnold and Wade 1984b; Arnold and Wade 1984a), so having the ability to examine the effects of selection at different episodes on the genome might be useful in linking theory to empirical work. Therefore,

a method to detect the signature of each component of selection within a natural population would be an important addition to an evolutionary biologist's toolkit.

Currently, three principal analytical methods are used to diagnose the effects of selection on the genome. First, quantitative traits can be mapped to specific loci using linkage mapping techniques. Quantitative trait locus mapping is very effective, but requires crossing specific parents, generating numerous offspring, and having a trait of interest to map. Second, genome-wide association studies can be used to correlate a specific trait (often disease related) with loci that differ between groups with different values of the trait (e.g., a group with diabetes compared to a group without; reviewed in Carlson et al. (2004). Finally, population genomics methods compare summary statistics describing allele frequencies, genetic diversity, and linkage disequilibrium between multiple populations of the same species to identify loci that lie outside of a specified significance threshold (Hohenlohe et al. 2010b). This method can be very powerful at detecting signatures of positive selection (e.g., Gagnaire et al. 2013; Hess et al. 2013), balancing selection (e.g., Reitzel et al. 2013), local adaptation (e.g., Hohenlohe et al. 2010a; Miller et al. 2012; Catchen et al. 2013a; Vincent et al. 2013), and selective sweeps (e.g., Boitard and Rocha 2013; Clement et al. 2013; Harris et al. 2013; Hubner et al. 2013; Rellstab et al. 2013). One shortcoming of comparing population genomics statistics between multiple populations is that such comparisons do not facilitate a diagnosis of the type of selection (e.g., sexual selection or viability selection) causing the pattern.

A complementary approach, which has not yet been applied on a whole-genome scale, is to measure the effects of selection at various stages in the life cycle of a population. At least four major types of selection occur during a typical life cycle. These different components can be isolated within a single generation using a cross-sectional study design (e.g., Christiansen et al. 1973; Christiansen and Frydenberg 1973), or by tracking a population over multiple generations in a longitudinal design (Bundgaard and Christiansen 1972; Clark and Feldman 1981; Clark et al. 1981; Anderson et al. 2014). Although a longitudinal design allows researchers to track allele frequencies over multiple generations, it is not a feasible experimental design for many organisms and is difficult to implement in studies of natural populations.

Selection components analysis can be used to decompose total selection into its parts in a variety of ways. For instance, some researchers have compared preobservation and postobservation components of selection (Prout 1965, 1969, 1971a, b), while others have examined mother–offspring combinations, allowing a subset of the male breeding population to be inferred and compared to a random sample of adult males containing both mated and unmated individuals (e.g., Christiansen and Frydenberg 1973; Nadeau and Baccus 1981). Allele frequencies of individuals at different life history stages were commonly compared in studies using allozyme markers (e.g., Christiansen et al. 1973; Christiansen and Frydenberg 1973, 1974; Nadeau and Baccus 1981; Heath et al. 1988; McDonald 1989), but these studies usually did not target enough loci to detect selection. Selection components analysis was also used to investigate the patterns of selection on entire chromosomes (e.g., Anderson 1969; Prout 1971a; Bundgaard and Christiansen

1972; Anderson et al. 1979; Curtsinger and Feldman 1980; Clark and Feldman 1981; Clark et al. 1981; Barbadilla et al. 1994), but chromosomes were too broad of a target and so only crude estimates of selection were detectable. However, with next-generation sequencing approaches it is now possible to identify large numbers of single nucleotide polymorphisms distributed across the entire genome, opening up the possibility to detect a genome-wide signature of selection components.

There is still much to learn about how selection affects the genome, and selection components analysis may be one solution. In this paper, we present findings from an individual-based simulation model that tests the application of existing population genomic approaches in the context of selection components analysis. We show that this approach holds promise for detecting genome-wide signatures of strong selection, at least in a best-case scenario. Additionally, this model allows us to make predictions about characteristics of populations that might benefit most from a selection components analysis approach.

Methods

Modeled sampling procedure

This model, described in detail below, was designed to determine the power of an empirical selection components analysis. An empirical study would require a one-time collection of a population, including equal numbers of adults and offspring. The sampled individuals would then undergo some form of reduced representation sequencing, such as restriction-site-associated DNA sequencing (RAD-seq), to generate SNP data. From the genome-wide SNP data, loci with approximately uniform allele frequencies would be

selected for genome-wide selection components analysis (Figure 7). From this analysis, we expect to detect only loci of large effect, as every population genomics study struggles to detect loci of small effect (Lewontin and Krakauer 1973; Beaumont and Nichols 1996).

In the implementation of our simulation model, which encapsulates a best-case scenario for this type of empirical study, we wished to model a population with genetic variation upon which selection could act. Thus, we modeled initial generations without sexual selection (i.e., with random mating). Even though a natural population would not typically make a single-generation transition from random mating to strong sexual selection, our approach uses this modeling convenience to simulate populations in a way that gives us control over levels of genetic variation and patterns of linkage disequilibrium independent of the strength of sexual selection. We chose to model a polygynous mating system (females mate once, males mate multiply), with sexual selection acting on the male trait, which is constrained by viability selection because this is a well-studied sexual selection framework in quantitative genetics (e.g., Lande 1981). Although other mating systems certainly exist and have strong sexual selection, we restricted our analysis to this natural selection and sexual selection trade-off for the scope of this paper.

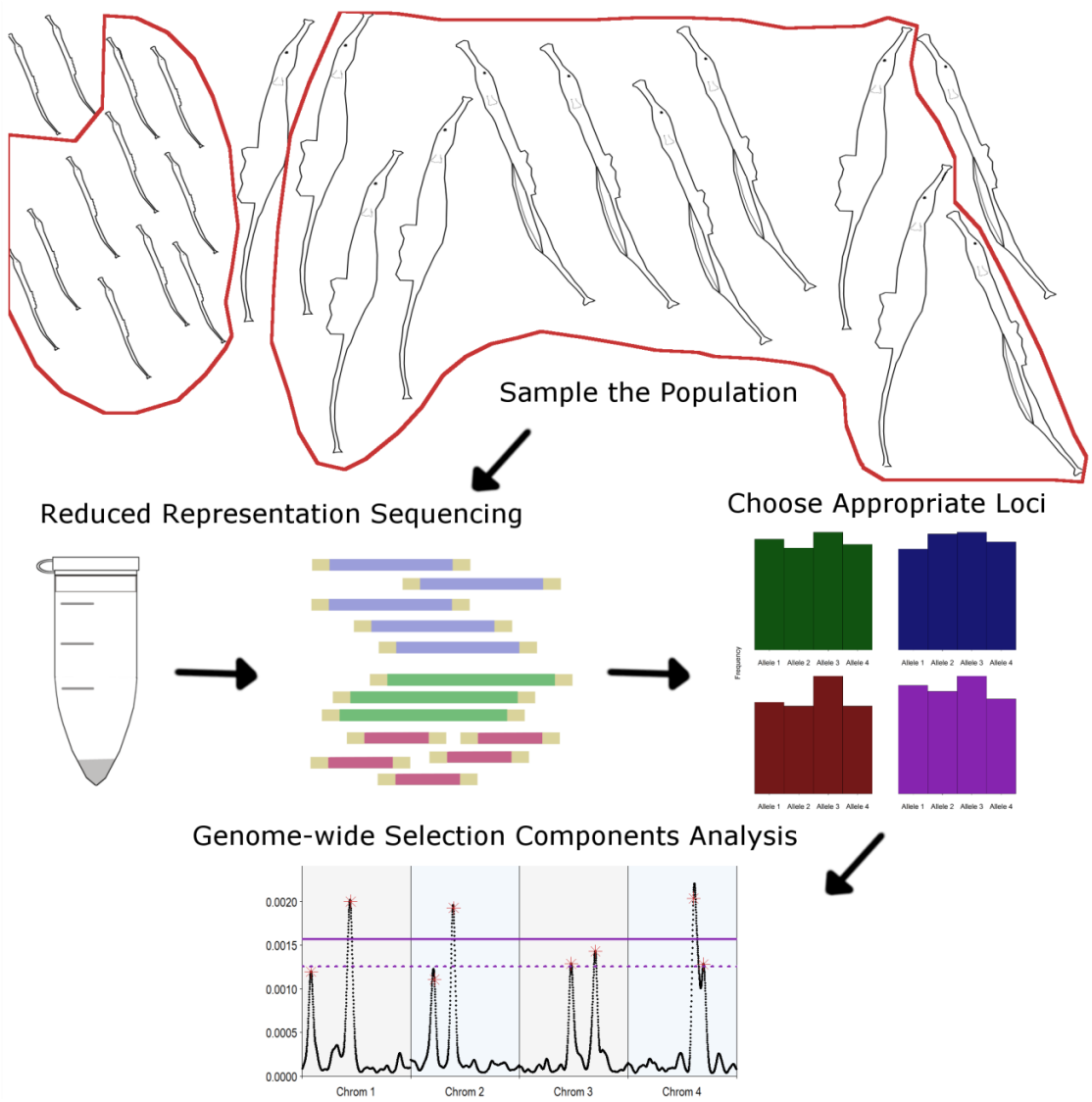

Figure 7. A schematic diagram of how to apply genome-wide selection components analysis in an empirical study. A population of some organism, for example, pipefish, is sampled so that DNA samples are obtained from roughly equal numbers of very young offspring and adults. Those DNA samples are then sequenced using a reduced representation sequencing method, such as RAD-sequencing. Loci with roughly even allele frequencies would then be selected for use in genome-wide selection components analysis, which will identify outlier loci that are putatively under selection.

Model overview

The model was written in C++, and the source code is available on Dryad (doi: 10.5061/dryad.5k84d). We modeled a population with a carrying capacity of N individuals, each of which had c chromosomes with m markers (i.e., single nucleotide polymorphisms) and q quantitative trait loci. The quantitative trait loci additively determined, sometimes with added environmental noise, the phenotype of each individual. In a life cycle, individuals produced gametes, mated, and produced offspring. Females chose mates based on the encountered males' phenotypes, putting sexual selection pressure on the male phenotype only. The male offspring then underwent viability selection on the same trait females used to choose a mate. Finally, the offspring matured into adults and replaced the previous generation.

The life cycle was repeated for a given number of initial generations, in which selection did not occur, to generate enough genetic variation upon which sexual selection could act. The initial generations were followed by one experimental generation, during which the population was randomly sampled and summary statistics calculated. Allele frequencies were also compared between adults and offspring (see below, "Sampling the population," for more detail) using weighted F_{ST} values. We tested some of the parameters, such as the number of initial generations, to fine-tune the model so that we could simulate the best-case scenario for applying genome-wide selection components analysis.

Because we wanted to focus our attention on the types of markers that would be most informative in an empirical RAD-seq type of study, namely quantitative trait loci

of large effect with moderate allele frequencies, our initial generations generated quantitative trait loci with relatively uniform distributions. This approach differs from previous work, which also used simulation models (e.g., Thornton et al. 2013), but instead focused on detecting rare alleles of moderate effect.

Genetics of the population

The simulated organism was assumed to be diploid. Both neutral markers and quantitative trait loci were evenly distributed among chromosomes. The locations of quantitative trait loci were randomly chosen per chromosome per run of the model, unless otherwise stated. For instance, under the basic parameter combinations, each of the four chromosomes had 1000 marker loci and two quantitative trait loci, so that the total number of observed markers was 4000 and the total number of quantitative trait loci was eight. Although a suite of 4000 loci is a modest number of markers in the scheme of all loci identified in RAD-seq studies, most studies do typically restrict their analyses to several thousand loci. Therefore, we believe that 4000 markers is a reasonable number. The alleles for the quantitative trait loci were drawn from a normal distribution with a mean of zero and a standard deviation of 0.5. Each locus could have up to four alleles, and we started each simulation run with chromosome-wide genotypes for each chromosome. In other words, each run started with complete linkage disequilibrium within particular chromosomes. Linkage disequilibrium then decayed during the initial generations due to recombination, which occurred during the production of gametes in the form of r crossing-over events, where r was drawn from a Poisson distribution with a constant mean of 0.2. Each recombination event was

randomly assigned a location between two marker loci. This approach allows the genome-wide level of linkage disequilibrium to be altered by merely changing the number of initial generations. No mutations occurred during the production of gametes, because the simulation runs consisted of so few generations that mutation would not be a major factor affecting allele frequencies. Phenotypes were calculated by summing across all alleles at all quantitative trait loci plus an added value, *e*, a random number from a normal distribution with a mean of 0 and a specified environmental standard deviation.

We tested different numbers of initial generations to see their effect on linkage disequilibrium and on the prospects for reliably detecting quantitative trait loci. For this analysis, we calculated pairwise linkage disequilibrium between 100 randomly chosen loci on each chromosome (i.e., all comparisons were from loci on the same chromosome). The pairwise linkage disequilibrium between randomly chosen locus A and locus B was calculated as follows. For each allele *Ai* and *Bj*, *D* was calculated as $f_{ij} - p_i q_j$, where f_{ij} is the frequency of the $A_i B_j$ haplotype, p_i is the frequency of allele *i*, and q_j is the frequency of allele *j*. $D_{\max}$ is the lesser of $p_i q_j$ or 1 - $p_i q_j$ when $D_{ij} < 0$ and is the minimum of $(1 - p_i)*q_i$ or $p_i*(1 - q_i)$ when $D > 0$. Finally, D' was evaluated as:

$$D' = \sum_{i}^{m} \sum_{j}^{n} \frac{p_i q_j |D_{ij}|}{D_{max_{ij}}}$$

where *m* is the number of alleles at locus A and *n* is the number of alleles at locus B.

Mating, production of gametes, and selection

In this model, each female mated with at most one male, and males were capable of mating with multiple females. Females randomly sampled 50 males in the population, and if they could not find an acceptable mate within those 50, they did not mate. We incorporated this cost of choosiness to add variability to the selection differentials in males. In our framework, males with identical trait values are not necessarily guaranteed the same number of matings. In the initial generations, females mated with the first male they encountered, so no sexual selection occurred. Sexual selection was introduced to the model during the experimental generation, after trait values were standardized to a mean of 0 and a standard deviation of 1. When mate choice was implemented, the probability that the female would mate with a given male was determined by a Gaussian-shaped function comparing the male's phenotype, z, to a population-level female preference value, θ,

$$P(z) = e^{\frac{-(z - \theta)^2}{2\omega_S^2}},$$

where ω_S^2 is the width of the selection surface (i.e., it determines the strength of selection). We set θ to an arbitrary value of 4 for all runs of the model. If a random number from a uniform distribution (0,1) was less than $P(z)$, the female mated with that male and they produced four offspring. Therefore, the probability of mating for a male was determined first by whether a female encountered him and then by his trait value (z) relative to the population-level preference optimum ($\theta = 4$). When selection was strong, few males possessed a trait value favored by the females (Figure 8).

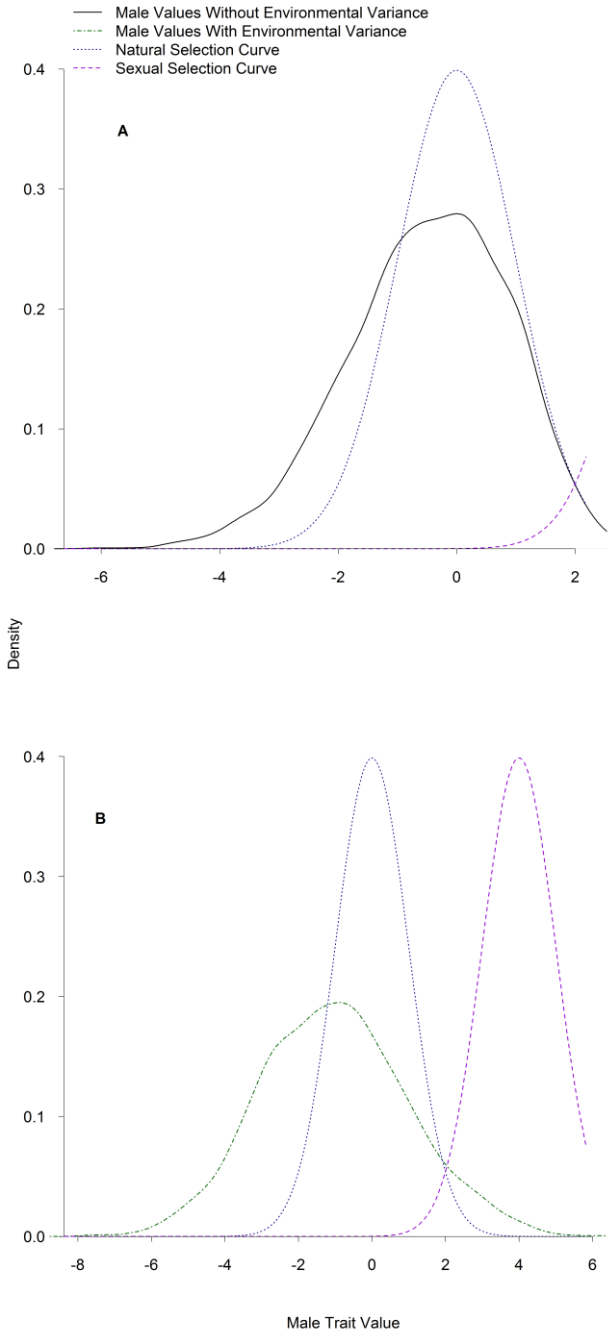

Figure 8. Representative distributions of male trait values under default parameters (A) and with an environmental variance of 1 (heritability = 0.5; B). Also shown are the uniform distributions based on the trait values and the preference optimum (sexual selection curve, θ = 4) and the viability selection optimum (natural selection curve, θ = 0) with default selection strengths (Table 5).

When females found a mate and produced offspring, we simulated meiosis in the following way. For each chromosome pair, one of the mother's two chromosomes was randomly chosen to be passed to the offspring. Before being passed to the zygote, recombination occurred. The number of recombination events on a given chromosome was a random number chosen from a Poisson distribution with a mean of 0.2. For each recombination event that occurred in a given mating event on a given chromosome, a randomly chosen chunk of one of the mother's chromosomes was exchanged with the matching region from the mother's other homologous chromosome, while maintaining the total size of each chromosome. The recombined chromosome was then passed to the zygote. A similar procedure was used for the father's chromosomes, so recombination occurred in both sexes. This procedure realistically simulates the process of meiosis for a species in which crossing-over occurs at a similar rate in both sexes. The sex of each offspring was determined randomly, such that on average 50% of the offspring were female and 50% were male.

After the zygotes were produced, viability selection acted on the male offspring. Viability selection was implemented in the model merely to maintain variation in the male trait and to constrain sexual selection, and thus viability selection was a weak force in the model. This selection was implemented as the following Gaussian fitness surface with a given width, ω_V^2:

$$W(z) = e^{\frac{-(z-\theta)^2}{2\omega_V^2}},$$

where z is an individual's phenotype and θ is the optimum value (zero). Viability selection was implemented during both the initial generations and the experimental

generations, although the strength of viability selection was weak ($\omega_{VI}^2 = \omega_{VE}^2 = 500$) For each male, if a random number drawn from a uniform distribution (0,1) was less than $W(z)$ for that individual, he survived to the next generation. As females did not express the trait, they were unaffected by viability selection. We implemented very weak viability selection, so that the majority of males survived the viability selection event (Figure 8A), even when environmental variance altered the distribution of male trait values (Figure 8B). After the viability selection event, offspring were randomly chosen to survive to adulthood, so that the number of surviving offspring was less than or equal to the carrying capacity.

Sampling the population

Population demographic statistics were calculated for the entire population each generation. Some of the statistics calculated were population size, sex ratios, and mean trait values for males and females. Additive genetic and phenotypic variances were calculated from the distribution of values in all adults. Heritability was calculated as the additive genetic variance divided by the phenotypic variance and was therefore always 1 whenever there was no environmental variation added to the trait. "Long-distance" linkage disequilibrium was calculated for randomly selected loci throughout the genome as described above (see "Genetics of the population"), and the same equations were used to calculate pairwise linkage disequilibrium between neighboring polymorphic loci. Mating differentials were calculated as the covariance between standardized trait values and relative mating success (Jones 2009).

During the experimental generation, the population was randomly sampled after mating occurred and offspring were produced, but before the offspring experienced viability selection. As females all produced the same number of offspring (4) and meiotic drive was not included in the model, this sampling strategy captured the effects of sexual selection on allele frequencies. Both parents and offspring were sampled without replacement, and genealogical relationships were assumed to be unknown. Summary statistics, including allele frequencies and observed and expected heterozygosities, were calculated for adults, offspring, and the total population. Expected heterozygosity, H_E, was calculated as $1 - \sum_{i=1}^{a} p_i^2$ for each locus with a alleles. We then compared allele frequencies in adults and offspring using the Nei (1986) F_{ST} calculation:

$$F_{ST} = \left(1 - \frac{H_{E_{progeny}} + H_{E_{adults}}}{2 * H_{E_{total\ population}}}\right).$$

F_{ST} values were weighted using a kernel-smoothing moving average, which incorporates the contribution of nearby values to the F_{ST} for each locus. Specifically, each polymorphic locus, k, was weighted by the F_{ST} values at each marker position, d, within the sliding window region in each direction, using the Gaussian function:

$$F_{ST}{}'_{k} = \frac{\sum_{k-\sigma_s}^{k+\sigma_s} F_{ST_k} * e^{\frac{-(d-k)^2}{2\sigma_s^2}}}{\sum_{k-\sigma_s}^{k+\sigma_s} e^{\frac{-(d-k)^2}{2\sigma_s^2}}},$$

where σs is the width of the sliding window region in each direction (Hohenlohe et al. 2010a).

Much work in the field of population genetics has been dedicated to detecting F_{ST} outliers, beginning with Lewontin and Krakauer (1973). They proposed the

idea that neutral markers all experience the same background selection, drift, and other demographic factors, so any loci with statistics such as F_{ST} lying outside of the distribution of the other loci are likely experiencing selection (Lewontin and Krakauer 1973). Improvements on the original method have been suggested, such as weighting F_{ST} values by heterozygosity (Beaumont and Nichols 1996) and using Bayesian methods (Beaumont and Rannala 2004). Other studies have tested the importance of the neutral distribution, by comparing null models to the dataset (e.g., Foll and Gaggiotti 2008; Lotterhos and Whitlock 2014). Indeed, other work has shown that increased neutral variance in F_{ST} values leads to high rates of false positives (Bierne et al. 2013). Despite the acknowledged importance of the distributions of F_{ST} values in determining outliers, the distribution of the smoothed F_{ST} values used commonly in modern population genomics studies is unknown, and the neutral distributions are often not mentioned in population genomics analyses. We were therefore interested in evaluating different common methods for determining significance of our outlier summary statistics.

We implemented three methods of determining cutoffs, two of which are commonly used approaches in the literature. First, we calculated *P*-values for each $F_{ST}'_k$ statistic at locus *k* using the χ^2 distribution, as F_{ST} values are known to have a χ^2 distribution in a neutral model (Workman and Niswander 1970; Lewontin and Krakauer 1973; Weir and Cockerham 1978; Beaumont and Nichols 1996). Specifically, the transformation $2N(m_k\text{-}1)F_{STk}$ is the χ^2 statistic, where *m* is the number of alleles at locus *k* in *N* individuals, with $(m-1)(n-1)$ degrees of freedom, where *n* is the number

of subgroups within a population (Workman and Niswander 1970). The Benjamini and Hochberg (1995) false discovery rate was then calculated to establish a cutoff value by ranking all of the *P*-values from smallest to largest. For each *P*-value, its relative rank (its order in the sorted list of *P*-values divided by the total number of *P*-values) was multiplied by the significance value, 0.05. The largest *P*-value that was less than or equal to this weighted rank was the false discovery rate significance threshold. Second, we implemented the bootstrapping algorithm used by the software package STACKS (Catchen et al. 2011; Catchen et al. 2013b), a common population genomics bioinformatics program, re-sampling the genome 10,000 times. This algorithm re-weights the weighted F_{ST}' values using the kernel-smoothing approach described above, but the nucleotide positions (d) are randomly chosen loci from anywhere in the genome, rather than the neighboring nucleotides. Confidence intervals were then calculated from the distribution of the 10,000 bootstrapped F_{ST}' values in the same way as described below for the genome-wide confidence intervals. Finally, we determined the genome-wide distribution of F_{ST}' values and calculated confidence intervals.

Although F_{ST} values have a χ^2 distribution (Workman and Niswander 1970; Lewontin and Krakauer 1973; Beaumont and Nichols 1996; Lotterhos and Whitlock 2014), the distribution of smoothed F_{ST}' values is unknown and appears to only approximate a χ^2 distribution. Therefore, rather than calculating confidence intervals from a χ^2 distribution, we chose to use a Gaussian confidence interval, which is based on two basic descriptors of the F_{ST}' distribution: the mean and the variance. To calculate the confidence intervals, the mean F_{ST}' and the variance and standard deviation in F_{ST}'

values were calculated across all sampled loci on all chromosomes. Genome-wide confidence intervals were then calculated as the mean F_{ST}' value plus the appropriate value from the cumulative normal distribution function multiplied by the standard deviation of F_{ST}' values. For example, the 95% genome-wide confidence interval is calculated as follows:

$$95\%\ \text{CI} = \overline{F_{ST}'} \pm 1.95996 * \sigma_{F_{ST}'}.$$

We present the 95% and 99% confidence intervals, as those are two significance thresholds commonly used in biology, although other confidence intervals certainly could be used instead. After determining these various cutoff values, each peak in F_{ST}' value was detected and the value compared to the cutoffs. If the peak was above the cutoff value, and if a known quantitative trait locus was within *x* marker loci of the peak, then it was counted as a "real" peak. If the peak was above the cutoff value but a quantitative trait locus was not within *x* marker loci, then it was counted as a "spurious" peak. The average and standard errors of both the number of real and spurious peaks were calculated. The average number of real peaks detected compared to the overall number of quantitative trait loci reflected the amount of type II error in the analysis. In contrast, the average number of spurious peaks indicated the extent to which type I error occurred (i.e., the frequency of false positives). To test various peak widths, we varied *x* and tested values from 1 to 100 loci.

Testing parameter combinations

The default parameters from the model are in Table 1. To address whether genome-wide selection components analysis could be used in empirical studies of

natural populations, we focused on the effects of sample size, strength of sexual selection, and environmental variance in the focal trait. We also assessed the effects of the architecture of marker loci (covarying the number of marker loci and number of chromosomes), population size, and the number of quantitative trait loci underlying the trait on this type of selection components analysis. We tested many of these parameters in combination. The pairwise parameter combinations tested included sample size and carrying capacity; the number of markers and the number of chromosomes; the number of markers and sample size; the strength of sexual selection and number of quantitative trait loci; the strength of selection and linkage disequilibrium; environmental variation and the number of quantitative trait loci; and environmental variation and linkage disequilibrium.

Table 5. The baseline parameters for running the simulation model. Selection variances refer to the Gaussian selection surface width. "Initial" refers to the width during the initial generations before sexual selection was imposed, and "Experimental" refers to the width during the subsequent generation during which the population was sampled.

Parameter	Starting Value
Carrying capacity	5000
Sample size (adults)	4000
Sample size (offspring)	4000
Number of markers per chromosome	1000
Number of QTL per chromosome	2
Number of chromosomes	4
Initial mate choice strength (ω_{SI}^2)	Random mating
Experimental mate choice strength (ω_{SE}^2)	2
Initial viability selection strength (ω_{VI}^2)	500
Experimental viability selection strength (ω_{VE}^2)	500
Environmental variance	0
Number of populations	1

Results

Peak detection

We explored how the peak detection width, or the distance from an actual quantitative trait locus required to call a peak a "real" peak as opposed to a spurious peak, affected the results. All of the values we tested beyond 2 loci resulted in equivalent results (Figure 9). We used a peak detection width of 50 loci for all of the other runs of the model.

Replication

To determine whether running the model with only ten replicates would negatively impact detection rates, we ran the default parameters (Table 5) with both 10 replicates and 100 replicates. We found qualitatively similar detection rates (Table 6), so to conserve time we ran the model for 10 replicates for all parameter combinations.

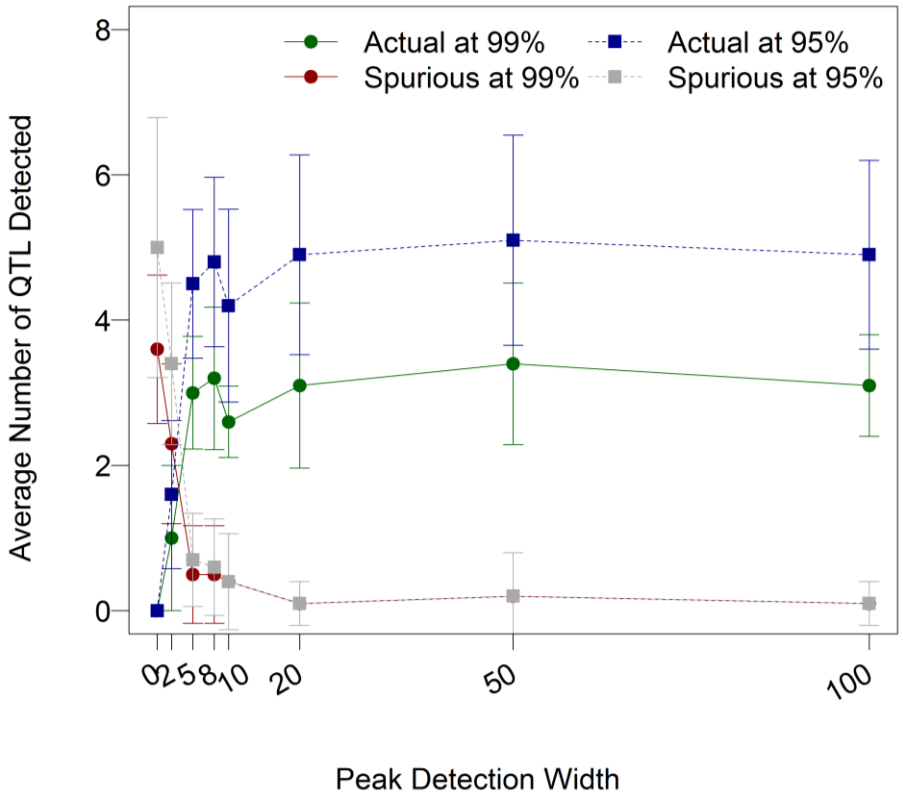

Figure 9. The effect of peak detection width on average number of quantitative trait loci detected. When a peak was identified, it was either designated "actual" or "spurious" based on whether there was a quantitative trait locus *x* markers away. The value of *x* is the "peak detection width," represented on the *x*-axis here. To test peak detection width, the model was run with default parameters (Table 5), with 10 replicates for each peak detection width tested. Bars are the standard error of the mean.

Determining significance

Our three methods of choosing cutoff values for determining whether a peak was significant showed strikingly different patterns. The false discovery rate was highly unpredictable, such that in some cases nearly every locus was significant, and at other times nearly none of the loci were significant, when the parameters remained constant.

This unpredictability is reflected in the standard errors of the mean number of spurious peaks detected and especially in the mean proportion of peaks detected (Table 7). Additionally, the false discovery rate detected very few actual peaks. The bootstrapped confidence intervals were better than the false discovery rate and detected a high number of real peaks, but consistently detected spurious peaks (Table 7). In contrast, the genome-wide confidence intervals were more conservative in the number of peaks detected, but consistently detected over 30% of the real peaks, and importantly very rarely detected spurious peaks (Table 7). Thus, for the rest of our results, significance was determined by 95% or 99% genome-wide confidence intervals. It is important to note that rarely were all quantitative trait loci detected, largely because quantitative trait loci of small effect tended not to show strong signatures of selection. The best detection rate achieved was 92.5% of the quantitative trait loci, with a spurious detection rate of 0, but more commonly a "good" detection rate was 50-70%.

Table 6. A comparison of running the model with default parameters (Table 1) and with either 100 replicates or 10 replicates. Here we display both the 99% and 95% cutoffs as determined by the genome-wide confidence interval and the bootstrapped confidence interval. We also present the 95% false discovery rate. Running 100 replicates instead of 10 replicates did not significantly increase the average number of real peaks ("real") or decrease the average number of spurious peaks ("spurious").

Detection Method	Significance Level	Number of Replicates	Real	±	SE	Spurious	±	SE
Genome-wide confidence interval	**99%**	100	3.300	±	1.22	0.000	±	0.00
		10	3.800	±	1.25	0.100	±	0.30
	95%	100	4.970	±	1.45	0.000	±	0.00
		10	5.200	±	1.33	0.100	±	0.30
Bootstrapped	**99%**	100	0.948	±	0.85	0.113	±	0.84
		10	0.875	±	0.79	0.088	±	0.84
	95%	100	0.948	±	0.08	0.145	±	0.15
		10	0.875	±	0.30	0.100	±	0.09
False Discovery Rate	**95%**	100	0.169	±	0.36	0.580	±	1.46
		10	0.200	±	0.40	0.838	±	1.65

Table 7. The reliability of three methods to determine significance cutoff thresholds for weighted F_{ST} values was compared using the mean proportion of actual peaks detected and the mean number of spurious peaks detected and their standard errors. These means were generated by running the model with its default parameters (Table 1) in 10 replicates, each of which had 200 initial generations where no sampling occurred, followed by one experimental generation. Allele frequencies and F_{ST} measures were calculated between adults and offspring. Viability selection was weak during both the initial and the experimental generations ($\omega_{VI}^2 = \omega_{VE}^2 = 500$), and strong sexual selection was introduced at the start of the experimental generations (ω_{SI}^2 = random mating, $\omega_{SE}^2 = 2$).

	Mean Proportion of Actual Peaks Detected	SE	Mean Number of Spurious Peaks Detected	SE
99% Genome-wide CI	0.3475	0.0245	0.1000	0.0428
95% Genome-wide CI	0.4925	0.0318	0.1000	0.0428
99% Bootstrapped CI	0.8000	0.0404	1.1400	0.1874
95% Bootstrapped CI	0.8075	0.0395	1.5600	0.2063
False Discovery Rate	0.1525	0.0455	4.0400	1.5367

Linkage disequilibrium

The number of initial generations determined the degree of linkage disequilibrium present when sexual selection was introduced in the experimental generations. We measured long-distance linkage disequilibrium per chromosome (D') at the end of the initial generations (see Methods: Genetics of the population). The number of initial generations tested varied from 1 to 1000 to examine how linkage disequilibrium affected our ability to detect selection. We found that after 200 initial generations linkage disequilibrium was 0.1007 and that detection rates appeared to peak at this level of linkage disequilibrium (Figure 9). We chose to use 200 generations in the rest of our permutations of the model to present the best-case scenario for our genome-wide selection components analysis approach.

We also explored the effects of linkage disequilibrium on the detection rate when sexual selection strength was varied (Figure 10) and when environmental variation in the trait was introduced (Figure 11). In both cases, there was not a large amount of variation in detection rates with different levels of linkage disequilibrium. Very low linkage disequilibrium (0.077–0.078, resulting from 1000 initial generations; Figures 10, 11) resulted in reduced detection rates in both cases, as did high levels of linkage disequilibrium (≥0.2, resulting from 50 initial generations or fewer; Figures 10, 11). This further solidifies our choice of 200 initial generations as providing us with a best-case scenario for testing genome-wide selection components analysis.

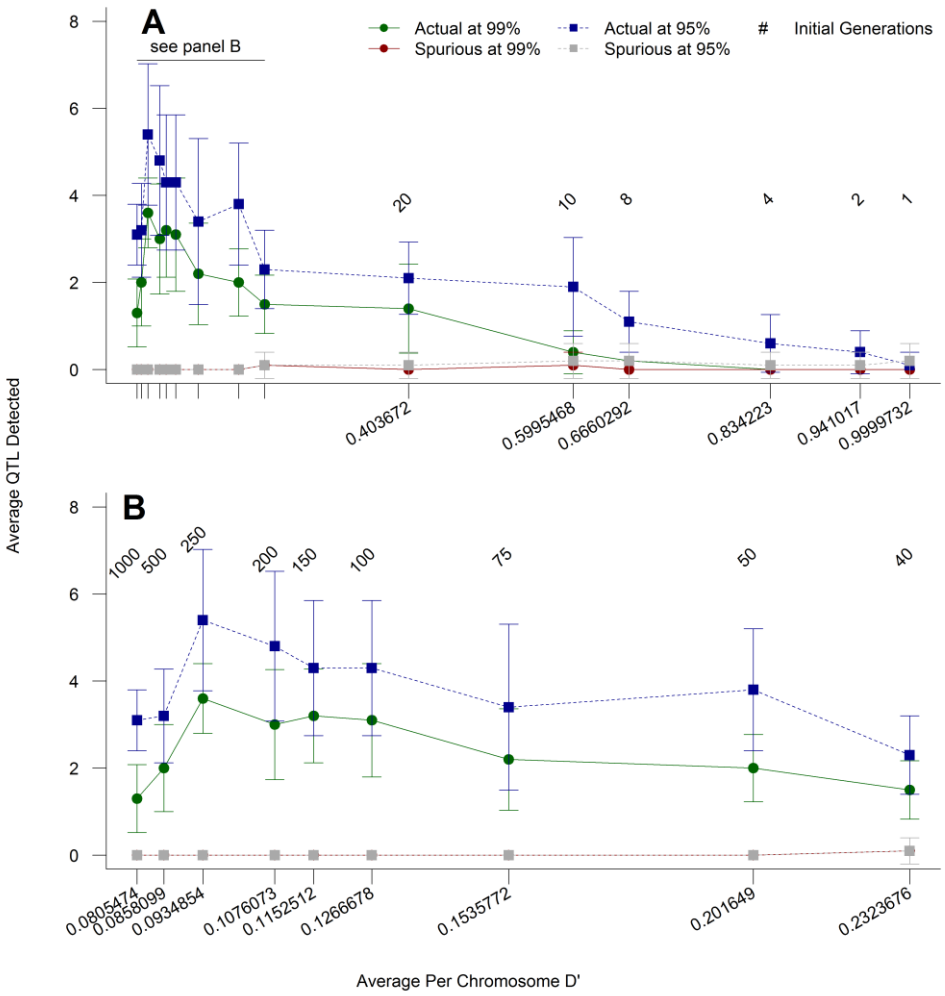

Figure 10. The effect of linkage disequilibrium (determined by the number of initial generations) on the percentage of quantitative trait loci accurately detected and the number of spurious loci called as significant by 99% and 95% genome-wide confidence intervals for weighted F_{ST} values. The measure of linkage disequilibrium presented here is *D'* calculated as a pairwise measure between 100 loci randomly selected from each chromosome and averaged across chromosomes and replicates. Linkage disequilibrium was calculated in the final initial generation, and the number of initial generations was varied to change linkage disequilibrium (initial generation numbers are presented above the points on the graphs). Panel A shows all permutations of the number of initial generations (1, 2, 4, 8, 10, 20, 40, 50, 75, 100, 150, 200, 250, 500, and 1000). Panel B presents a close-up view of generations 40, 50, 75, 100, 150, 200, 250, 500, and 1000 to highlight the changes that occur at low levels of linkage disequilibrium (below 0.3). The model was run with the parameters presented in Table 5. Values presented here are averages from 10 replicates. Bars are the standard error of the mean.

Figure 11. The effects of linkage disequilibrium and sexual selection on detection rates. The measure of linkage disequilibrium is *D′*, a pairwise measure of linkage disequilibrium between 100 loci randomly selected from each chromosome and averaged across chromosomes and replicates, calculated in the final initial generation. The number of initial generations was varied to change linkage disequilibrium. Because most of the effects on detection rates occurred at low levels of linkage disequilibrium (below 0.3; Figure 9), we restricted analysis to those measures, which represent 40, 50, 75, 100, 150, 200, 250, 500, and 1000 initial generations. The number of initial generations is presented above the points, and *D′* is presented on the *x*-axis. The model was run with default parameters (Table 5), except for the altered number of initial generations and values of sexual selection in the experimental generations. Values presented are averages from 10 replicates with bars showing the standard error of the mean.

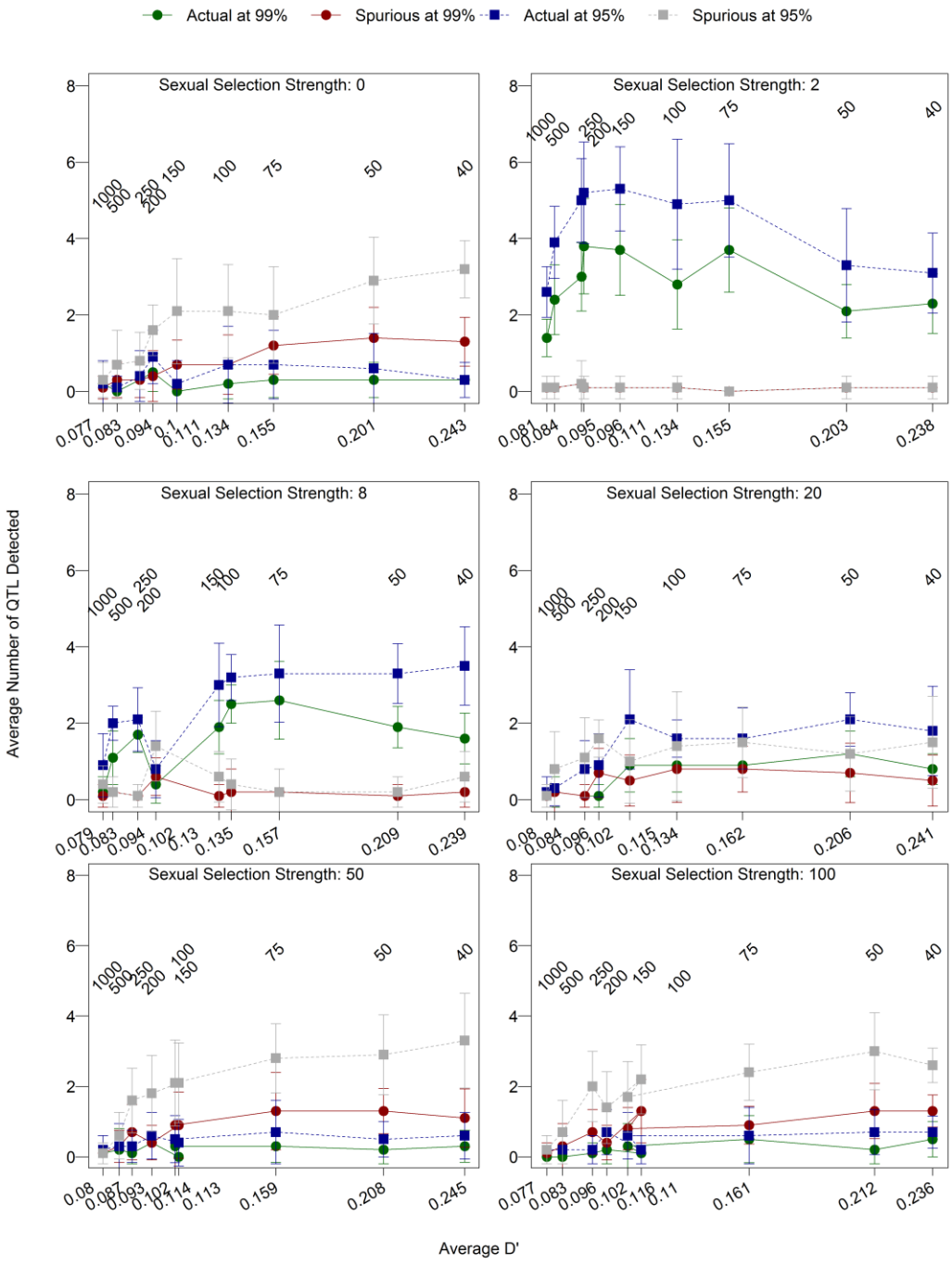
Actual at 99%
Spurious at 99%
Actual at 95%
Spurious at 95%
Sexual Selection Strength: 0
Sexual Selection Strength: 2
Sexual Selection Strength: 8
Sexual Selection Strength: 20
Sexual Selection Strength: 50
Sexual Selection Strength: 100
Average Number of QTL Detected
Average D'

Figure 12. The effect of linkage disequilibrium and environmental variation on detection rates. Linkage disequilibrium, *D′*, was calculated as a pairwise measure between 100 randomly selected loci from each chromosome and averaged across chromosomes in the final initial generation. The number of initial generations is presented above the points, and *D′* is on the *x*-axis. We ran the model with default parameters (Table 5), except for the number of initial generations and environmental variance. We present the average heritabilities generated by various environmental variance settings. Values shown are the means of 10 replicates with standard error bars.

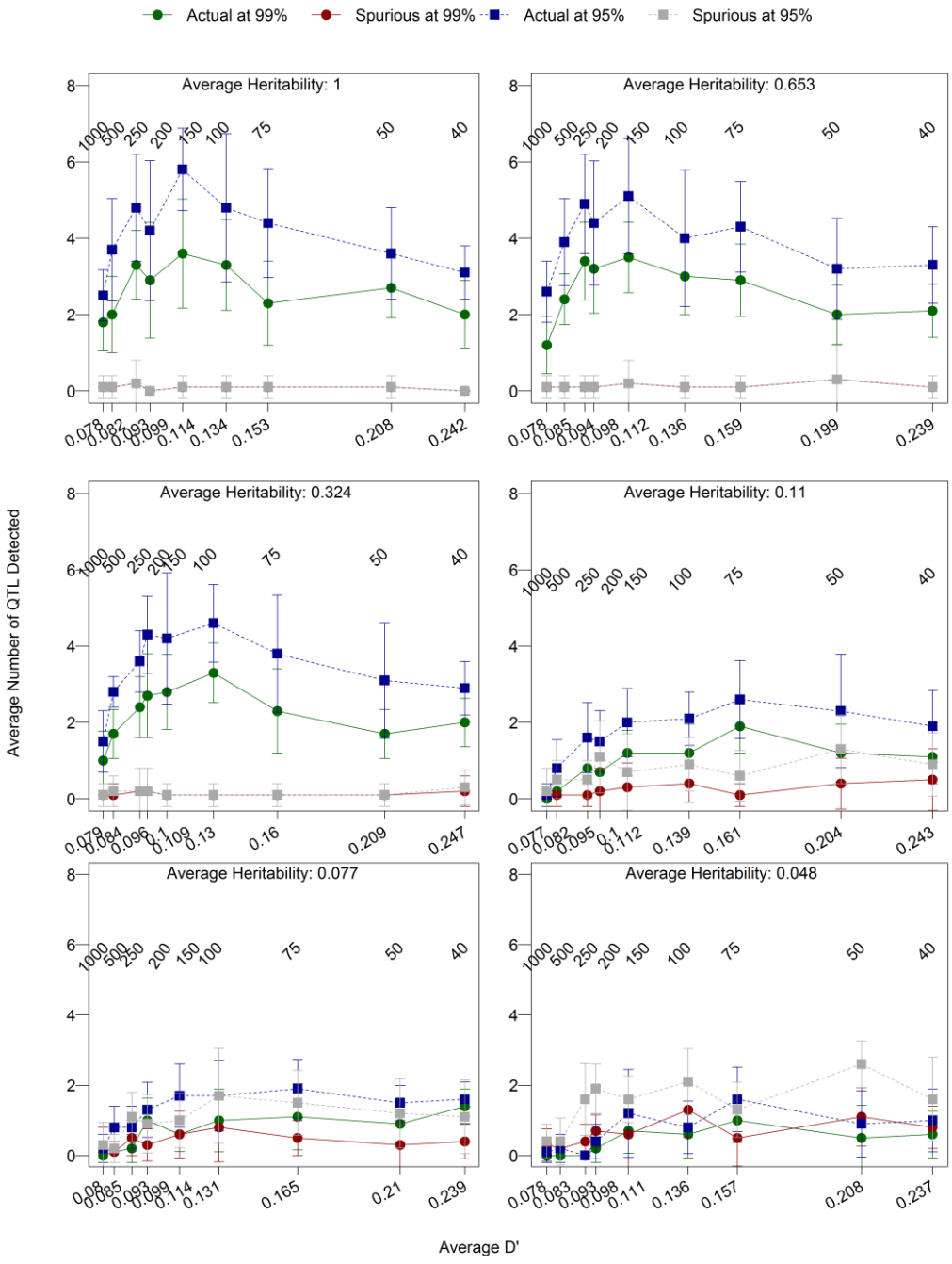
Actual at 99%
Spurious at 99%
Actual at 95%
Spurious at 95%
Average Heritability: 1
Average Heritability: 0.653
Average Heritability: 0.324
Average Heritability: 0.11
Average Heritability: 0.077
Average Heritability: 0.048
Average Number of QTL Detected
Average D'

The effects of population size and sample size

Population genetics theory predicts that selection will have a stronger effect in larger populations due to a reduction in the effects of drift (Hartl and Clark 2007). Thus, we tested how well our selection components analysis detected selection in populations of varying sizes (1000, 2500, 5000, and 10,000) with different sample sizes (100, 250, 500, 1000, 2000, and 4000). Sample size and population size both impacted the detection rates, and they appeared to have an interactive effect. The minimum sample size tested, 100 adults and 100 offspring, had a high average number of spurious peaks detected (but this number was still below 1, suggesting that on average fewer than one spurious peak was detected) and a low proportion of peaks detected (only 18.5% at the 99% confidence level, which means that between 1 and 2 of the eight actual quantitative trait loci were detected; Figure 13). This pattern was consistent across population sizes. In other words, regardless of the actual population size, a sample of 100 adults and 100 offspring was barely adequate to detect any quantitative trait loci. However, increasing the sample size improved detection rates dramatically, especially in larger populations. As the population size increased, the mean number of spurious loci fell below the mean detection rate (Figure 13). Large sample sizes alone improved detection rates, but the combination of a large sample with a large population led to high detection rates as well as very low numbers of spurious loci detected.

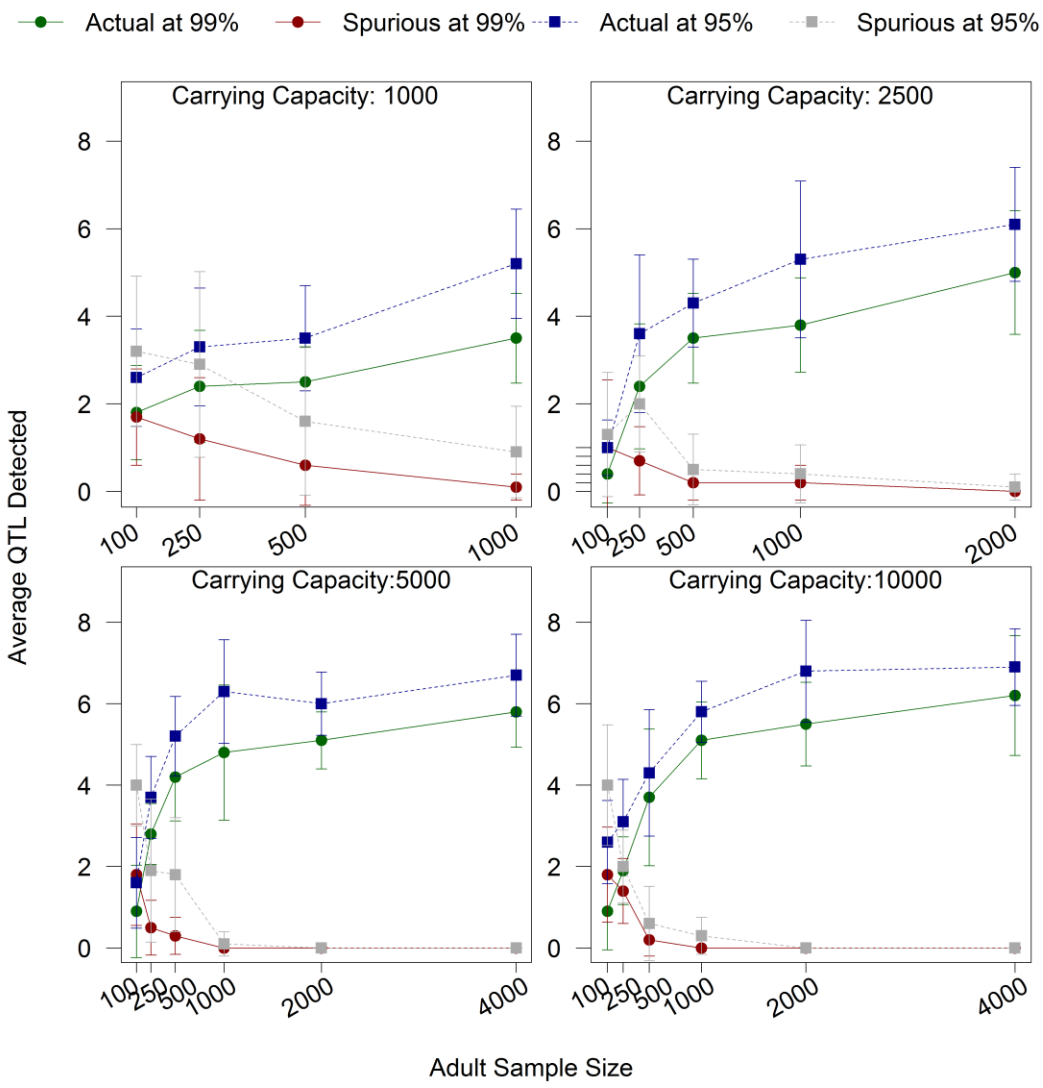

Figure 13. The effect of population size and sample size on detection rates. For each of 10 replicates, the model ran for 200 initial generations followed by one experimental generation. The number of real and spurious peaks detected was averaged across all ten replicates. The carrying capacity and sample size were constant throughout all initial and experimental generations, and the same number of adults and offspring was sampled in the experimental generation. All other parameters were the default parameters shown in Table 5. Bars show the standard error of the mean.

The effects of the number of neutral markers

In this model, the total number of neutral markers could be manipulated by changing the number of chromosomes, changing the number of markers per chromosome, or changing both. We investigated the interaction between the total number of markers (1000, 2000, 4000, and 9000) and chromosome number (1, 2, 4, and 8) on the detection of real and spurious peaks, and two major patterns emerged. First, regardless of how many chromosomes among which the loci were distributed, having more marker loci increased the average proportion of real peaks detected, but also slightly increased the number of spurious loci detected. The number of chromosomes seemed to determine the magnitude of the increase in spurious peaks. Low numbers of neutral markers (1000 and 2000) consistently had low detection rates (Figure 14). However, with the markers distributed across many chromosomes, the detection rate increased dramatically once there were more than 2000 markers. Indeed, with 12,000 markers spread evenly across 8 chromosomes, the quantitative trait locus detection rate was 87.3% at the 99% confidence level and 94.3% at the 95% confidence level, which are some of the highest values we recorded. The average F_{ST}' value for runs with 8 chromosomes was lower than the average F_{ST}' in runs with fewer chromosomes (e.g., with 9000 total neutral loci and eight quantitative trait loci, mean $F_{ST}'_{8\ chrom} = 0.00016$ and mean $F_{ST}'_{1chrom} = 0.00072$). Essentially no spurious peaks were detected (Figure 14) under these parameter combinations. This pattern may be due to the fact that the quantitative trait loci were equally distributed among chromosomes, so with 8

chromosomes and 8 quantitative trait loci, there was exactly 1 quantitative trait locus on each chromosome.

The effects of sample size and number of neutral markers

As the number of neutral markers in our model represents the number of sampled markers in an empirical study, we explored how varying adult sample size and the number of neutral markers affected our results. We found a significant increase in the number of real quantitative trait loci detected when both sample size and the number of neutral markers were increased. When sample size was small (100 or 250 adults), we found an increase in the number of spurious markers detected with increasing number of neutral markers (Figure 15). This suggested that more peaks were likely to be detected, whether they were spurious or not, with an increased number of neutral markers, and that increasing the adult sample size allowed real peaks to be detected, as opposed to spurious peaks. This may be due to the fact that having more neutral markers diluted the effect of outlier F_{ST}' values on the mean background F_{ST}' values, allowing outliers to be even more differentiated from the background when there were more neutral markers.

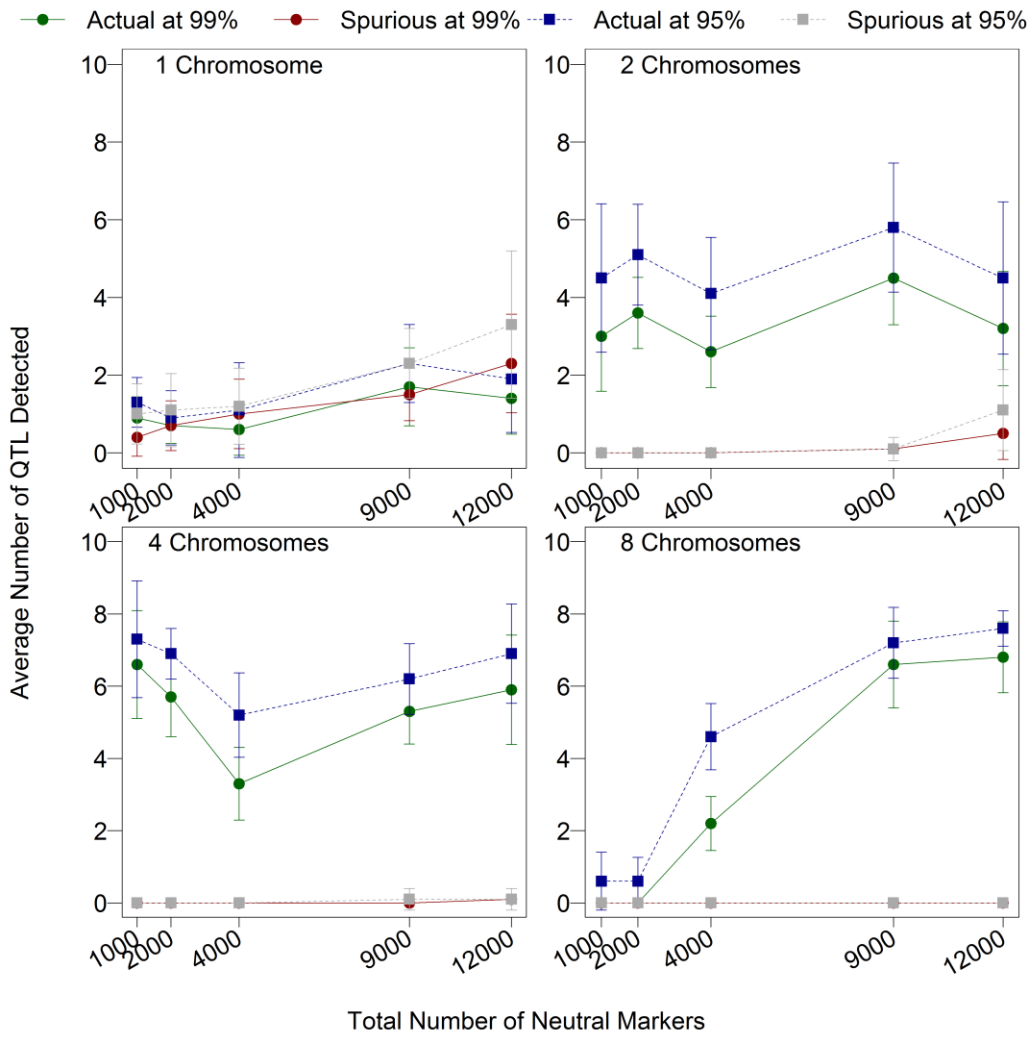

Figure 14. The effect of the number of neutral markers and number of chromosomes on detection rates. These data represent averages from ten replicates, each of which had a carrying capacity of 5000, adult and offspring sample sizes of 4000 each, and ran for an initial 200 generations followed by one experimental generation. A constant number of 8 quantitative trait loci were distributed equally across the chromosomes (so with 4 chromosomes, there were 2 quantitative trait loci on each, but the location of each quantitative trait locus on the chromosome was randomly chosen). Other than the number of chromosomes and the number of neutral markers, all other parameters were set to the defaults (Table 5). Bars indicate the standard error of the mean.

Figure 15. The effect of sample size and the number of neutral markers on detection rates. Each panel is a different sample size. The offspring sample size was set to be equal to adult sample size in each case. The neutral markers were distributed evenly across four chromosomes, each of which contained two quantitative trait loci. Besides sample size and the number of neutral markers, all other parameters were set to the defaults (Table 5). The values presented here are means from 10 replicates with standard error bars.

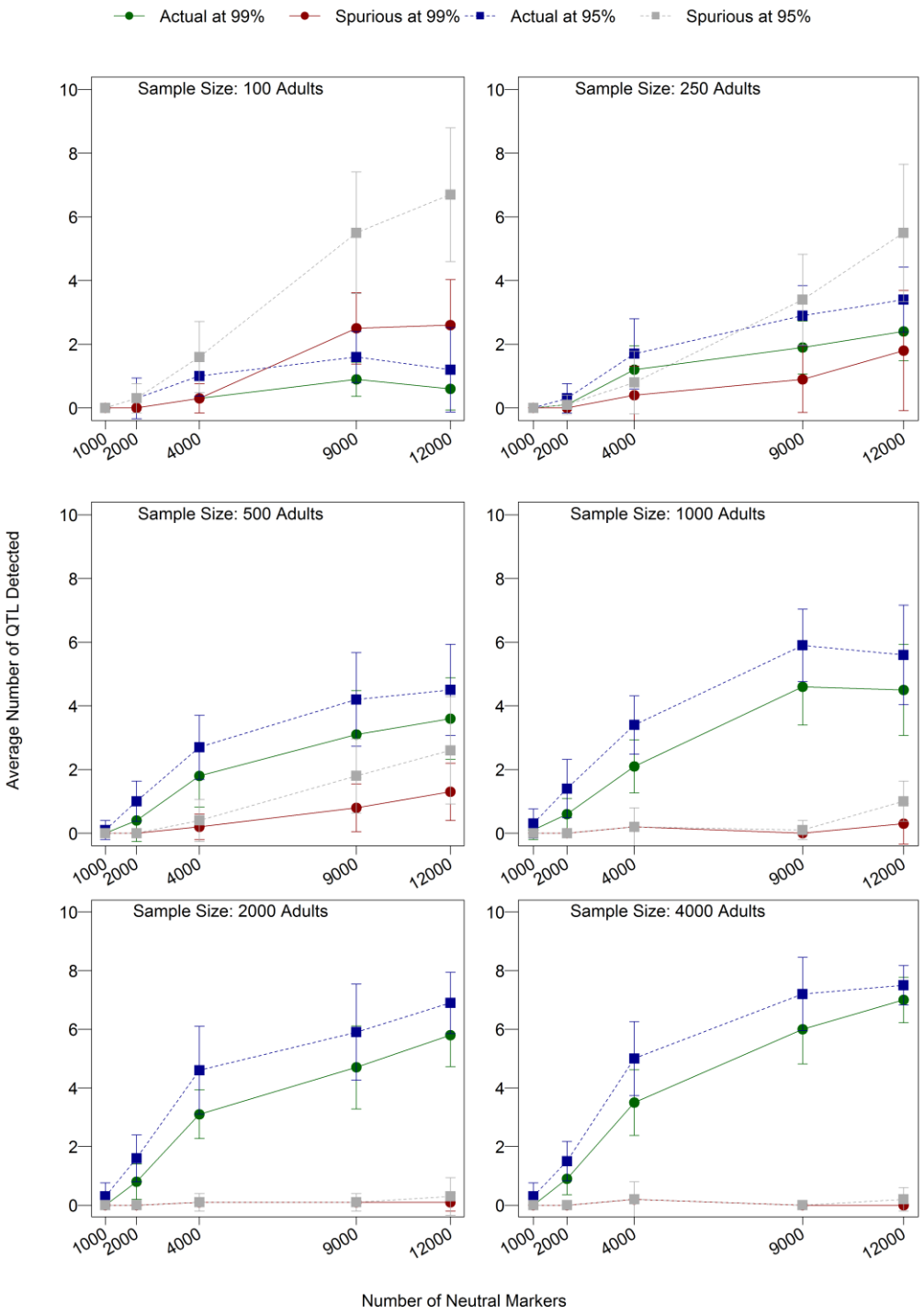
Actual at 99%
Spurious at 99%
Actual at 95%
Spurious at 95%
Sample Size: 100 Adults
Sample Size: 250 Adults
Sample Size: 500 Adults
Sample Size: 1000 Adults
Sample Size: 2000 Adults
Sample Size: 4000 Adults
Average Number of QTL Detected
Number of Neutral Markers
0
2
4
6
8
10
1000
2000
4000
9000
12000

The effects of number of quantitative trait loci and strength of selection

The number of quantitative trait loci had a strong effect on the ability to detect real peaks, as we had predicted. The total strength of selection was distributed among all of the quantitative trait loci, so with fewer quantitative trait loci, each locus received a greater portion of the total selection. We tested sexual selection surface widths in the experimental generations (ω_{SE}^2) of 2, 8, 20, 50, 100, and 500 acting on a total of 4, 8, 16, and 32 quantitative trait loci distributed equally on 4 chromosomes. We also included a test with random mating in the experimental generation for comparison. Selection strength was greatest at $\omega_{SE}^2 = 2$ in each case (male $m' \approx 1.2$). The number of quantitative trait loci had a large effect on the detection of selection: When strong selection was acting on a total of 32 quantitative trait loci, only 6.5% real peaks were detected at the 99% confidence level (~2 of the quantitative trait loci), whereas with only 4 quantitative trait loci, 89.5% were detected on average (Figure 16). The improvement in detection rates with few quantitative trait loci when selection was strong came with a cost when selection was weak: The number of spurious peaks detected at low selection strengths and few quantitative trait loci was higher than the number of peaks detected at low selection strengths but many quantitative trait loci (Figure 16). Overall, these results suggested that accurately and reliably detecting selection required that selection acted strongly on phenotypes that were mainly determined by a few quantitative trait loci of major effect. Although this result was unsurprising, as it is well established that population genetics techniques can only detect loci of major effect (Lewontin and

Krakauer 1973; Beaumont and Nichols 1996), it is worth noting that our within-population approach conforms to population genetics expectations.

The effects of environmental variation

The phenotype of an individual was determined by two components: the genotype derived from the quantitative trait loci and environmental effects. We tested how adding environmental variation to individuals' phenotypes affected the reliability of our genome-wide selection components analysis by changing the environmental variance from zero (0, 0.1, 0.5, 1, 2, 8, 12, and 20) and the number of quantitative trait loci underlying the phenotype (4, 8, 16, and 32). Adding a small amount of environmental variance (0.1 or 0.5) did not have a large effect on our ability to detect quantitative trait loci under selection and even led to a slight increase in the proportion of real peaks detected (Figure 17). Once the environmental variance reached values greater than 1, the ability to detect loci under selection declined and the number of spurious loci detected increased (Figure 17). However, the variance in male trait values without added environmental variance was typically between 0 and 1 in this model, so adding a value of up to 20 to the phenotype may not be biologically relevant. Adding perhaps more relevant values (0.1, 0.5, 1, and 2) did not substantially alter the ability to detect selection (Figure 17).

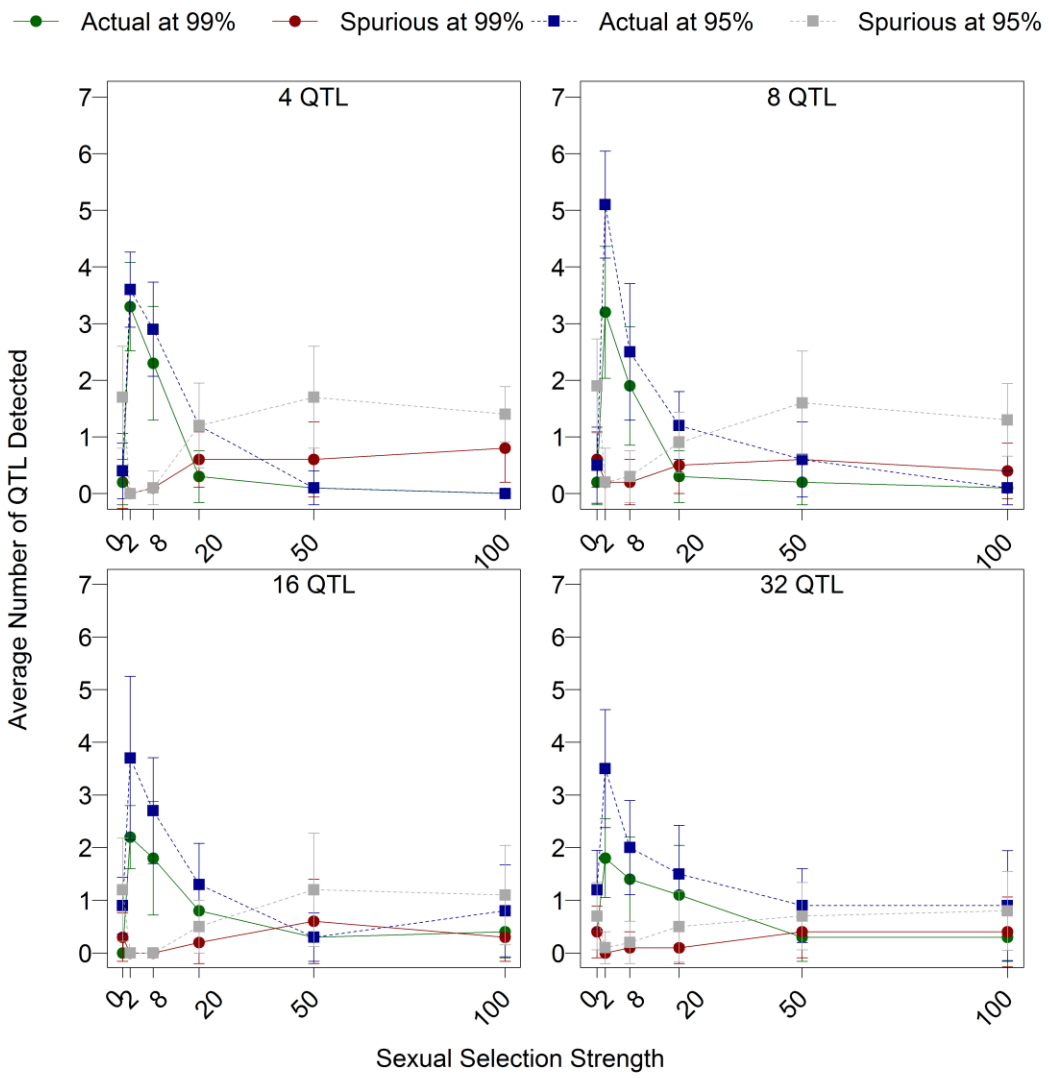

Figure 16. The effect of sexual selection strength and the number of quantitative trait loci on detection rates. We tested random mating and female choice with selection surface widths (ω_{SE}^2) of 2, 8, 20, 50, and 100 during the experimental generation. There was random mating during the initial 200 generations, and these selection strengths were implemented during the experimental generation. The quantitative trait loci were distributed equally among the chromosomes, and the total number of quantitative trait loci tested was 4, 8, 16, and 32. These data are averages and standard errors from the experimental generation of 10 replicates.

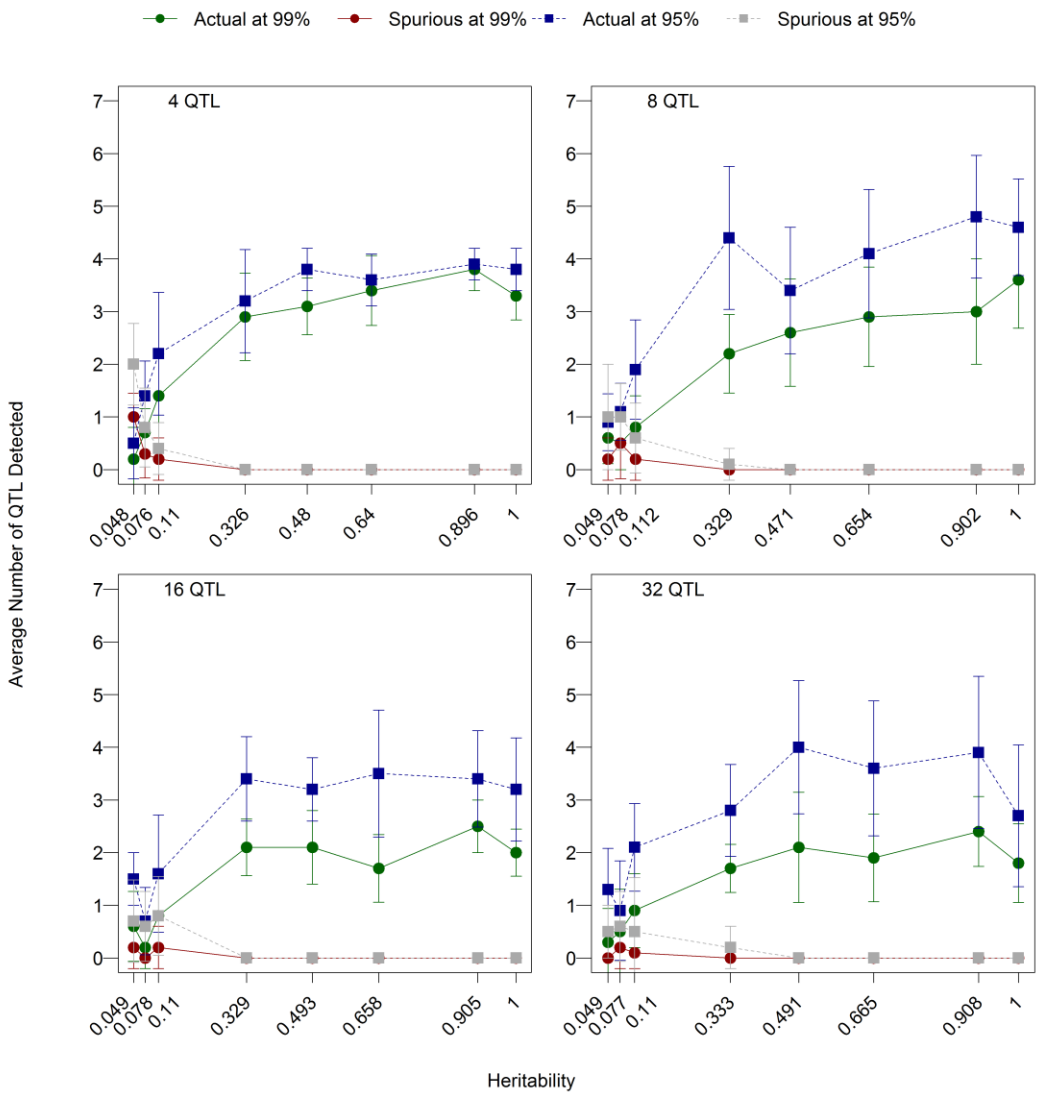

Figure 17. The effects of environmental variation on the ability to detect quantitative trait loci using an outlier F_{ST} approach. Environmental variation was implemented by drawing a number from a normal distribution with variances of 0, 0.1, 0.5, 1, 2, 8, 12, and 20 and adding that value to the phenotype of the individual. We calculated the average heritability from all 10 replicates for each environmental variance and present those values on the *x*-axis, rather than the environmental variances. The environmental variances were tested with 4, 8, 16, and 32 total quantitative trait loci, which were distributed equally among the chromosomes. All other parameters were set to the defaults (Table 5). Error bars are the standard error of the mean.

The number of quantitative trait loci underlying the trait also affected the prospects for detecting selection but buffered the effects of environmental variation; when 32 quantitative trait loci affected the trait, the proportion of quantitative trait loci detected was consistently below 20%, but did not decline significantly with added amounts of environmental variation, and the number of spurious loci detected remained near zero (Figure 17). So although environmental variance added noise to the data, especially when many quantitative trait loci affected the trait of interest, it was still possible to detect some loci under selection even with low heritabilities. Our ability to detect a small subset of quantitative trait loci was likely due to random chance placing a spurious locus near a quantitative trait locus, so it is unclear how these detection rates would translate into empirical studies in natural populations.

Comparing multiple populations

We ran the model on multiple populations that all had the same quantitative trait loci, but that experienced no gene flow, to determine whether comparing even distant populations of the same species might help improve the detection of quantitative trait loci. We found that there was no increase in the reliability of detection (within a population, the average number of real and spurious loci remained the same). However, as predicted, the spurious loci differed between populations, allowing peaks that were at consistent loci to be identified as "real" loci (Figure 18).

Figure 18. Sampling multiple populations can improve the detection of real quantitative trait loci, if the same loci underlie the trait affected by selection. The model was run with 10 replicates, but in each replicate the 8 same quantitative trait loci were designated, rather than being randomly assigned. Thus, each replicate was essentially another population with the same loci under selection, but without gene flow between populations. The model was run with the default parameters (Table 5). Comparing the significant weighted F_{ST} values uncovered in each population, it is obvious that the peaks that reappear in each population are the quantitative trait loci (whose locations are designated by red asterisks). The four chromosomal regions are delineated by different colored backgrounds, and we show two genome-wide confidence intervals (99% and 95%) on the graph.

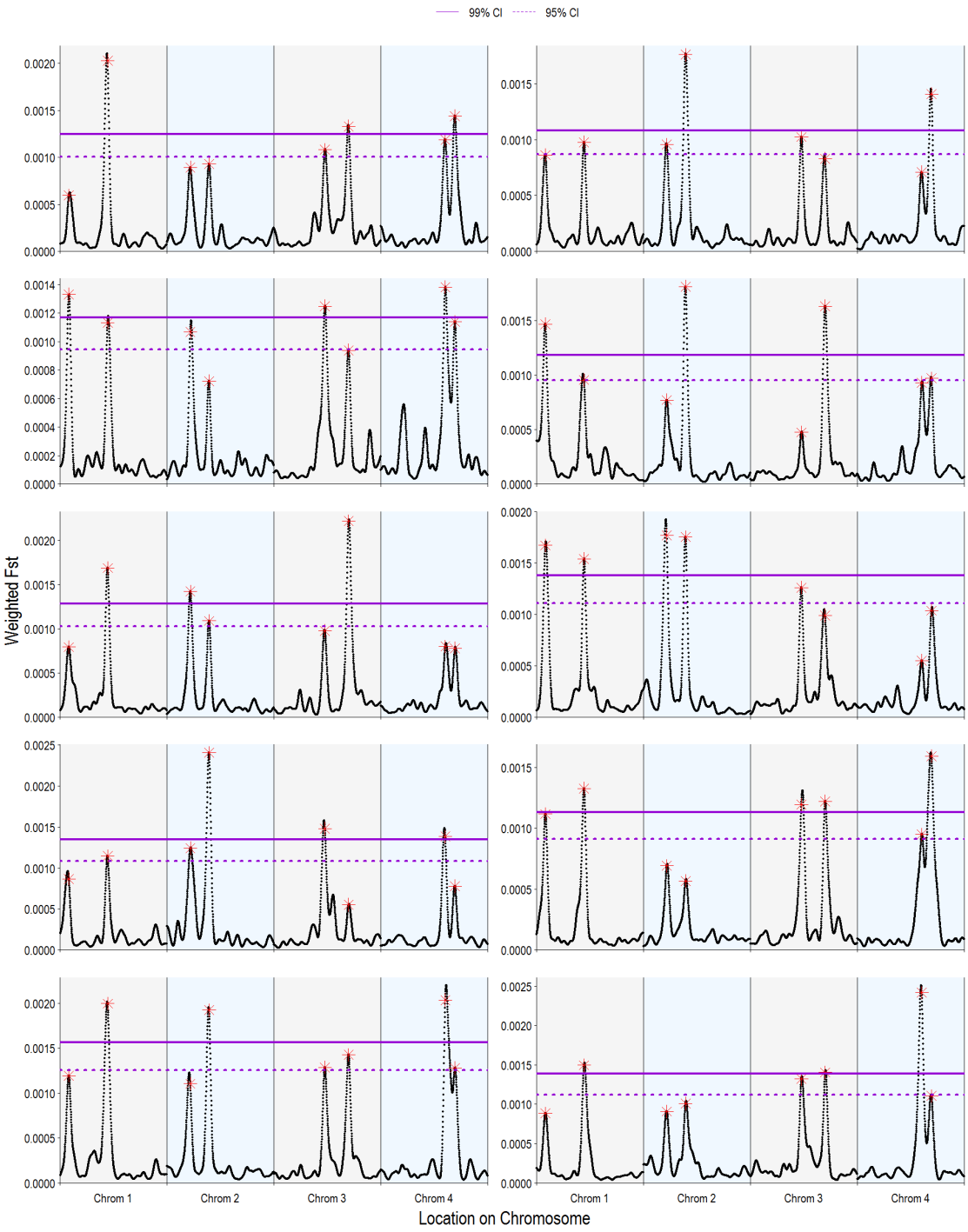
99% CI
95% CI
Weighted Fst
Chrom 1
Chrom 2
Chrom 3
Chrom 4
Location on Chromosome

We also explored whether multiple populations will help identify real quantitative trait loci even when sexual selection was weak. We found that with moderate sexual selection strengths ($\omega_{SE}^2 = 8$ and $\omega_{SE}^2 = 20$), having multiple populations with the same quantitative trait loci helped validate peaks as real, and the locus of each spurious peak was restricted to a single population (Figure 19). In an empirical study, this approach would allow a researcher to focus on those outlier peaks that are present in multiple populations.

When multiple populations were compared at different levels of linkage disequilibrium, the populations generally followed the same patterns. With only a few initial generations (1-2), there were no meaningful genome-wide patterns, as linkage disequilibrium was still nearly 1 (Figure 20). However, as linkage disequilibrium decayed with the addition of more initial generations, loci that were significant in one population were also often significant in others and contained a quantitative trait locus.

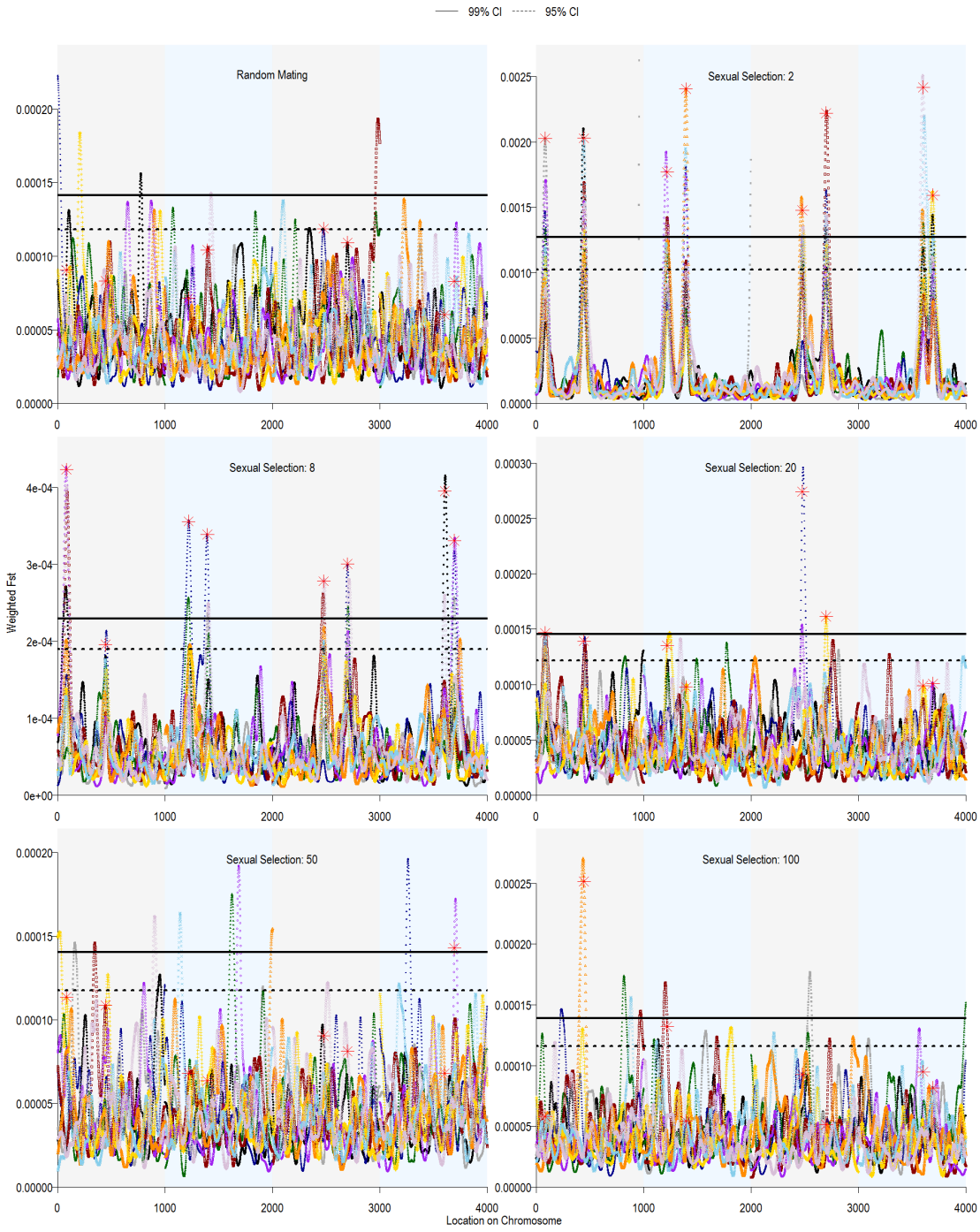

Figure 19. Sampling multiple populations improves the detection of real quantitative trait loci even when selection is weak. Each panel shows 10 replicates for that value of sexual selection strength. Each replicate is given a different color and shape. Both the 95% and 99% genome-wide confidence intervals are shown on the graphs, averaged across replicates.

Figure 20. Detection of real quantitative trait loci is improved by sampling multiple populations at various levels of linkage disequilibrium, *D′*. Each panel shows 10 replicates for each value of *D′*, with a different color and shape for each replicate. Linkage disequilibrium was altered by changing the number of initial generations, and *D′* was calculated as the average per-chromosome pairwise linkage disequilibrium between 100 randomly chosen loci on a chromosome. We show the average 95% and 99% genome-wide confidence intervals.

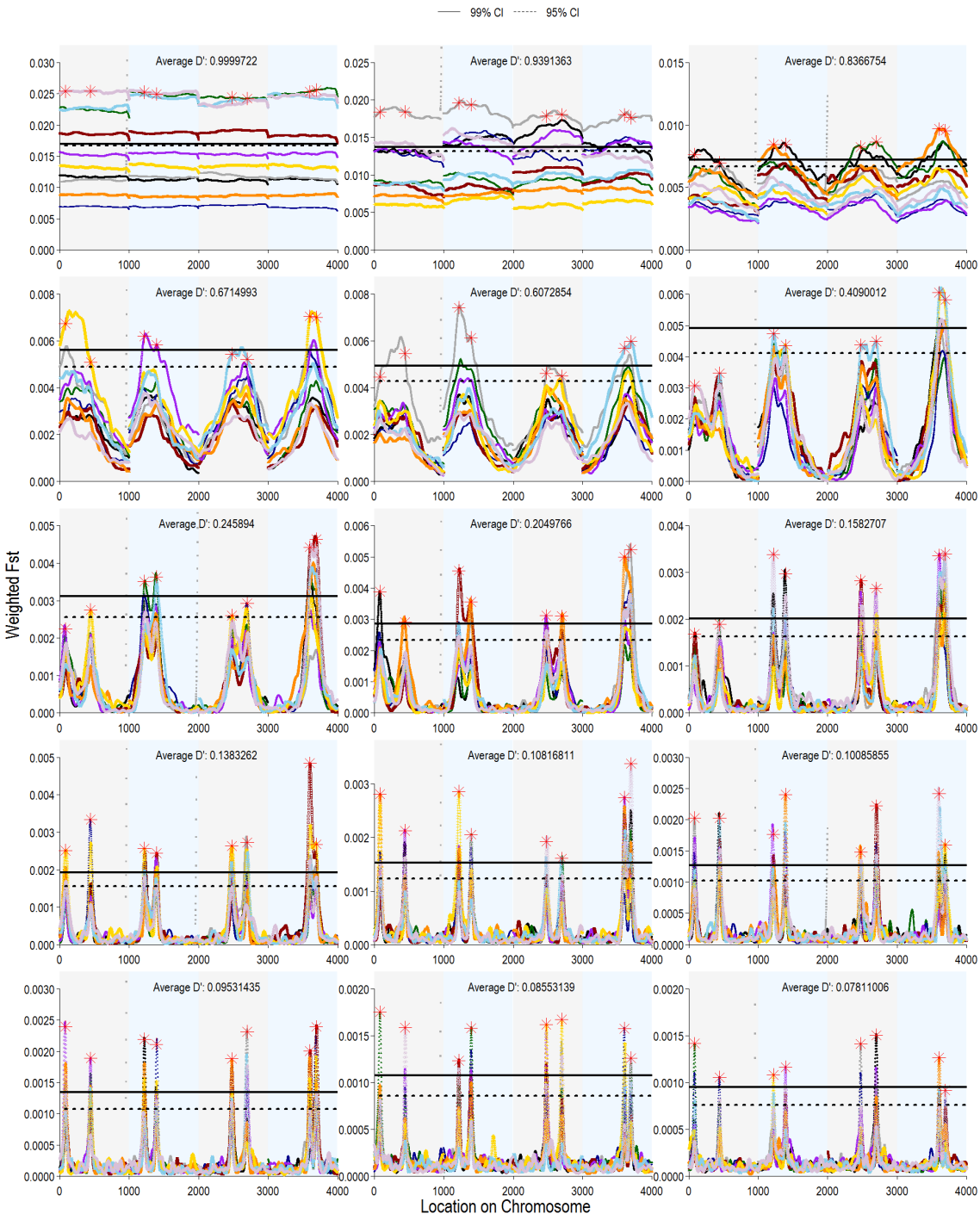
99% CI
95% CI
Average D': 0.9999722
Average D': 0.9391363
Average D': 0.8366754
Average D': 0.6714993
Average D': 0.6072854
Average D': 0.4090012
Average D': 0.245894
Average D': 0.2049766
Average D': 0.1582707
Average D': 0.1383262
Average D': 0.10816811
Average D': 0.10085855
Average D': 0.09531435
Average D': 0.08553139
Average D': 0.07811006
Weighted Fst
Location on Chromosome

Discussion

With this model, we set out to investigate the prospects for detecting a signature of sexual selection by comparing allele frequencies in adults and in offspring from one population using the type of data generated by next-generation sequencing approaches. We found that the genetic architecture of the trait was one of the most important factors determining the ability to detect selection. As expected, more real peaks were detected when fewer quantitative trait loci contributed to variation in the trait. When sexual selection was strong and acted on a phenotype determined by few quantitative trait loci, even small sample sizes (i.e., 100 parent–offspring pairs) could accurately detect some of the real quantitative trait loci without generating prohibitively huge numbers of spurious peaks. Overall, we showed that a genome-wide selection components analysis has the potential to detect signatures of sexual selection within a single population, at least in a best-case scenario with strong sexual selection, few loci of major effect, and optimal linkage disequilibrium.

The results from our simulations suggest that current empirical methods for assessing significance may be unreliable. The Benjamini–Hochberg false discovery rate, in particular, was unpredictable. Although the observed unreliability may be a feature of selection components analysis, this finding is worth noting, as many studies have used the false discovery rate in the analysis of RAD-seq and genome-wide scans (e.g., Hohenlohe et al. 2010a; Helyar et al. 2011; Narum et al. 2013b). Another approach to determining outliers is to compare the overall distribution of F_{ST} values to a distribution from a set of putatively neutral loci from an empirical dataset to identify outlier loci

(e.g., Lotterhos and Whitlock 2014). This approach requires a way to know which loci are likely to be neutral, however, and so is less versatile and may be more difficult to apply in RAD-seq studies of nonmodel organisms. We instead suggest that using the very simple measure of genome-wide confidence intervals, based on the empirical variance of the smoothed F_{ST} values, would not only be appropriate but also be an accurate and repeatable method for defining cutoff values, as it best excluded spuriously significant loci while catching the majority of real peaks in our model.

Even though the occurrence of spurious loci was rare in our model, spurious peaks occurred occasionally. In empirical studies, identifying which significant peaks are real and which are spurious may be challenging, but our results suggest that comparing multiple populations could help differentiate between real and spurious peaks. Even when genome scans are utilized to identify candidate regions that will later undergo further screening, it would be preferable to reduce the number of spurious loci detected to save time and resources. Although spurious loci occurred occasionally in our model, with multiple populations it was possible to identify the real peaks as those that occur consistently in all populations. Screening for peaks in multiple populations helped identify peaks when sexual selection was weak. This observation is consistent with recent evidence from empirical work that spurious loci should not be repeatable between populations or replicates. For instance, Tobler et al. (2014) showed that comparing replicates of laboratory-reared populations of *Drosophila melanogaster* was a very effective way to filter out false positives when looking for single nucleotide polymorphisms that responded to artificial selection regimes.

Environmental variation is expected to contribute to quantitative traits in real-world settings. We included environmental variation in our model and found encouraging results. Although large amounts of environmental variation dramatically reduced quantitative trait locus detection rates and increased the number of spurious loci, small amounts of environmental variation had very little effect on the detection of selection, even with many quantitative trait loci contributing to the trait. These small amounts of environmental variation (up to an environmental variance of 8) led to average heritability values within the range of 0.1 to 0.8, which is the range reported in studies with animal models (Visscher et al. 2008), so our genome-wide selection components analysis was robust to biologically relevant amounts of environmental variation.

Genome-wide selection components analysis was most effective at detecting only real peaks and not spurious ones when the sample size was large (>1000 adults and >1000 offspring). Such large samples may be difficult to collect and also would be very costly to genotype. Fortunately, even small sample sizes identified real quantitative trait loci, at least when sexual selection was strong, with little change in the average number of spurious loci detected: In a large population (carrying capacity = 10,000), sampling 100 adults and 100 offspring identified on average 14.5% of the quantitative trait loci (at least one real peak), but only detected 0.228 spurious peaks (less than one spurious peak, on average). If 100 parent–offspring pairs were sampled from each of two distant populations (assuming both populations had the same genetic architecture of the trait and similar selection pressures), then a real peak could be identified. This plan would not be

logistically prohibitive, especially if other population genomics questions could be answered in the comparison of the two populations. Additionally, as many population genomics studies aim to identify candidate regions, it may be reasonable to use a less stringent cutoff than we used here (e.g., 90% instead of 99% confidence intervals), and increase the number of both real and spurious peaks detected.

Empirical work suggests that most quantitative traits in several model organisms appear to have many underlying quantitative trait loci of small effect (Flint and Mackay 2009). Our model's ability to detect signatures of sexual selection was negatively impacted by an increase in the number of quantitative trait loci, which suggests that there may be limitations to the applicability of this method. However, we observed that a larger number of neutral markers included in our model increased detection rates of real peaks, suggesting that scanning a larger number of neutral markers may improve the ability to detect quantitative trait loci of smaller effect. Thus, genome-wide selection components analysis may indeed be able to capture signatures of selection on traits that are determined by many loci of small effect.

If researchers want to apply genome-wide selection components analysis to natural populations, we can provide several recommendations. First, this analysis was most effective in populations experiencing strong sexual selection, so it would be best applied to a species with clear evidence that sexual selection is occurring. Additionally, although larger sample sizes are always better, small sample sizes had the most spurious loci when the carrying capacity was small. Therefore, if the species of interest is known to have a small population size (as might be the case in some endangered species),

investing in more comprehensive sampling may be especially worthwhile (although sampling may be invasive and could raise additional conservation concerns). Finally, it is important to note that we detected signatures of selection with this model and did not necessarily identify the exact locus underlying the trait. When we identified peaks as "real," the quantitative trait locus had to be within 50 loci in either direction from the peak F_{ST}' value. We tested different distances (peak detection widths, Figure 9) and found that any distance greater than 2 loci up to 100 loci had generally equivalent detection rates. In empirical work, the quantitative trait locus would be unknown, so additional work will probably be necessary in most cases to identify the actual DNA-level variant affecting fitness.

Caveats

Several factors beyond the scope of this paper could affect genome-wide selection components analysis. First, our model of genetic architecture was not realistic in every way. For example, we did not incorporate variable recombination rates, although these are likely to occur in natural populations and could play a very important role in the effects of selection on the genetic architecture. It would be interesting to investigate how different patterns of recombination within the genome might affect selection components analysis. This could be done, for example, by making use of the *Drosophila* Genetic Reference Panel (Mackay et al. 2012; Huang et al. 2014), which encapsulates real patterns of recombination. Additionally, we allocated the same number of quantitative trait loci to each chromosome, which is an unlikely genetic architecture for a trait, and which may affect the ability of selection components analysis to identify

real quantitative trait loci. Lastly, we implemented a contrived setup of our population to generate sufficient genetic variation before selection was imposed. We have also restricted our analysis to loci with relatively high minor allele frequencies in the population, even though quantitative trait loci could have small minor allele frequencies. A more realistic model might use coalescent simulations to generate uneven allele frequencies more commonly seen in the wild.

Additionally, viability selection was present in our model only to control the levels of additive genetic variation, so the model was not set up to address how strong viability selection might affect the power of selection components analysis, with or without strong sexual selection. However, investigating trade-offs between the strength of sexual and viability selection could be very interesting for further research. Also of interest would be the degree of the trade-off between natural and sexual selection. We set our natural selection optimum to 0 and sexual selection optimum to 4, so that trait values would be restrained. Testing different values of both optima could be very interesting and could result in intriguing changes at the genomic level. Similarly beyond the scope of this paper, but of great interest, is how genome-wide selection components analysis might be affected by viability selection on a trait separate from the target of sexual selection; that is, if sexual selection and viability selection both affected males, but acted on different traits with different genetic architectures.

In our model, the initial generations set up the population with genetic variation upon which sexual selection could act, so we did not model a long history of sexual selection in our simulated populations. Therefore, we could only address the case where

sexual selection has been recently introduced to a system or where genetic variation is somehow maintained in the presence of strong sexual selection. We also did not investigate different types of mating systems, or those in which there are other costs to mating. We incorporated a cost of female choice (if females did not find an acceptable mate after sampling 50 males, they did not mate), but the impact of this parameter was not addressed in our analysis. There could be subtle effects of these details of the mating system on the detection of selection at the genomic level, but addressing how mating system parameters affect genome-wide selection components analysis is beyond the scope of this paper.

Although F_{ST} has been used as a measure of differentiation and population structure between populations, there is some murkiness surrounding its application between life stages within a population. More population genetics theoretical work is needed to evaluate whether there are any confounding factors in applying F_{ST} within a generation. Additionally, F_{ST} is sensitive to other modes of selection (e.g., background or positive selection), so it is possible that these forces may confound the effects of sexual selection. Although ideally we would be able to follow genotypes over multiple generations, F_{ST} is the most convenient summary statistic at this time. We believe that applying genome-wide selection components analysis using F_{ST} statistics to capture differentiation between life stages is the best method currently available, but that the same principle could be applied as genomics statistics are improved and refined.

In addition to these factors that we could not test with our model, our model is different from empirical studies in several ways. Importantly, empirical genomics studies would

be affected by sources of error such as sampling bias and sequencing errors. We chose not to include these factors in our model, as these are problems that plague all current population genomics studies and have been evaluated by other researchers (Arnold et al. 2013; Davey et al. 2013; Gautier et al. 2013). Finally, what we present here can be called a best-case scenario, in which sexual selection is recent and strong, linkage disequilibrium and genetic variance are at ideal levels, and there are few quantitative trait loci with large effects.

Conclusion

In summary, we investigated the potential for genome-wide selection components analysis to detect signatures of sexual selection using an individual-based simulation model, in which allele frequencies in adults and offspring from a single population were compared. We were able to accurately detect some or most of the quantitative trait loci underlying the trait under selection, even when sample sizes were low or the trait was highly polygenic. However, selection must be very strong and there must only be few loci of major effect for a high detection rate to occur. Implementation of this method in studies of natural populations could provide another tool to identify genomic regions that are affected by sexual selection, leading to a better understanding of how selection affects the phenotype and results in the heritable changes that allow evolutionary change in natural populations.

CHAPTER IV

GENOME-WIDE SELECTION COMPONENTS ANALYSIS IN A SEX-ROLE-REVERSED PIPEFISH

Overview

A major goal of evolutionary biology has been to identify the genome-level targets of natural and sexual selection. With the advent of next-generation sequencing, whole-genome selection components analysis provides a promising avenue in the search for loci affected by selection in nature. Here, we implement a genome-wide selection components analysis in the sex-role-reversed Gulf pipefish, *Syngnathus scovelli.* Our approach involves a double-digest restriction-site associated DNA sequencing (ddRADseq) technique, applied to adult females, non-pregnant males, pregnant males and their offspring. A comparison of allele frequencies among these groups reveals 180 genomic regions putatively experiencing sexual selection, as well as 271 regions showing a signature of differential viability selection between males and females. Our ddRADseq dataset displays an error rate of approximately 10 percent, which is similar to previously reported error rates for reduced representation sequencing studies. We discuss some potential pitfalls of implementing selection components analysis with current sequencing technologies. Ultimately, we conclude that genome-wide selection components analysis can be a useful tool to complement other approaches in the effort to pinpoint genome-level targets of selection in the wild.

Introduction

A major goal in evolutionary biology is to understand the effects of selection on the genome (Nielsen 2005). The proliferation of next-generation sequencing has made this topic an even more active target of research, as population genomics approaches are becoming increasingly feasible in non-model systems. One common approach to study the effects of selection in wild populations is to compare allele frequencies among populations and identify genomic regions that show too much or too little divergence to be explained by genetic drift alone (reviewed in Hohenlohe et al. 2010). However, among-population studies have limitations, because they require samples from multiple populations, perform well under only certain patterns of migration, and cannot diagnose the type of selection contributing to divergence unless specific traits under selection are known (Leinonen et al. 2006).

Selection in nature can be divided into multiple episodes, including viability selection, sexual selection, and possibly other forms of selection, such as meiotic drive. Episodes of selection can provide valuable insights into important aspects of a species' biology, such as mating systems (Emlen and Oring 1977), ecology (Loehle and Pechmann 1988), and conservation-related attributes (Stockwell et al. 2003). In the context of how selection affects the genome, it would be useful to link empirical work to quantitative genetics theory. Quantitative genetics theory often isolates or focuses on individual episodes of selection (Arnold and Wade 1984b; Arnold and Wade 1984a), so using a tool to identify the genomic signature of selection at different episodes would be ideal. Genome-wide selection components analysis partitions the genomic effects of

selection episodes (Flanagan and Jones 2015; Monnahan et al. 2015) and so could be the solution to linking empirical genomics work and quantitative genetics theory.

Selection components analysis is conceptually simple in that it compares allele frequencies among individuals at various stages in the life cycle to infer the components of total selection that are causing allele frequency changes across the lifecycle. The original implementation of selection components analysis used a maximum-likelihood approach to test sequential hypotheses regarding gametic selection, sexual selection, and viability selection (Christiansen and Frydenberg 1973). More recently, selection components analysis has been revisited with next-generation sequencing data. A maximum-likelihood approach has been developed to apply selection components analysis to genomic datasets (Monnahan et al. 2015), and an F_{ST}-outlier-based approach has also been proposed to detect components of selection across the genome (Flanagan and Jones 2015). In each of these cases, many individuals from a single population must be sampled, and the sample must contain adults and very young offspring. The method works best when one of the parents (either the mother or the father) can be matched with its offspring, so that each parent can be compared to its offspring to infer the allele contributed by the unknown parent (Table 8). Such a dataset allows sexual selection on the courting sex to be evaluated and facilitates all of the other comparisons to infer selection listed in Table 8.

Table 8. The comparisons that allow signatures of gametic, sexual, and viability selection to be inferred from genetic data. In parentheses are the groups that we used in the population of pipefish we investigated here. The final column describes the method of comparison we used in this study to address each episode of selection.

Group 1	Group 2	Type of selection	Mode of Comparison
Heterozygosity in parents and offspring (Mated pipefish males)	Offspring	Chooser gametic	None
Parent-offspring combination (Inferred pipefish female allele)	Adult courters (Adult pipefish females)	Sexual selection	F_{ST}
Mated choosers (Mated pipefish males)	Non-mated choosers (Non-mated pipefish males)	Sexual selection	None
Adult Males (All collected pipefish males)	Adult Females (All collected pipefish females)	Sex-biased viability	F_{ST}
Adults (All collected pipefish males and females)	Offspring (One offspring per pregnant male pouch)	Viability, Multiple episodes	F_{ST}

An ideal species in which to evaluate the signature of selection on the genome using selection components analysis has two main characteristics: (1) the offspring can be collected with one parent and (2) at least one component of selection is known to be strong. The second point is important because current methods are not effective when selection is weak (Flanagan and Jones 2015), and knowledge of which component of selection is likely to be important in the system allows the researcher to approach the study with *a priori* hypotheses. The Gulf pipefish (*Syngnathus scovelli*) fits both of these characteristics. Gulf pipefish exhibit male pregnancy, and males that have mated carry their offspring in a translucent pouch, permitting pregnant males to be collected with their offspring. In addition, female pipefish have been shown to be under strong sexual

selection (Jones et al. 2001), with sexual selection acting on iridescent banding patterns that run dorso-ventrally on their torso (Flanagan et al. 2014).

In this study, we used double-digest restriction-site associated DNA sequencing (ddRADseq) to generate genome-wide single-nucleotide polymorphism (SNP) data for a single population of Gulf pipefish and implemented a genome-wide selection components analysis (Table 8). We used the F_{ST}-outlier genome-wide selection components analysis approach to characterize the signature of sexual selection by comparing allele frequencies in females and the inferred maternal allele deduced from the father-offspring pairs. We also compared allele frequencies in males and females to establish whether viability selection acts differently on the sexes. Finally, we compared offspring genotypes to adult genotypes. If the population is at equilibrium and is not experiencing other forms of selection, differences in allele frequencies between adults and offspring are generally interpreted as viability selection (Christiansen and Frydenberg 1973). However, assuming other forms of selection are affecting the population, differences in allele frequencies between adults and offspring can be attributed to multiple evolutionary forces, including the three forms of selection listed above (Monnahan et al. 2015) as well as genetic drift (Flanagan and Jones 2015). Therefore, the adult-offspring comparison is best considered as a summary of the evolutionary forces affecting the population. We demonstrate that genome-wide selection components analysis can identify signatures of multiple forms of selection within a wild population of pipefish, and that those signatures span the entire genome.

Methods

Sample collection

Gulf pipefish were collected from a single continuous seagrass bed approximately 30 meters long and 5 meters wide in Corpus Christi, TX, in September 2011. By pulling a seine net through seagrass beds, we captured 57 females, 160 pregnant males, and 11 non-pregnant males. Each individual was euthanized with MS-222, photographed, and stored in ethanol at -20°C. Embryos were removed from the pouches of pregnant males.

RAD-seq library preparation

DNA was extracted from adult head tissues and from entire embryos using the PureGene DNA extraction kit (QIAGEN). Genomic DNA quality was evaluated by visualizing each sample on an agarose gel and each sample was quantified using a Qubit Fluorometer 2.0 (Life Technologies).

Double-digest restriction-site associated DNA sequencing (ddRAD-seq) was completed following the methods of Peterson et al. (2012) with several modifications. Briefly, we used 100 units of *PstI*-HF (New England Biolabs) and 25 units of *MboI* (New England Biolabs) to fragment 1µg of genomic DNA per individual in a 37°C incubation lasting 3 hours. Following purification by AMPure XP beads (Agilent), T4 ligase (Epicentre) was used to ligate 250ng of each DNA sample to a unique adapter containing a 6-bp barcode and the Illumina sequencing primers to the DNA fragments in a 23°C incubation lasting 30 minutes followed by a 10 minute 65°C heat shock. These adapters were identical to those used in single-digest RAD protocols (Miller et al. 2007;

Baird et al. 2008). Ninety-six unique barcodes were used so that ligated DNA fragments from 96 individuals could be pooled following an AMPure XP bead (Agilent) purification to form a single ddRAD-seq library. Fragments in the range of 300-500 bp were extracted from a 1% agarose gel stained with SafeView (ABMGood) and amplified by twelve rounds of PCRs (cycle conditions: 98°C for 30s; 12 cycles of 98°C for 10s, 60°C for 30s, 72°C for 10s; 72°C for 5min) using Phusion polymerase (New England Biolabs). Four separate rounds of PCR on the size-selected library were pooled and cleaned with AMPure XP beads (Agilent). Library quality was evaluated by visualizing DNA on a gel and quantifying it with a Qubit Fluorometer 2.0 (Invitrogen). A total of four libraries were sent to the University of Oregon Genomics Core Facility for single-end Illumina HiSeq 2000 sequencing.

Processing of raw reads and genotyping

Raw reads were filtered for quality and grouped by barcode using the Stacks v. 1.29 function process_radtags (Catchen et al. 2011; Catchen et al. 2013b). Bowtie 2.0 (Langmead and Salzberg 2012) was used to map the filtered reads to a draft *S. scovelli* genome assembly (pers. comm. William Cresko), using the default 'sensitive' parameters (--sensitive). A catalog of RAD loci was created and individuals were genotyped using the ref_map.pl program in Stacks v1.37 (Catchen et al. 2011; Catchen et al. 2013b). A minimum of three reads was required to report a stack in the catalog-building process, and two mismatches were allowed between loci when assembly the catalog. To call SNPs, Stacks uses a multinomial-based likelihood model, which incorporates a bounded error rate and calculates the likelihood of the two most

frequently observed nucleotides at each SNP location (Catchen et al. 2013b). The populations module in Stacks (Catchen et al. 2013b) was run to generate variant call format files containing loci found in 50% of the individuals and with a minor allele frequency of at least 0.05.

Estimating error rates

Four individuals were included in two different libraries, so we were able to compare the genotypes called for each technical replicate. We calculated the proportion of SNPs missing in both libraries, the proportion of SNPs that were given the same genotype in both libraries, and the proportion of SNPs that were not missing in both but were assigned a different genotype.

Inferring maternal alleles

The genotypes of pregnant males and their offspring were compared at each SNP locus and the maternal allele was inferred based on exclusion using a custom C++ program (available on github). For example, if the father's genotype was TT and the offspring had CT, the mother's allele was inferred to be C. If both the father and the offspring were heterozygous for the same genotype, then no maternal allele could be inferred. Custom R scripts were used to reformat and merge files for further analysis.

Genome-wide selection components analysis

To implement a genome-wide selection components analysis, we needed to compare allele frequencies to identify regions of the genome potentially experiencing sexual and viability selection. A custom C++ program (available on github) calculated summary statistics (allele frequencies, observed and expected heterozygosity) for each

group within the population and for the population as a whole. Expected heterozygosity was calculated from allele frequencies, *p*, as $1 - \sum_{i=1}^{a} p_i^2$ for each locus with *a* alleles. Pairwise F_{ST} was calculated between the following groups: collected females and inferred maternal alleles (females-mothers), males and females (males-females), and collected adults and offspring (adults-offspring). Because very few non-pregnant males were collected, we did not include a pregnant male versus non-pregnant male analysis. F_{ST} was calculated as:

$$F_{ST} = 1 - \frac{\sum_{i=1}^{k} H_{w_i}}{kH_b}$$

where *k* is the number of groups being compared, H_w is the expected heterozygosity within each group, and H_b is the overall expected heterozygosity calculated among all groups lumped into a single population (Nei 1986). Using custom R scripts, we pruned loci to retain SNPs in Hardy-Weinberg equilibrium, SNPs with a major allele frequency between 0.05 and 0.95, and SNPs genotyped in at least 75% of all individuals and in at least 50% of the individuals in their group. Using the pruned loci, the 99% quantiles were calculated so that SNPs in the top 1% of each F_{ST} distribution were designated as outliers.

Annotation of outliers

Outliers were compared among our various pairwise F_{ST} tests to identify SNPs that were outliers in multiple comparisons. Thus, we obtained two sets of outliers for each F_{ST} comparison: unique outliers and shared outliers. Although the goal of selection components analysis is to identify regions unique to each episode of selection, SNPs that

have extreme F_{ST} values in every comparison are probably the most likely candidates to be affected by sexual and natural selection.

To annotate regions of the genome containing outliers, the 2500 bp in either direction of outlier SNPs were extracted from the draft genome assembly. These 5kb regions were compared to the non-redundant nucleotide database using blastx. Gene ontologies were assigned to blastx hits using Blast2Go.

Results

The four ddRADseq libraries resulted in 827,690,623 raw reads, 445,488,822 of which were retained after the filtering steps implemented by process_radtags. Each individual had an average of 1,119,858 reads, and these reads mapped to the reference genome with an average alignment rate of 69.49%. Individuals were genotyped by Stacks and had an average coverage of 9.98X. The populations module of Stacks returned 51,356 SNPs with a minimum allele frequency of 0.05 and that were found in 50% of the individuals.

Four individuals were genotyped twice, in separate RAD libraries. The genotyping calls were compared between these technical replicates to estimate genotyping errors. The mean proportion of SNPs that were genotyped in both replicates but assigned different gentoypes was 0.169 ± 0.099 sd (Table 9).

Table 9. Error rates calculated from technical replicates. Each row represents an individual that was genotyped in two different libraries (Lib. 1 and Lib. 2). The numbers in each cell are proportions of the total number of SNPs, except in "Total Number SNPs". The proportion of SNPs with identical genotype calls are in the first column ("Same Genotype") and the proportion of SNPs that were not genotyped in that individual in both libraries are in the column "Missing in Both". The column "Different Genotypes" refers to SNPs that had a genotype call in both libraries, but the genotype call was different. The proportion that were missing in one library or the other are in "Missing in Lib. 1" and "Missing in Lib. 2", and the sum of those two columns is the column "Missing in Lib. 1 or Lib. 2". The remaining columns ("Genotyped in Lib. 1" and "Genotyped in Lib. 2") are the overall proportions of loci that were genotyped in each library (regardless of whether the genotype call was the same or different in the two libraries).

	Same Genotype	Missing in Both	Different Genotypes	Missing in Lib. 1	Missing in Lib. 2	Missing in Lib. 1 or Lib. 2	Genotyped in Lib. 1	Genotyped in Lib. 2	Total Number SNPs
OFF016	0.543	0.052	0.188	0.096	0.121	0.216	0.852	0.827	47199
OFF027	0.612	0.030	0.194	0.101	0.063	0.164	0.869	0.907	47199
OFF032	0.397	0.064	0.265	0.113	0.161	0.275	0.823	0.775	47199
PRM177	0.562	0.103	0.029	0.081	0.225	0.306	0.816	0.672	47472

Maternal alleles were inferred from 130 pairs of pregnant males and their offspring. Following pruning for Hardy-Weinberg Equilibrium and coverage in the subsets, 28,435 SNPs were retained for the females-mothers F_{ST} comparison, which characterizes sexual selection. These SNPs had a mean F_{ST} of 0.005171 ± 0.000048 (SEM; Figure 21). The females-mothers F_{ST} comparison had 180 unique outlier RAD loci (containing a total of 217 outlier SNPs), distributed on 162 scaffolds. The 5kb regions surrounding the unique outlier SNPs had 109 blastx hits and 92 gene ontology annotations (Supplemental File 4). The outlier SNP regions unique to the females-mothers F_{ST} comparison were the only regions to be involved in ten biological gene ontology categories, including regulation of response to stimulus, intracellular signal transduction, and cell cycle (Figure 22). They also share 10 categories with other comparisons, including animal organ development and anatomical structure morphogenesis, which include unique outlier regions from all three F_{ST} comparisons.

The F_{ST} comparison identifying differential viability selection between males and females used 40,334 SNPs, which had a mean F_{ST} of 0.00470 ± 0.000041. Of the top 1% of F_{ST} values, 271 of those RAD loci (363 outlier SNPs) on 237 scaffolds were unique to the male-female comparison. The 5kb regions surrounding the unique outliers had 193 matches to the non-redundant database, and 159 of those hits had associated gene ontology terms (Supplemental File 5). The unique male-female outliers fall into 11 gene ontology categories that are not found in other comparisons and 11 categories shard with other comparisons (Figure 22).

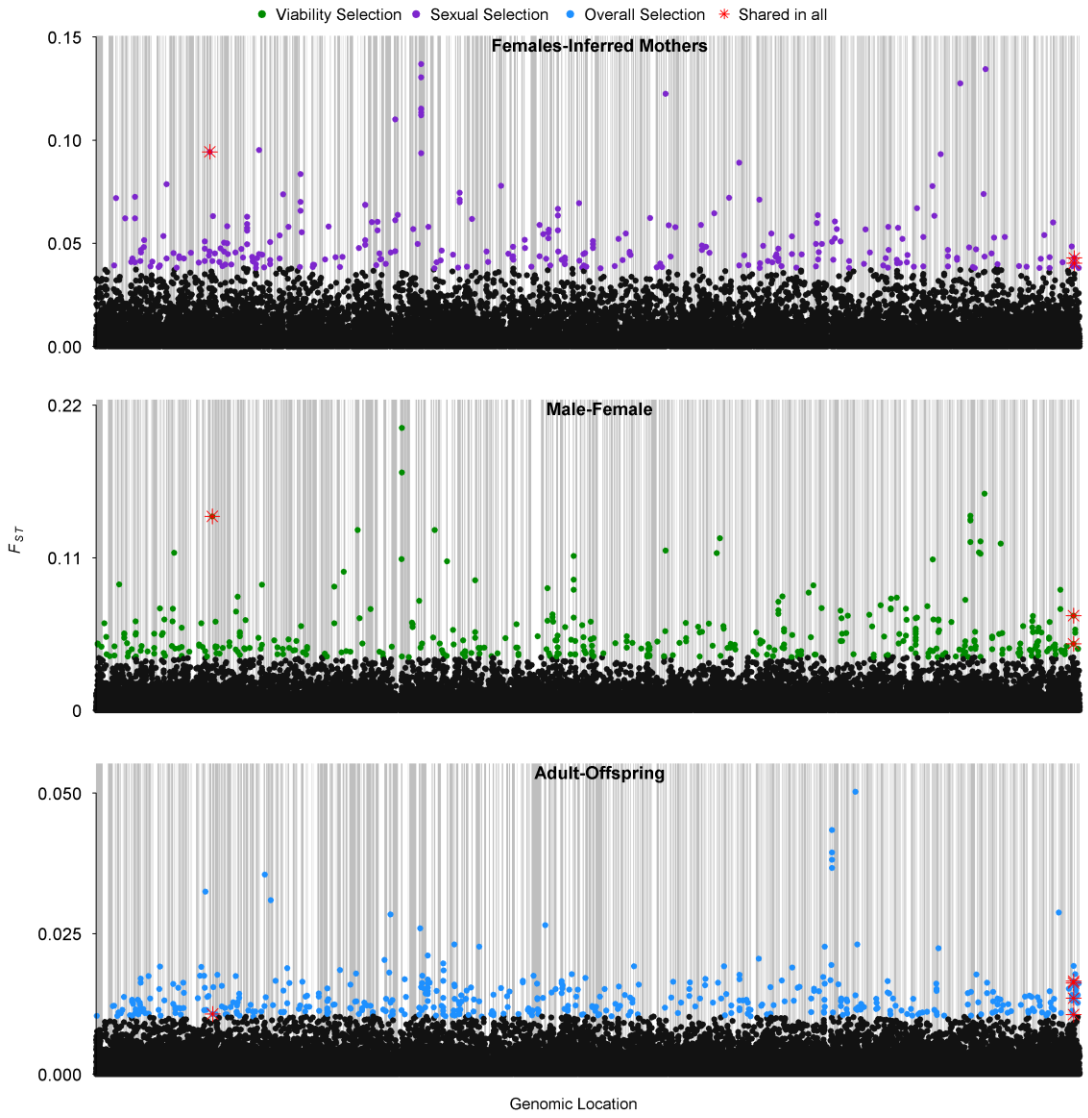

Figure 21. Outlier plots for the three comparisons. The top panel shows the F_{ST} values comparing inferred maternal allele frequencies and allele frequencies in collected females, which represents sexual selection. The middle panel shows the F_{ST} values comparing allele frequencies in males and females, which depicts differential viability selection in the sexes. The bottom panel shows the F_{ST} values comparing the adults and offspring, which summarizes multiple evolutionary forces affecting the population. The dark rectangles in the background delineate different scaffolds in the draft genome. The colored points are those that exceed the 1% threshold. One RAD locus was shared among all three, and the F_{ST} values for SNPs on that locus represented in each comparison are depicted with a red star.

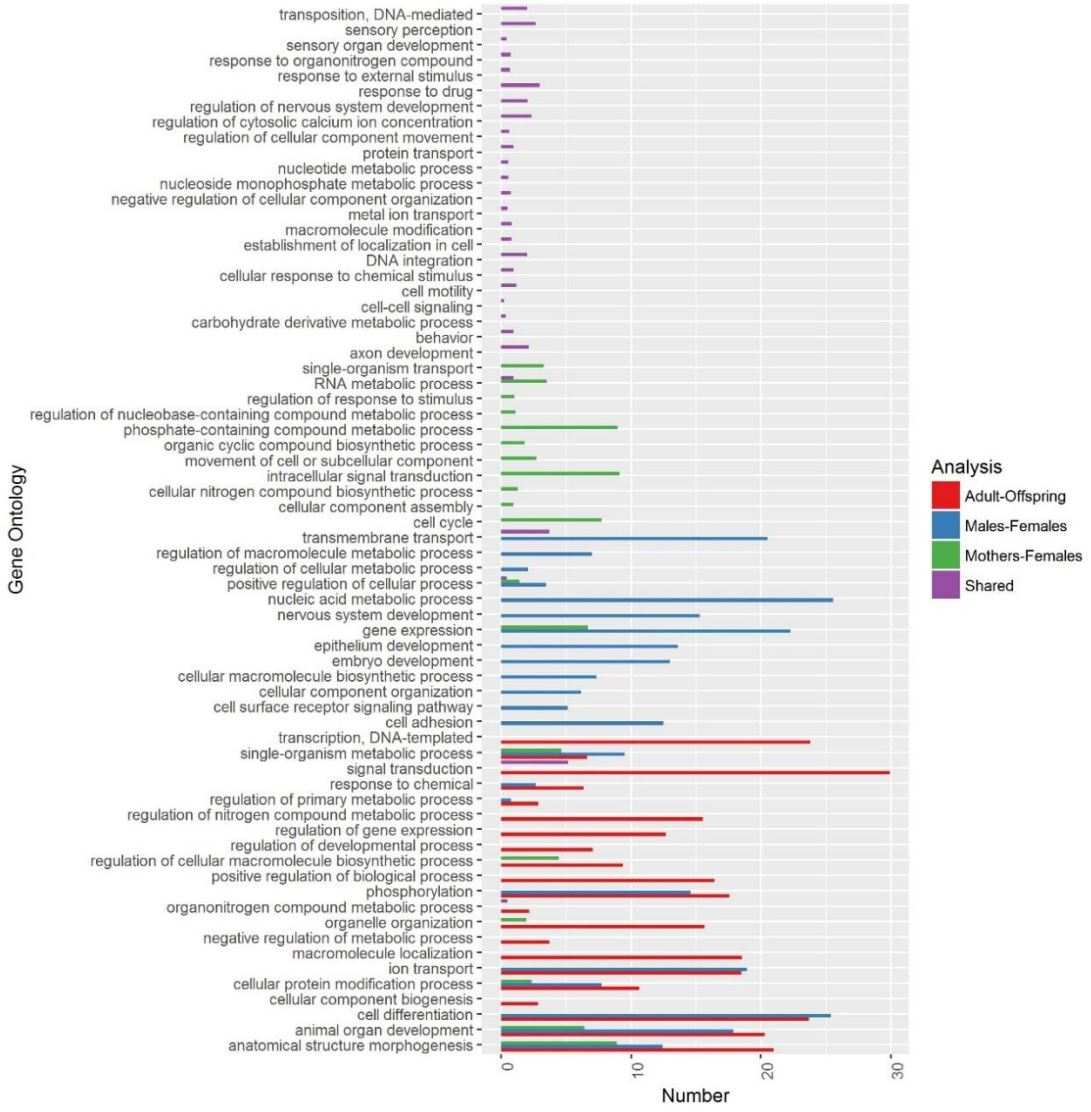

Figure 22. Gene ontologies describing biological functions for the 5kb regions surrounding outlier SNPs unique to each of the three F_{ST} comparisons and outlier SNPs shared by at least two F_{ST} comparisons. The mothers-females comparison includes 92 outlier regions with gene ontology annotations, the males-females comparison has 159, the adults-offspring comparison contains 158, and 44 of the shared outlier regions had gene ontology matches.

The F_{ST} comparison of adults and offspring used 44,937 SNPs with a mean F_{ST} of 0.001372 ± 0.000010. We identified 258 unique RAD loci (comprising 302 outlier SNPs) on 222 scaffolds. The 5kb regions surrounding those outliers had 184 blastx hits, of which 158 could be matched to gene ontology labels (Supplemental File 4). Of the 21 gene ontology categories identified for the unique adult-offspring outlier regions, nine are alone in their gene ontology category (cellular component biogenesis, macromolecule localization, negative regulation of metabolic process, organelle organization, positive regulation of biological process, regulation of cellular macromolecule biosynthetic process, regulation of gene expression, regulation of nitrogen compound metabolic process, and signal transduction; Figure 22).

Two RAD loci, each containing 9 SNPs, had at least one significant SNP in each of the three comparisons (Figure 21). One is located on scaffold_985 and does not have any blast hits within 5kb of the RAD locus, but is within 10kb of *partitioning defective 3 homolog*, characterized in other fish species. The other is located on scaffold_125 and is within 5kb of *macrophage mannose receptor 1-like* and *C-type lectin domain family 4-like* protein sequences. An additional 69 RAD loci, distributed among 67 scaffolds and containing 105 outlier SNPs, were shared in two of the three F_{ST} comparisons ("shared outliers"). Of those, 48 had blastx hits in the 5kb region surrounding the RAD locus, 43 of which matched at least one gene ontology term (Supplemental File 4). The gene ontology categories include sensory perception, sensory organ development, regulation of nervous system development, protein transport, metal ion transport, cell-cell signaling, and behavior (Figure 22).

Discussion

In this study, we used genome-wide selection components analysis to identify loci putatively under sexual selection in a sex-role reversed pipefish. We identified 180 RAD loci showing a signature of sexual selection, 271 SNPs implicated in differential viability selection between males and females, and 72 RAD loci that were outliers in multiple F_{ST} comparisons. Each F_{ST} comparison had unique outlier SNPs that fell into unique gene ontology categories, suggesting that viability selection and sexual selection may affect genes with different functions. Altogether, we have identified several hundred genomic regions putatively experiencing sexual selection and viability selection, demonstrating that genome-wide selection components analysis is a useful approach for discerning signatures of selection in an empirical study.

The only other empirical study that has implemented genome-wide selection components analysis took a different approach from the one that we used here. The other study applied selection components analysis to examine viability selection in the plant *Mimulus guttatus* and the authors identified 367 SNPs exhibiting a signature of viability selection (Monnahan et al. 2015). Their study was able to pinpoint viability selection in a way that was impossible in our study system, but our study was better poised to identify signatures of sexual selection. These discrepancies show that selection components analysis is flexible and can be adapted to very different study systems experiencing different modes of selection.

In this study, 72 RAD loci contained outlier SNPs in multiple F_{ST} comparisons that tested for sexual and viability selection. Genomic regions that are significant in

multiple analyses could be a result of several factors. Significance in multiple comparisons would suggest that those loci might be experiencing multiple forms of selection. Trade-offs between sexual and viability selection have been observed at the level of the phenotype (Delph and Herlihy 2012; Sentinella et al. 2013; Kim and Velando 2016), and such trade-offs could be have similar effects at the genomic level. Similarly, both episodes of selection could act in the same direction (Andersson 1986; Kokko et al. 2002), at least within one sex (Martin et al. 2014). An important consideration is whether there is a characteristic of the RAD-seq data that could cause overlapping outliers, perhaps if shared regions have polymorphic restriction sites or if those sequences have more sequencing errors than other regions, thus inflating F_{ST} values in any analysis.

The F_{ST} comparisons suggest that both sexual selection and viability selection affect allele frequencies in the Gulf pipefish. The comparison with the highest mean F_{ST} value was the mother-female comparison, suggesting that sexual selection is the stronger evolutionary force (although this result could also arise from sequencing artifacts; see below). We expected to find a signature of selection because Gulf pipefish females are known to be under strong sexual selection (Jones et al. 2001; Rose et al. 2013; Flanagan et al. 2014), so this result supports our hypothesis. Somewhat surprisingly, the mean F_{ST} between males and females was within one standard error of the mean mother-female F_{ST}, suggesting that viability selection is acting differentially on males and females at a similar strength as sexual selection. Strong sexual selection is often associated with viability tradeoffs (Salvador et al. 1996; Delph and Herlihy 2012; Sentinella et al. 2013;

Kim and Velando 2016), however, and since sexual selection is known to act on females and not males (Rose et al. 2013), a tradeoff could explain allele frequency differences between the sexes.

One of the drawbacks of using F_{ST} values to compare groups is the problem of spurious outliers. We used a 1% cutoff to identify potential outlier loci, which will always identify outliers, regardless of whether 1% of the loci are expected to be under selection. A cutoff-based approach was used because most methods such as FDIST2 (Beaumont and Nichols 1996; Beaumont 2000) are based on specific demographic models that are not applicable for use in a single population. The outlier identification approach is additionally limited because loci not experiencing selection do not necessarily have a distribution of F_{ST} values that is markedly different from that of loci experiencing selection. Whether or not the two distributions can be differentiated depends on factors such as the strength of selection and the number of loci underlying the traits experiencing selection (Flanagan and Jones 2015). Better, more comprehensive theory and models are required if more precise outlier approaches are desired. For the time being, the best the analysis can do is pinpoint putative genomic regions experiencing selection, but these regions will require further validation through experimentation or complementary population genomics analyses, since we do not expect that all of the outliers are truly under selection.

All of these results must be taken with a grain of salt, however, as many caveats arise due to limitations of current sequencing technologies and the reduced representation sequencing approach. First, restriction sites can be polymorphic, so allelic

dropout can cause false homozygous genotyping calls (Davey et al. 2013), resulting in inconsistent depth of coverage for different RAD loci (Davey et al. 2013; Andrews and Luikart 2014) and summary statistics that deviate dramatically from true values (Arnold et al. 2013). Although allelic dropout causes an underestimation of polymorphism, it can also sometimes increased apparent heterozygosity if mutations altering the restriction site tend to be in regions containing SNP alleles that tend to be at high frequency in the population (Gautier et al. 2013). Duplicates from PCR can also contribute to the calling of false heterozygotes (Puritz et al. 2014; Monnahan et al. 2015). Regardless of where these errors originate, PCR duplicates are the most important source of random errors in RAD-seq datasets, resulting in error rates above 2% even with stringent (30X) coverage filters (Henning et al. 2014). These PCR duplication errors generally result in inflated F_{ST} values (Arnold et al. 2013). Genome-wide selection components analysis relies on comparing genotypes to infer parental alleles to assess sexual selection. The problem of erroneous genotyping calls is therefore particularly relevant to selection components analysis, because the effect of errors could be amplified in the inferred allele frequencies (inferred mothers in this study), inflating F_{ST} values and resulting in an excess of false positives.

Despite these limitations, genome-wide selection components analysis has the potential to be an exciting approach for identifying candidate genomic regions involved in different types of selection. Here, we found evidence that viability selection and sexual selection are likely acting mostly on different genomic regions, but that there are some regions that might be experiencing both types of selection. These findings suggest

that trade-offs or concordant selection may be contributing to total selection in Gulf pipefish, a result that would not be easily discerned from a similar population genomics study. The ability to partition selection episodes at the genomic level will allow us to link genotypic and phenotypic changes in a quantitative genetics framework (Arnold and Wade 1984a; Arnold and Wade 1984b) in future studies. Further analyses will be required to differentiate spurious and real results, but that is the case with all next-generation sequencing data analysis. It is becoming obvious that understanding evolution at the genomic level will require investigations from multiple avenues, and selection components analysis is poised to be a useful tool in combination with other approaches.

CHAPTER V

CONCLUSION

In this thesis I have investigated the signature of selection on the genome using multiple approaches. These three studies reveal a complex, interconnected, and dynamic interaction between selection and the genome, in which selection, along with neutral forces, shape the genome while the structure of the genome also impacts the effects of selection.

In the first study (Chapter II), I investigated differentiation among 12 populations of the Gulf pipefish, *Syngnathus scovelli* by comparing allele frequencies at thousands of SNPs distributed throughout the genome. These twelve populations group into four or five genetically distinct clusters that are linked by limited migration to show a pattern of isolation by distance. Outlier loci, which do not follow the background pattern of isolation by distance, were linked to phenotypic variation. Phenotypic divergence followed a pattern different from geographic distance, and the traits driving the majority of variation among populations were body size and the number of female bands, which is a sexually-selected trait.

A complementary approach to the population genomics analysis presented in Chapter II is a selection components analysis, in which allele frequencies in groups within a population are compared to differentiate the signatures of the types of selection, such as viability selection or sexual selection. Before applying this approach empirically, I developed a simulation model in which a diploid, sexually reproducing population

experienced strong sexual selection on a quantitative trait. Weighted F_{ST} values were calculated between adults and offspring of the population to compare allele frequencies genome-wide. This model allowed me to test the effects of sample size, the number of markers sampled, selection strength, population size, the genetic architecture of the trait, and environmental variance affecting the traits on the ability to detect a signature of sexual selection. When selection was strong and the quantitative trait was determined by few quantitative trait loci, genome-wide selection components analysis was very effective at detecting loci experiencing selection, even with environmental variation.

The findings in Chapter III encouraged me to proceed with an empirical application of selection components analysis in one population of the Gulf pipefish. Using RAD-seq, I compared allele frequencies in adults and offspring, males and females, and inferred maternal genotypes and females. These comparisons highlighted approximately 300-400 genomic loci that are likely candidates for regions experiencing selection spread throughout the genome. We found a strong signature of sexual selection, accompanied by a signature of viability selection that differs between the sexes. However, this study also highlighted many of the pitfalls and shortcomings of current sequencing methodologies, since we found a ~10% error rate that likely impacted our analysis.

Together, this thesis demonstrates the importance of tackling a problem from multiple sides. Especially in the era of next-generation sequencing, which suffers from a lack of grounding theory to robustly test hypotheses, these sorts of multi-pronged approaches to understanding a large problem such as how selection affects the genome

are necessary. In the process of analyzing these datasets, new and challenging problems have emerged that impact the way RAD-seq datasets should be interpreted. Identifying and pinpointing these issues will help the fields of evolutionary and population genomics gain a better understanding of the interplay between selection and the genome. Additionally, these studies contribute to the growing body of next-generation sequencing data that will shed light on the complex issue of how genomes evolve and respond to evolutionary forces.

REFERENCES

Aguirre, J. D., E. Hine, K. McGuigan, and M. W. Blows. 2014. Comparing **G**: multivariate analysis of genetic variation in multiple populations. Heredity 112:21-29.

Ahnesjo, I. 1995. Temperature affects male and female potential reproductive rates differently in the sex-role reversed pipefish, *Syngnathus typhle*. Behavioral Ecology 6:229-233.

Ahnesjo, I. 2008. Behavioural temperature preference in a brooding male pipefish *Syngnathus typhle*. Journal of Fish Biology 73:1039-1045.

Anderson, J. T., C. R. Lee, and T. Mitchell-Olds. 2014. Strong selection genome-wide enhances fitness trade-offs across environments and episodes of selection. Evolution 68:16-31.

Anderson, W. W. 1969. Selection in experimental populations. I. Lethal genes. Genetics 62:653.

Anderson, W. W., L. Levine, O. Olvera, J. R. Powell, M. E. de la Rosa, V. M. Salceda, M. I. Gaso, and J. Guzmán. 1979. Evidence for selection by male mating success in natural populations of *Drosophila pseudoobscura*. Proceedings of the National Academy of Sciences 76:1519-1523.

Andersson, M. 1986. Evolution of condition-dependent sex ornaments and mating preferences: sexual selection based on viability differences. Evolution 40:804-816.

Andrews, K. R. and G. Luikart. 2014. Recent novel approaches for population genomics data analysis. Molecular Ecology 23:1661-1667.

Arnold, B., R. B. Corbett-Detig, D. Hartl, and K. Bomblies. 2013. RADseq underestimates diversity and introduces genealogical biases due to nonrandom haplotype sampling. Molecular Ecology:3179-3190.

Arnold, S. J. and M. J. Wade. 1984a. On the measurement of natural and sexual selection: applications. Evolution:720-734.

Arnold, S. J. and M. J. Wade. 1984b. On the measurement of natural and sexual selection: theory. Evolution 38:709-719.

Asgharian, H., P. L. Chang, S. Lysenkov, V. A. Scobeyeva, W. K. Reisen, and S. V. Nuzhdin. 2015. Evolutionary genomics of *Culex pipiens*: global and local adaptations associated with climate, life-history traits and anthropogenic factors. Proceedings of the Royal Society of London B: Biological Sciences 282.

Avise, J. C. 1992. Molecular population structure and the biogeographic history of a regional fauna - A case history with lessons for conservation biology. Oikos 63:62-76.

Baird, N. A., P. D. Etter, T. S. Atwood, M. C. Currey, A. L. Shiver, Z. A. Lewis, E. U. Selker, W. A. Cresko, and E. A. Johnson. 2008. Rapid SNP discovery and genetic mapping using sequenced RAD markers. PLoS ONE 3:e3376.

Barbadilla, A., A. Ruiz, M. Santos, and A. Fontdevila. 1994. Mating pattern and fitness-component analysis associated with inversion polymorphism in a natural population of *Drosophila buzzatii*. Evolution:767-780.

Barley, A. J., P. J. Monnahan, R. C. Thomson, L. L. Grismer, and R. M. Brown. 2015. Sun skink landscape genomics: assessing the roles of micro-evolutionary processes in shaping genetic and phenotypic diversity across a heterogeneous and fragmented landscape. Molecular Ecology 24:1696-1712.

Beaumont, M. A. 2000. Fdist2–a program to detect loci that might be under selection in samples from structured populations.

Beaumont, M. A. and R. A. Nichols. 1996. Evaluating loci for use in the genetic analysis of population structure. Proceedings of the Royal Society of London. Series B: Biological Sciences 263:1619-1626.

Beaumont, M. A. and B. Rannala. 2004. The Bayesian revolution in genetics. Nature Reviews Genetics 5:251-261.

Becker, R. A., A. R. Wilks, and R. Brownrigg. 2014a. mapdata: Extra map databases, http://CRAN.R-project.org/package=mapdata.

Becker, R. A., A. R. Wilks, R. Brownrigg, and T. P. Minka. 2014b. maps: Draw geographical maps, http://CRAN.R-project.org/package=maps.

Benjamini, Y. and Y. Hochberg. 1995. Controlling the false discovery rate: a practical and powerful approach to multiple testing. Journal of the Royal Statistical Society: Series B (Methodological):289-300.

Berg, P. R., S. Jentoft, B. Star, K. H. Ring, H. Knutsen, S. Lien, K. S. Jakobsen, and C. André. 2015. Adaptation to low salinity promotes genomic divergence in Atlantic cod (*Gadus morhua* L.). Genome Biology and Evolution 7:1644-1663.

Bierne, N., D. Roze, and J. J. Welch. 2013. Pervasive selection or is it…? why are F_{ST} outliers sometimes so frequent? Molecular Ecology 22:2061-2064.

Blanco-Bercial, L. and A. Bucklin. 2016. New view of population genetics of zooplankton: RAD-seq analysis reveals population structure of the North Atlantic planktonic copepod *Centropages typicus*. Molecular Ecology 25:1566-1580.

Boehm, J. T., J. Waldman, J. D. Robinson, and M. J. Hickerson. 2015. Population genomics reveals seahorses (*Hippocampus erectus*) of the western mid-Atlantic coast to be residents rather than vagrants. PLoS ONE 10:e0116219.

Boitard, S. and D. Rocha. 2013. Detection of signatures of selective sweeps in the Blonde d'Aquitaine cattle breed. Animal Genetics 44:579-583.

Bolland, J. and A. Boettcher. 2005. Population structure and reproductive characteristics of the Gulf pipefish, *Syngnathus scovelli*, in Mobile Bay, Alabama. Estuaries 28:957-965.

Brommer, J. E. 2011. Whither Pst? The approximation of Qst by Pst in evolutionary and conservation biology. Journal of Evolutionary Biology 24:1160-1168.

Buerkle, A. C. and Z. Gompert. 2013. Population genomics based on low coverage sequencing: how low should we go? Molecular Ecology 22:3028-3035.

Bundgaard, J. and F. Christiansen. 1972. Dynamics of polymorphisms. I. Selection components in an experimental population of *Drosophila melanogaster*. Genetics 71:439.

Candy, J. R., N. R. Campbell, M. H. Grinnell, T. D. Beacham, W. A. Larson, and S. R. Narum. 2015. Population differentiation determined from putative neutral and

divergent adaptive genetic markers in Eulachon (*Thaleichthys pacificus*, Osmeridae), an anadromous Pacific smelt. Molecular Ecology Resources 15:1421-1434.

Carlson, C. S., M. A. Eberle, L. Kruglyak, and D. A. Nickerson. 2004. Mapping complex disease loci in whole-genome association studies. Nature 429:446-452.

Catchen, J., S. Bassham, T. Wilson, M. Currey, C. O'Brien, Q. Yeates, and W. A. Cresko. 2013a. The population structure and recent colonization history of Oregon threespine stickleback determined using restriction-site associated DNA-sequencing. Molecular Ecology 22:2864-2883.

Catchen, J., P. A. Hohenlohe, S. Bassham, A. Amores, and W. A. Cresko. 2013b. Stacks: an analysis tool set for population genomics. Molecular Ecology 22:3124-3140.

Catchen, J. M., A. Amores, P. Hohenlohe, W. Cresko, and J. H. Postlethwait. 2011. Stacks: building and genotyping loci de novo from short-read sequences. G3: Genes, Genomes, Genetics 1:171-182.

Chiang, Y.-C., B.-H. Huang, C.-W. Chang, Y.-T. Wan, S.-J. Lai, S. Huang, and P.-C. Liao. 2013. Asymmetric introgression in the horticultural living fossil *Cycas* Sect. *Asiorientales* using a genome-wide scanning approach. International Journal of Molecular Sciences 14:8228-8251.

Christiansen, F., O. Frydenberg, and V. Simonsen. 1973. Genetics of *Zoarces* populations IV. Selection component analysis of an esterase polymorphism using population samples of mother-offspring combinations. Hereditas 73:291-304.

Christiansen, F. B. and O. Frydenberg. 1973. Selection component analysis of natural polymorphisms using population samples including mother-offspring combinations. Theoretical Population Biology 4:425-445.

Christiansen, F. B. and O. Frydenberg. 1974. Geographical patterns of four polymorphisms in *Zoarces viviparus* as evidence of selection. Genetics 77:765-770.

Clark, A. and M. Feldman. 1981. The estimation of epistasis in components of fitness in experimental populations of *Drosophila melanogaster* II. Assessment of meiotic drive, viability, fecundity and sexual selection. Heredity 46:347.

Clark, A., M. Feldman, and F. Christiansen. 1981. The estimation of epistasis in components of fitness in experimental populations of *Drosophila melanogaster* I. A two-stage maximum likelihood model. Heredity 46:321.

Clement, J. A. J., E. Toulza, M. Gautier, H. Parrinello, D. Roquis, J. Boissier, A. Rognon, H. Mone, G. Mouahid, J. Buard, G. Mitta, and C. Grunau. 2013. Private selective sweeps identified from next-generation pool-sequencing reveal convergent pathways under selection in two inbred *Schistosoma mansoni* strains. PLoS Neglected Tropical Diseases 7.

Combosch, D. J. and S. V. Vollmer. 2015. Trans-Pacific RAD-Seq population genomics confirms introgressive hybridization in Eastern Pacific *Pocillopora* corals. Molecular Phylogenetics and Evolution 88:154-162.

Coop, G., D. Witonsky, A. Di Rienzo, and J. K. Pritchard. 2010. Using environmental correlations to identify loci underlying local adaptation. Genetics 185:1411-1423.

Curtsinger, J. W. and M. W. Feldman. 1980. Experimental and theoretical analysis of the" sex-ratio" polymorphism in *Drosophila pseudoobscura*. Genetics 94:445-466.

Davey, J. L. and M. W. Blaxter. 2010. RADSeq: next-generation population genetics. Briefings in Functional Genomics 9:416-423.

Davey, J. W., T. Cezard, P. Fuentes-Utrilla, C. Eland, K. Gharbi, and M. L. Blaxter. 2013. Special features of RAD Sequencing data: implications for genotyping. Molecular Ecology 22:3151-3164.

Davey, J. W., P. A. Hohenlohe, P. D. Etter, J. Q. Boone, J. M. Catchen, and M. L. Blaxter. 2011. Genome-wide genetic marker discovery and genotyping using next-generation sequencing. Nature Reviews Genetics 12:499-510.

Dawson, C. E. 1982. Order Gasterosteiformes, Suborder Syngnathoidei: Part 8, Syngnathidae (Doryrhamphinae, Syngnathinae, Hippocampinae). Sears Foundation for Marine Research, Yale University, New Haven, CT, USA.

Delph, L. F. and C. R. Herlihy. 2012. Sexual, fecundity, and viability selection on flower size and number in a sexually dimorphic plant. International Journal Of Organic Evolution 66:1154-1166.

Diaz-Ruiz, S., A. Aguirre-Leon, and O. Perez-Soli. 2000. Distribution and abundance of *Syngnathus louisianae* and *Syngnathus scovelli* (Syngnathidae) in Tamiahua lagoon, Gulf of Mexico. Ciencias Marinas 26:125-143.

Dierickx, E. G., A. J. Shultz, F. Sato, T. Hiraoka, and S. V. Edwards. 2015. Morphological and genomic comparisons of Hawaiian and Japanese Black-

footed Albatrosses (Phoebastria nigripes) using double digest RADseq: implications for conservation. Evolutionary Applications 8:662-678.

Dionne, M., K. M. Miller, J. J. Dodson, F. Caron, and L. Bernatchez. 2007. Clinal variation in MHC diversity with temperature: evidence for the role of host-pathogen interaction on local adaptation in Atlantic salmon. Evolution 61:2154-2164.

Dray, S. and A. Dufour. 2007. The ade4 package: implementing the duality diagram for ecologists. Journal of Statistical Software 22:1-20.

Duforet-Frebourg, N., E. Bazin, and M. Blum. 2014. Genome scans for detecting footprints of local adaptation using a Bayesian factor model. Molecular Biology and Evolution 31:2483-2495.

Earl, D. A. and B. M. vonHoldt. 2012. STRUCTURE HARVESTER: a website and program for visualizing STRUCTURE output and implementing the Evanno method. Conservation Genetics Resources 4:359-361.

Ekblom, R. and J. Galindo. 2011. Applications of next generation sequencing in molecular ecology of non-model organisms. Heredity 107:1-15.

Emlen, S. T. and L. W. Oring. 1977. Ecology, sexual selection, and the evolution of mating systems. Science 197:215-223.

Engelhardt, B. E. and M. Stephens. 2010. Analysis of population structure: a unifying framework and novel methods based on sparse factor analysis. PLoS Genetics 6:e1001117.

Evanno, G., S. Regnaut, and J. Goudet. 2005. Detecting the number of clusters of individuals using the software structure: a simulation study. Molecular Ecology 14:2611-2620.

Everett, M. V. and J. E. Seeb. 2014. Detection and mapping of QTL for temperature tolerance and body size in Chinook salmon (*Oncorhynchus tshawytscha*) using genotyping by sequencing. Evolutionary Applications 7:480-492.

Falush, D., M. Stephens, and J. K. Pritchard. 2003. Inference of population structure using multilocus genotype data: linked loci and correlated allele frequencies. Genetics 164:1567-1587.

Falush, D., M. Stephens, and J. K. Pritchard. 2007. Inference of population structure using multilocus genotype data: dominant markers and null alleles. Molecular Ecology Notes 7:574-578.

Flanagan, S. P., J. B. Johnson, E. Rose, and A. G. Jones. 2014. Sexual selection on female ornaments in the sex-role-reversed Gulf pipefish (*Syngnathus scovelli*). Journal of Evolutionary Biology 27:2457-2467.

Flanagan, S. P. and A. G. Jones. 2015. Identifying signatures of sexual selection using genomewide selection components analysis. Ecology and Evolution 5:2722-2744.

Flint, J. and T. F. C. Mackay. 2009. Genetic architecture of quantitative traits in mice, flies, and humans. Genome Research 19:723-733.

Foll, M. and O. Gaggiotti. 2008. A genome-scan method to identify selected loci appropriate for both dominant and codominant markers: A Bayesian perspective. Genetics 180:977-993.

Fournier-Level, A., A. Korte, M. D. Cooper, M. Nordborg, J. Schmitt, and A. M. Wilczek. 2011. A map of local adaptation in *Arabidopsis thaliana*. Science 334:86-89.

Fraser, B. A., A. Künstner, D. N. Reznick, C. Dreyer, and D. Weigel. 2015. Population genomics of natural and experimental populations of guppies (*Poecilia reticulata*). Molecular Ecology 24:389-408.

Futuyma, D. J. 1998. Evolutionary Biology. Sinauer Associates, Incorporated.

Gagnaire, P.-A., S. A. Pavey, E. Normandeau, and L. Bernatchez. 2013. The genetic architecture of reproductive isolation during speciation-with-gene-flow in Lake Whitefish species pairs assessed by RAD sequencing. Evolution 67:2483-2497.

Gautier, M., K. Gharbi, T. Cezard, J. Foucaud, C. Kerdelhué, P. Pudlo, J.-M. Cornuet, and A. Estoup. 2013. The effect of RAD allele dropout on the estimation of genetic variation within and between populations. Molecular Ecology 22:3165-3178.

Guo, B., J. DeFaveri, G. Sotelo, A. Nair, and J. Merilä. 2015. Population genomic evidence for adaptive differentiation in Baltic Sea three-spined sticklebacks. BMC Biology 13:19.

Günther, T. and G. Coop. 2013. Robust identification of local adaptation from allele frequencies. Genetics 195:205-220.

Harris, S. E., J. Munshi-South, C. Obergfell, and R. O'Neill. 2013. Signatures of rapid evolution in urban and rural transcriptomes of white-footed mice (*Peromyscus leucopus*) in the New York metropolitan area. PLoS ONE 8.

Hartl, D. L. and A. G. Clark. 2007. Principles of population genetics. Sinauer associates Sunderland, Massachusetts.

Harvey, M. G. and R. T. Brumfield. 2015. Genomic variation in a widespread Neotropical bird (*Xenops minutus*) reveals divergence, population expansion, and gene flow. Molecular Phylogenetics and Evolution 83:305-316.

Heath, D., B. Riddoch, D. Childs, and J. Ratford. 1988. Selection component analysis of the PGI polymorphism in *Sphaeroma rugicauda*. Heredity 60:229-235.

Helyar, S. J., J. Hemmer-Hansen, D. Bekkevold, M. I. Taylor, R. Ogden, M. T. Limborg, A. Cariani, G. E. Maes, E. Diopere, G. R. Carvalho, and E. E. Nielsen. 2011. Application of SNPs for population genetics of nonmodel organisms: new opportunities and challenges. Molecular Ecology Resources 11:123-136.

Henning, F., H. J. Lee, P. Franchini, and A. Meyer. 2014. Genetic mapping of horizontal stripes in Lake Victoria cichlid fishes: benefits and pitfalls of using RAD markers for dense linkage mapping. Molecular Ecology 23:5224-5240.

Hess, J. E., N. R. Campbell, D. A. Close, M. F. Docker, and S. R. Narum. 2013. Population genomics of Pacific lamprey: adaptive variation in a highly dispersive species. Molecular Ecology 22:2898-2916.

Hine, E., S. F. Chenoweth, H. D. Rundle, and M. W. Blows. 2009. Characterizing the evolution of genetic variance using genetic covariance tensors. Philosophical

Transactions of the Royal Society of London B: Biological Sciences 364:1567-1578.

Hohenlohe, P. A., S. Bassham, P. D. Etter, N. Stiffler, E. A. Johnson, and W. A. Cresko. 2010a. Population genomics of parallel adaptation in threespine stickleback using sequenced RAD tags. PLoS Genetics 6:e1000862.

Hohenlohe, P. A., M. D. Day, S. J. Amish, M. R. Miller, N. Kamps-Hughes, M. C. Boyer, C. C. Muhlfeld, F. W. Allendorf, E. A. Johnson, and G. Luikart. 2013. Genomic patterns of introgression in rainbow and westslope cutthroat trout illuminated by overlapping paired-end RAD sequencing. Molecular Ecology 22:3002-3013.

Hohenlohe, P. A., P. C. Phillips, and W. A. Cresko. 2010b. Using population genomics to detect selection in natural populations: Key concepts and methodological considerations. International Journal of Plant Science 171:1059-1071.

Houle, D., C. Pelabon, G. Wagner, and T. F. Hansen. 2011. Measurement and meaning in biology. The Quarterly Review of Biology 86:3-34.

Huang, W., A. Massouras, Y. Inoue, J. Peiffer, M. Ràmia, A. M. Tarone, L. Turlapati, T. Zichner, D. Zhu, R. F. Lyman, M. M. Magwire, K. Blankenburg, M. A. Carbone, K. Chang, L. L. Ellis, S. Fernandez, Y. Han, G. Highnam, C. E. Hjelmen, J. R. Jack, M. Javaid, J. Jayaseelan, D. Kalra, S. Lee, L. Lewis, M. Munidasa, F. Ongeri, S. Patel, L. Perales, A. Perez, L. Pu, S. M. Rollmann, R. Ruth, N. Saada, C. Warner, A. Williams, Y.-Q. Wu, A. Yamamoto, Y. Zhang, Y. Zhu, R. R. H. Anholt, J. O. Korbel, D. Mittelman, D. M. Muzny, R. A. Gibbs, A. Barbadilla, J.

S. Johnston, E. A. Stone, S. Richards, B. Deplancke, and T. F. C. Mackay. 2014. Natural variation in genome architecture among 205 *Drosophila melanogaster* Genetic Reference Panel lines. Genome Research 24:1193-1208.

Hubner, S., E. Rashkovetsky, Y. B. Kim, J. H. Oh, K. Michalak, D. Weiner, A. B. Korol, E. Nevo, and P. Michalak. 2013. Genome differentiation of *Drosophila melanogaster* from a microclimate contrast in Evolution Canyon, Israel. Proceedings of the National Academy of Sciences of the United States of America 110:21059-21064.

Jombart, T. 2008. adegenet: a R package for the multivariate analysis of genetic markers. Bioinformatics 24:1403-1405.

Jombart, T. and I. Ahmed. 2011. adegenet 1.3-1: new tools for the analysis of genome-wide SNP data. Bioinformatics 27:3070-3071.

Jones, A. G. 2009. On the opportunity for sexual selection, the Bateman gradient and the maximum intensity of sexual selection. Evolution 63:1673-1684.

Jones, A. G. and J. C. Avise. 1997. Microsatellite analysis of maternity and the mating system in the Gulf pipefish *Syngnathus scovelli*, a species with male pregnancy and sex-role reversal. Molecular Ecology 6:203-213.

Jones, A. G., D. Walker, and J. C. Avise. 2001. Genetic evidence for extreme polyandry and extraordinary sex-role reversal in a pipefish. Proceedings of the Royal Society B-Biological Sciences 268:2531-2535.

Jones, F. C., M. G. Grabherr, Y. F. Chan, P. Russell, E. Mauceli, J. Johnson, R. Swofford, M. Pirun, M. C. Zody, S. White, E. Birney, S. Searle, J. Schmutz, J.

Grimwood, M. C. Dickson, R. M. Myers, C. T. Miller, B. R. Summers, A. K. Knecht, S. D. Brady, H. Zhang, A. A. Pollen, T. Howes, C. Amemiya, E. S. Lander, F. Di Palma, K. Lindblad-Toh, and D. M. Kingsley. 2012. The genomic basis of adaptive evolution in threespine sticklebacks. Nature 484:55-61.

Kim, S.-Y. and A. Velando. 2016. Genetic conflict between sexual signalling and juvenile survival in the three-spined stickleback. BMC Evolutionary Biology 16:1-7.

Kokko, H., R. Brooks, J. M. McNamara, and A. I. Houston. 2002. The sexual selection continuum. Proceedings of the Royal Society of London B: Biological Sciences 269:1331-1340.

Krzanowski, W. 1979. Between-groups comparison of principal components. Journal of the American Statistical Association 74:703-707.

Lande, R. 1981. Models of speciation by sexual selection on polygenic traits. Proceedings of the National Academy of Sciences 78:3721-3725.

Landis, S. H., M. Kalbe, T. B. H. Reusch, and O. Roth. 2012a. Consistent pattern of local adaptation during an experimental heat wave in a pipefish-trematode host-parasite system. PLoS ONE 7:e30658.

Landis, S. H., J. Sundin, G. Rosenqvist, and O. Roth. 2012b. Behavioral adjustments of a pipefish to bacterial Vibrio challenge. Behavioral Ecology and Sociobiology 66:1399-1405.

Langmead, B. and S. L. Salzberg. 2012. Fast gapped-read alignment with Bowtie 2. Nature Methods 9:357-359.

Leinonen, T., J. M. Cano, H. Makinen, and J. Merila. 2006. Contrasting patterns of body shape and neutral genetic divergence in marine and lake populations of threespine sticklebacks. Journal of Evolutionary Biology 19:1803-1812.

Lewontin, R. C. and J. Krakauer. 1973. Distribution of gene frequency as a test of the theory of the selective neutrality of polymorphisms. Genetics 74:175-195.

Liao, P.-C., C.-C. Tsai, C.-H. Chou, and Y.-C. Chiang. 2012. Introgression between cultivars and wild populations of *Momordica charantia* L.(Cucurbitaceae) in Taiwan. International Journal of Molecular Sciences 13:6469-6491.

Loehle, C. and J. H. Pechmann. 1988. Evolution: the missing ingredient in systems ecology. American Naturalist 132:884.

Lotterhos, K. E. and M. C. Whitlock. 2014. Evaluation of demographic history and neutral parameterization on the performance of F_{ST} outlier tests. Molecular Ecology 23:2178-2192.

Lotterhos, K. E. and M. C. Whitlock. 2015. The relative power of genome scans to detect local adaptation depends on sampling design and statistical method. Molecular Ecology 24:1031-1046.

Mackay, T. F. C., S. Richards, E. A. Stone, A. Barbadilla, J. F. Ayroles, D. Zhu, S. Casillas, Y. Han, M. M. Magwire, J. M. Cridland, M. F. Richardson, R. R. H. Anholt, M. Barron, C. Bess, K. P. Blankenburg, M. A. Carbone, D. Castellano, L. Chaboub, L. Duncan, Z. Harris, M. Javaid, J. C. Jayaseelan, S. N. Jhangiani, K. W. Jordan, F. Lara, F. Lawrence, S. L. Lee, P. Librado, R. S. Linheiro, R. F. Lyman, A. J. Mackey, M. Munidasa, D. M. Muzny, L. Nazareth, I. Newsham, L.

Perales, L.-L. Pu, C. Qu, M. Ramia, J. G. Reid, S. M. Rollmann, J. Rozas, N. Saada, L. Turlapati, K. C. Worley, Y.-Q. Wu, A. Yamamoto, Y. Zhu, C. M. Bergman, K. R. Thornton, D. Mittelman, and R. A. Gibbs. 2012. The *Drosophila melanogaster* genetic reference panel. Nature 482:173-178.

Martin, A. M., M. Festa-Bianchet, D. W. Coltman, and F. Pelletier. 2014. Sexually antagonistic association between paternal phenotype and offspring viability reinforces total selection on a sexually selected trait. Biology Letters 10:20140043.

Masonjones, H. D., E. Rose, L. B. McRae, and D. Dixson. 2010. An examination of the population dynamics of syngnathid fishes within Tampa Bay, Florida, USA. Current Zoology 56:118-133.

Mastretta-Yanes, A., N. Arrigo, N. Alvarez, T. H. Jorgensen, D. Piñero, and B. C. Emerson. 2015. Restriction site-associated DNA sequencing, genotyping error estimation and de novo assembly optimization for population genetic inference. Molecular Ecology Resources 15:28-41.

McDonald, J. 1989. Selection component analysis of the *Mpi* locus in the amphipod *Platorchestia platensis*. Heredity 62:243-249.

Meier, K., M. M. Hansen, E. Normandeau, K.-L. D. Mensberg, J. Frydenberg, P. F. Larsen, D. Bekkevold, and L. Bernatchez. 2014. Local adaptation at the transcriptome level in brown trout: evidence from early life history temperature genomic reaction norms. PLoS ONE 9:e85171.

Meirmans, P. G. 2012. The trouble with isolation by distance. Molecular Ecology 21:2839-2846.

Miller, M. R., J. P. Brunelli, P. A. Wheeler, S. Liu, C. E. Rexroad, Y. Palti, C. Q. Doe, and G. H. Thorgaard. 2012. A conserved haplotype controls parallel adaptation in geographically distant salmonid populations. Molecular Ecology 21:237-249.

Miller, M. R., J. P. Dunham, A. Amores, W. A. Cresko, and E. A. Johnson. 2007. Rapid and cost-effective polymorphism identification and genotyping using restriction site associated DNA (RAD) markers. Genome Research 17:240-248.

Mitton, J. B. and R. K. Koehn. 1975. Genetic organization and adaptive response of allozymes to ecological variables in *Fundulus heteroclitus*. Genetics 79:97-111.

Mobley, K. B. and A. G. Jones. 2007. Geographical variation in the mating system of the dusky pipefish (*Syngnathus floridae*). Molecular Ecology 16:2596-2606.

Mobley, K. B. and A. G. Jones. 2009. Environmental, demographic, and genetic mating system variation among five geographically distinct dusky pipefish (*Syngnathus floridae*) populations. Molecular Ecology 18:1476-1490.

Mobley, K. B., C. M. Small, N. K. Jue, and A. G. Jones. 2010. Population structure of the dusky pipefish (*Syngnathus floridae*) from the Atlantic and Gulf of Mexico, as revealed by mitochondrial DNA and microsatellite analyses. Journal of Biogeography 37:1363-1377.

Monnahan, P. J., J. Colicchio, and J. K. Kelly. 2015. A genomic selection component analysis characterizes migration-selection balance. Evolution 69:1713-1727.

Monteiro, N. M. and D. O. Lyons. 2012. Stronger sexual selection in warmer waters: the case of a sex role reversed pipefish. PLoS ONE 7:e44251.

Morris, G. P., P. Ramu, S. P. Deshpande, C. T. Hash, T. Shah, H. D. Upadhyaya, O. Riera-Lizarazu, P. J. Brown, C. B. Acharya, S. E. Mitchell, J. Harriman, J. C. Glaubitz, E. S. Buckler, and S. Kresovich. 2013. Population genomic and genome-wide association studies of agroclimatic traits in sorghum. Proceedings of the National Academy of Sciences 110:453-458.

Nadeau, J. H. and R. Baccus. 1981. Selection components of four allozymes in natural populations of *Peromyscus maniculatus*. Evolution:11-20.

Narum, S. R., C. A. Buerkle, J. W. Davey, M. R. Miller, and P. A. Hohenlohe. 2013a. Genotyping-by-sequencing in ecological and conservation genomics. Molecular Ecology 22:2841-2847.

Narum, S. R., N. R. Campbell, K. A. Meyer, M. R. Miller, and R. W. Hardy. 2013b. Thermal adaptation and acclimation of ectotherms from differing aquatic climates. Molecular Ecology 22:3090-3097.

Nei, M. 1986. Definition and estimation of fixation indices. Evolution 40:643-645.

Nielsen, R. 2005. Molecular signatures of natural selection. Annual Review of Genetics 39:197-218.

Ocean Climate Laboratory, N. O. D. C. N. N. U. S. D. o. C. 1984. World Ocean Database and World Ocean Atlas. Research Data Archive at the National Center for Atmospheric Research, Computational and Information Systems Laboratory, Boulder, CO.

Oksanen, J., F. G. Blanchet, R. Kindt, P. Legendre, P. R. Minchin, R. B. O'Hara, G. L. Simpson, P. Solymos, M. H. H. Stevens, and H. Wagner. 2013. vegan: Community Ecology Package.

Oneal, E. and L. L. Knowles. 2013. Ecological selection as the cause and sexual differentiation as the consequence of species divergence? Proceedings of the Royal Society B: Biological Sciences 280:20122236.

Ozerov, M. Y., M. Himberg, T. Aykanat, D. S. Sendek, H. Hägerstrand, A. Verliin, T. Krause, J. Olsson, C. R. Primmer, and A. Vasemägi. 2015. Generation of a neutral F_{ST} baseline for testing local adaptation on gill raker number within and between European whitefish ecotypes in the Baltic Sea basin. Journal of Evolutionary Biology 28:1170-1183.

Paczolt, K. A. and A. G. Jones. 2010. Post-copulatory sexual selection and sexual conflict in the evolution of male pregnancy. Nature 464:401-U494.

Partridge, C., A. Boettcher, and A. G. Jones. 2012. Population structure of the Gulf pipefish in and around Mobile Bay and the northern Gulf of Mexico. Journal of Heredity 103:821-830.

Peterson, B. K., J. N. Weber, E. H. Kay, H. S. Fisher, and H. E. Hoekstra. 2012. Double digest RADseq: an inexpensive method for de novo SNP discovery and genotyping in model and non-model species. PLoS ONE 7:e37135.

Picq, S., W. O. McMillan, and O. Puebla. 2016. Population genomics of local adaptation versus speciation in coral reef fishes (*Hypoplectrus* spp, Serranidae). Ecology and Evolution 6:2109-2124.

Pinheiro, J., D. Bates, S. DebRoy, and D. Sarkar. 2016. nlme: Linear and nonlinear mixed effects models.

Pritchard, J. K., M. Stephens, and P. Donnelly. 2000. Inference of population structure using multilocus genotype data. Genetics 155:945-959.

Prout, T. 1965. The estimation of fitnesses from genotypic frequencies. Evolution:546-551.

Prout, T. 1969. The estimation of fitnesses from population data. Genetics 63:949-967.

Prout, T. 1971a. The relation between fitness components and population prediction in *Drosophila.* I: the estimation of fitness components. Genetics 68:127-149.

Prout, T. 1971b. The relation between fitness components and population prediction in *Drosophila.* II: population prediction. Genetics 68:151-167.

Purcell, S., B. Neale, K. Todd-Brown, L. Thomas, M. Ferreira, D. Bender, J. Maller, P. Sklar, P. de Bakker, M. Daly, and P. Sham. 2007. PLINK: a toolset for whole-genome association and population-based linkage analysis. American Journal of Human Genetics 81:559-575.

Puritz, J. B., M. V. Matz, R. J. Toonen, J. N. Weber, D. I. Bolnick, and C. E. Bird. 2014. Demystifying the RAD fad. Molecular Ecology 23:5937-5942.

R Core Team. 2013. R: A Language and Environment for Statistical Computing *in* R. F. f. S. Computing, ed, Vienna, Austria.

Rasband, W. S. 1997-2012. ImageJ, U. S. National Institutes of Health, Bethesda, Maryland, USA.

Rausher, M. D. D., Lynda F. 2015. Commentary: When does understanding phenotypic evolution require identification of the underlying genes? Evolution 69:1655-1664.

Reitzel, A. M., S. Herrera, M. J. Layden, M. Q. Martindale, and T. M. Shank. 2013. Going where traditional markers have not gone before: utility of and promise for RAD sequencing in marine invertebrate phylogeography and population genomics. Molecular Ecology 22:2953-2970.

Rellstab, C., S. Zoller, A. Tedder, F. Gugerli, and M. C. Fischer. 2013. Validation of SNP allele frequencies determined by pooled next-generation sequencing in natural populations of a non-model plant species. PLoS ONE 8: e80422.

Rohlf, F. J. 2005. tpsDig2, digitize landmarks and outlines, Department of Ecology and Evolution, State University of New York at Stony Brook.

Rose, E., K. A. Paczolt, and A. G. Jones. 2013. The contributions of premating and postmating selection episodes to total selection in sex-role-reversed Gulf pipefish. The American Naturalist 182:410-420.

Salvador, A., J. P. Veiga, J. Martin, P. Lopez, M. Abelenda, and M. Puertac. 1996. The cost of producing a sexual signal: testosterone increases the susceptibility of male lizards to ectoparasitic infestation. Behavioral Ecology 7:145-150.

Schumer, M., R. Cui, D. L. Powell, R. Dresner, G. G. Rosenthal, and P. Andolfatto. 2014. High-resolution mapping reveals hundreds of genetic incompatibilities in hybridizing fish species. ELife 3:e02535.

Sentinella, A. T., A. J. Crean, and R. Bonduriansky. 2013. Dietary protein mediates a trade-off between larval survival and the development of male secondary sexual traits. Functional Ecology 27:1134-1144.

Spitze, K. 1993. Population structure in *Daphnia obtusa*: quantitative genetic and allozymic variation. Genetics 135:367-374.

Stockwell, C. A., A. P. Hendry, and M. T. Kinnison. 2003. Contemporary evolution meets conservation biology. Trends in Ecology & Evolution 18:94-101.

Thornton, K. R., A. J. Foran, and A. D. Long. 2013. Properties and modeling of GWAS when complex disease risk is due to non-complementing, deleterious mutations in genes of large effect. PLoS Genetics 9:e1003258.

Tobler, R., S. U. Franssen, R. Kofler, P. Orozco-terWengel, V. Nolte, J. Hermisson, and C. Schlötterer. 2014. Massive habitat-specific genomic response in *D. melanogaster* populations during experimental evolution in hot and cold environments. Molecular Biology and Evolution 31:364-375.

Vincent, B., M. Dionne, M. P. Kent, S. Lien, and L. Bernatchez. 2013. Landscape genomics in Atlantic Salmon (*Salmo salar*): searching for gene-environment interactions driving local adaptation. Evolution 67:3469-3487.

Visscher, P. M., W. G. Hill, and N. R. Wray. 2008. Heritability in the genomics era—concepts and misconceptions. Nature Reviews Genetics 9:255-266.

Warnes, G. R., B. Bolker, L. Bonebakker, R. Gengleman, W. Huber, A. Liaw, T. Lumley, M. Maechler, A. Magnusson, S. Moeller, M. Schwartz, and B.

Venables. 2015. gplots: various R programming tools for plotting data, http://CRAN.R-project.org/package=gplots.

Weir, B. S. and C. C. Cockerham. 1978. Testing hypotheses about linkage disequilibrium with multiple alleles. Genetics 88:633-642.

Whitlock, M. C. and F. Guillaume. 2009. Testing for spatially divergent selection: comparing Q_{ST} to F_{ST}. Genetics 183:1055-1063.

Workman, P. L. and J. D. Niswander. 1970. Population studies on southwestern Indian tribes. II. Local genetic differentiation in the Papago. American Journal of Human Genetics 22:24-49.

Wright, S. 1931. Evolution in Mendelian populations. Genetics 16:97-159.

Wright, S. 1943. Isolation by distance. Genetics 28:114-138.

APPENDIX I

List of supplemental files, archived data, and accessible code

Chapter II

Supplemental File 1. Table containing all of the SNPs identified as outliers in at least one of the local adaptation or isolation by ecology analyses. This is saved as a Microsoft Excel® file. The column "RAD locus" is the numerical ID assigned to the 100bp sequence in the "Sequence" column by Stacks, and the "SNP ID" column is the identifier for this SNP. The "Scaffold" is the scaffold in the reference genome this sequence mapped to, and the "BP" is the position on that scaffold that the SNP mapped to. The "Analysis" column designates which local adaptation or isolation by ecology analysis designated this SNP as an outlier.

Supplemental File 2. A Microsoft Excel® file with three tabs. The first tab, "MalePsts", contains all of the pairwise P_{ST} values for the male traits. The second tab, "FemalePsts", contains all of the pairwise P_{ST} values for the female traits. The third tab, "SignificantSNPs", contains the RAD locus and SNP IDs, the scaffold and position on the scaffold ("BP"), where the SNP mapped to in the reference genome, and the sequence. This table also shows which trait had a P_{ST} significantly associated with the F_{ST} for the SNP.

Supplemental File 3. A Microsoft Word® document containing detailed descriptions of the **P**-matrix comparisons, including tables and figures.

GitHub Repository. The github repository found at this web address: https://github.com/spflanagan/popgen.git contains all of the scripts and programs written to conduct the analyses in Chapter II.

Dryad Repository. Raw phenotypic data, genotypic data, the draft genome, and GPS coordinates of collecting sites are archived on Dryad. Sequence files will be uploaded to GenBank after the manuscript has been accepted.

Chapter III

Dryad Repository. Data and source code are archived on Dryad (doi: 10.5061/dryad.5k84d).

Chapter IV

Supplemental File 4. A Microsoft Excel® file containing the outliers shared among the three selection components analysis F_{ST} comparisons. The table contains the RAD locus information, including the sequence, blastx hit, and Blast2GO results.

Supplemental File 5. A Microsoft Excel® file containing the outliers unique to each of the three selection components analysis F_{ST} comparisons. The table contains the RAD locus information, including the sequence, blastx hit, and Blast2GO results.

GitHub Repository. All code and scripts for the analyses in Chapter IV can be found on GitHub at this web address: https://github.com/spflanagan/SCA.git.

APPENDIX II

Results of the MIGRATE-N analysis. The width of the arrows represents the migration rate; thicker arrows represent higher mutation-scaled migration rates (M = m/μ). The size of the points represent the estimates of θ ($4N_e\mu$) calculated by the program, such that larger points represent larger estimates. The numbers are the estimated *Nm* values, calculated as (θ*M)/4.

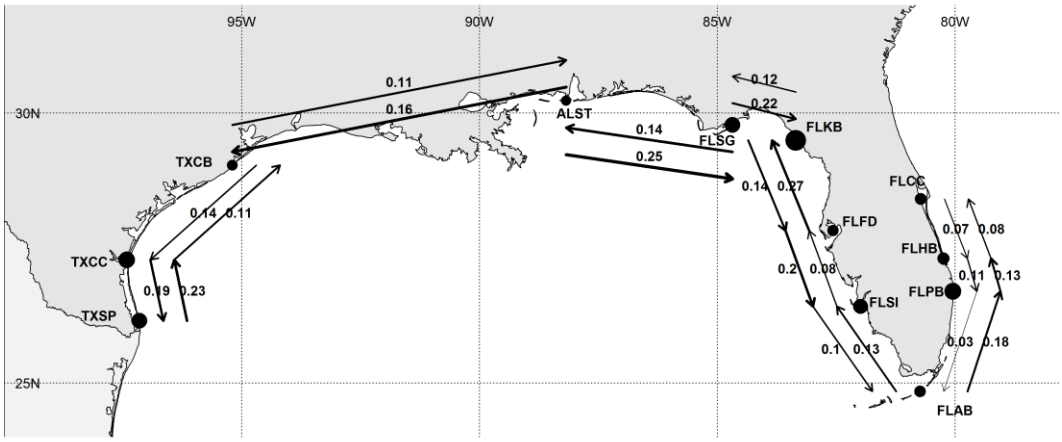

APPENDIX III

Overlapping RAD loci that are found in each of the three outlier analyses and the temperature association analysis. This Venn diagram shows the number of RAD loci (a) identified as outliers (in the top 1% of Bayes Factors) by all 10 runs of PCAdapt; (b) the top 1% of F_{ST} values; and (c) in the top 5% of the X^TX values computed by Bayenv2.0. One RAD locus was shared among all four analyses.

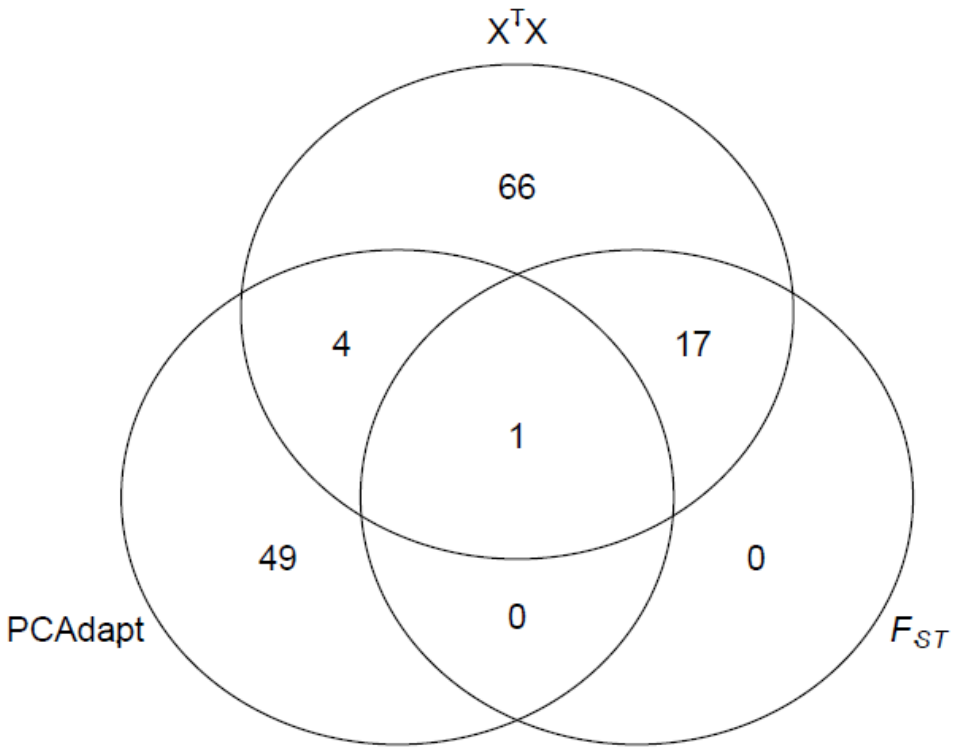

APPENDIX IV

Gene ontology categories relating to biological processes for the 5kb regions surrounding SNPs associated with the six environmental variables. A total of 383 SNPs were associated with at least one environmental variable, and each environmental variable has 88 SNPs associated with it. Of those, most had blastx hits (71 10-yr Salinity; 63 10-yr Temperature; 67 10-yr Temperature Variance; 61 Collection Salinity; 72 Collection Temperature; 67 Seagrass Cover).

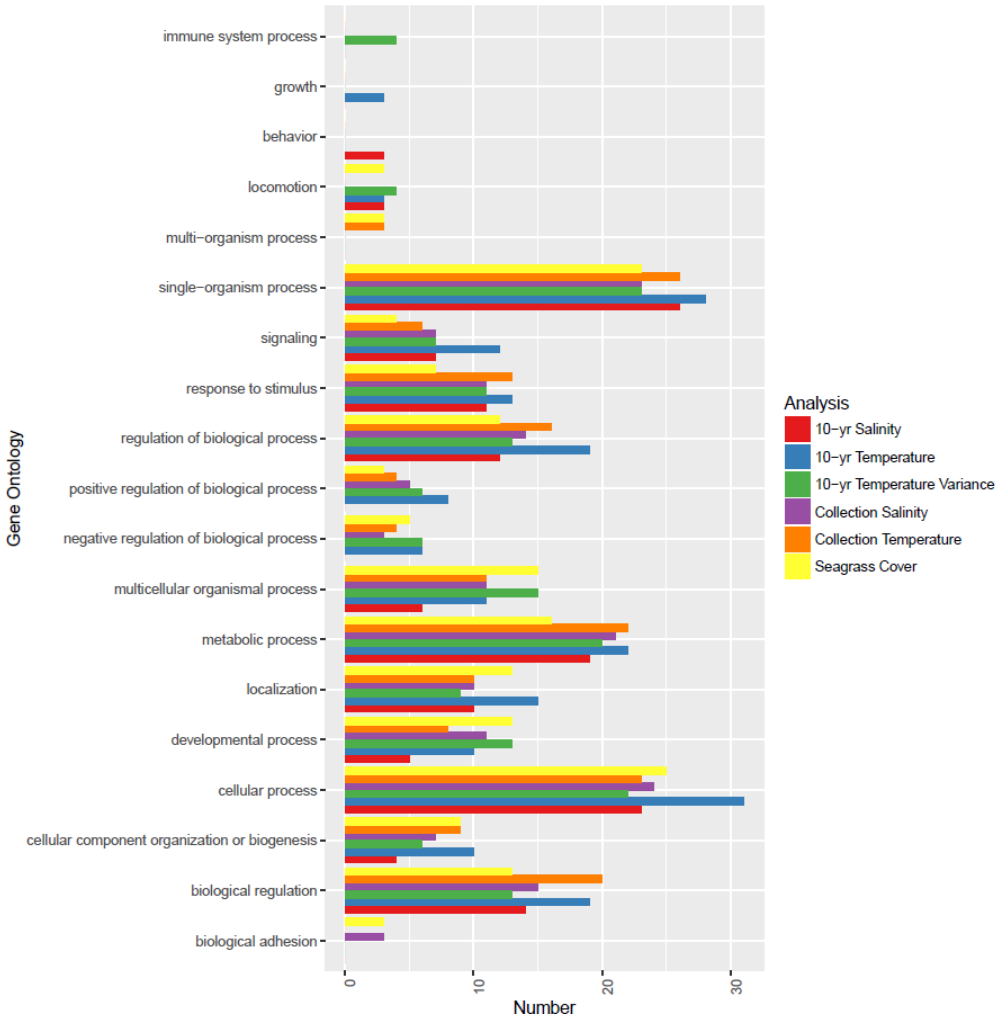

APPENDIX V

Female **P**-matrices. These are the unstandardized variances (diagonal), covariances (lower triangle), and correlations (upper triangle). The columns for $\boldsymbol{p}_1$, $\boldsymbol{p}_2$, and $\boldsymbol{p}_3$ show the three leading eigenvectors for each population.

	SVL	Tail Length	Body Depth	Snout Length	Snout Depth	Head Length	Mean Band Area	Band Number	p_1	p_2	p_3
TXSP											
SVL	10.019	0.969	0.995	0.997	0.981	0.754	0.971	0.640	-0.574	-0.254	0.693
Tail Length	11.626	18.354	0.977	0.962	0.994	0.581	0.892	0.452	-0.785	0.419	-0.419
Body Depth	1.459	1.785	0.381	0.994	0.982	0.718	0.955	0.603	-0.087	-0.029	0.090
Snout Length	1.088	1.276	0.206	0.202	0.972	0.753	0.977	0.665	-0.064	-0.039	0.040
Snout Depth	0.250	0.375	0.036	0.022	0.031	0.634	0.919	0.517	-0.017	0.002	-0.009
Head Length	0.933	0.428	0.141	0.096	0.032	0.368	0.842	0.847	-0.037	-0.106	0.357
Mean Band Area	0.311	0.323	0.041	0.046	0.005	0.045	0.024	0.801	-0.017	-0.023	0.005
Band Number	4.194	2.494	0.590	0.532	0.088	0.593	0.213	5.680	-0.202	-0.864	-0.456
TXCC											
SVL	6.650	0.986	0.992	0.998	0.853	0.998	0.995	-0.166	0.586	0.011	0.755
Tail Length	7.519	11.329	0.976	0.985	0.765	0.986	0.989	-0.144	0.792	0.025	-0.608
Body Depth	0.864	0.951	0.234	0.987	0.843	0.994	0.992	-0.108	0.076	-0.042	0.123
Snout Length	1.466	1.673	0.169	0.422	0.847	0.995	0.994	-0.165	0.131	-0.003	0.169
Snout Depth	0.199	0.101	0.040	0.038	0.029	0.834	0.809	-0.438	0.012	0.021	0.089
Head Length	0.850	0.981	0.131	0.177	0.023	0.163	0.995	-0.128	0.076	-0.023	0.091
Mean Band Area	0.138	0.166	0.021	0.032	0.007	0.014	0.008	-0.084	0.013	-0.007	0.011
Band Number	0.183	0.249	0.114	0.054	-0.043	0.076	0.021	2.211	0.021	-0.998	-0.013
TXCB											
SVL	11.709	0.852	0.979	0.999	0.771	0.974	0.989	0.921	-0.342	0.888	0.174
Tail Length	12.443	41.665	0.728	0.831	0.326	0.949	0.912	0.946	-0.927	-0.368	0.067
Body Depth	1.390	1.082	0.208	0.986	0.882	0.907	0.942	0.844	-0.033	0.125	-0.007
Snout Length	2.399	2.407	0.285	0.552	0.795	0.964	0.983	0.909	-0.067	0.191	0.014
Snout Depth	0.415	0.122	0.055	0.093	0.039	0.607	0.677	0.507	-0.006	0.046	0.017

	SVL	Tail Length	Body Depth	Snout Length	Snout Depth	Head Length	Mean Band Area	Band Number	p_1	p_2	p_3
Head Length	1.240	1.921	0.140	0.263	0.028	0.180	0.992	0.965	-0.048	0.067	0.020
Mean Band Area	0.166	0.218	0.020	0.036	0.006	0.016	0.003	0.968	-0.006	0.011	-0.011
Band Number	2.772	5.044	0.334	0.585	0.063	0.334	0.059	2.027	-0.126	0.136	-0.982
ALST											
SVL	2.483	0.876	0.812	0.973	0.845	0.913	0.679	0.610	-0.321	0.185	0.905
Tail Length	2.959	9.767	0.971	0.950	0.983	0.937	0.834	0.739	-0.899	0.212	-0.368
Body Depth	0.305	1.094	0.250	0.919	0.987	0.840	0.936	0.862	-0.106	-0.107	-0.042
Snout Length	0.608	0.987	0.145	0.241	0.942	0.927	0.813	0.740	-0.104	-0.016	0.178
Snout Depth	0.095	0.296	0.043	0.056	0.034	0.888	0.905	0.833	-0.029	-0.022	-0.001
Head Length	0.247	0.507	0.041	0.088	0.031	0.138	0.632	0.530	-0.048	0.063	0.041
Mean Band Area	0.031	0.101	0.028	0.022	0.006	0.001	0.006	0.980	-0.011	-0.031	0.001
Band Number	0.760	2.235	0.477	0.352	0.122	0.044	0.083	2.391	-0.251	-0.951	0.099
FLSG											
SVL	14.887	0.994	0.991	0.989	0.996	0.995	-0.515	0.750	-0.656	0.030	-0.635
Tail Length	14.839	17.333	0.984	0.975	0.999	0.982	-0.576	0.720	-0.704	-0.295	0.624
Body Depth	2.594	2.638	0.619	0.969	0.985	0.986	-0.423	0.823	-0.118	0.106	-0.017
Snout Length	1.971	1.726	0.267	0.461	0.980	0.983	-0.529	0.712	-0.081	-0.009	-0.238
Snout Depth	0.571	0.640	0.105	0.075	0.038	0.983	-0.570	0.724	-0.027	-0.008	0.013
Head Length	3.210	2.965	0.591	0.357	0.103	0.987	-0.480	0.745	-0.138	0.028	-0.312
Mean Band Area	0.006	-0.104	0.038	-0.004	0.004	0.042	0.050	0.116	0.001	0.054	-0.037
Band Number	3.898	3.454	1.055	0.406	0.137	0.834	0.162	4.390	-0.182	0.947	0.225
FLKB											
SVL	9.656	0.975	0.997	0.915	0.982	0.967	0.994	0.858	-0.509	0.704	-0.326

	SVL	Tail Length	Body Depth	Snout Length	Snout Depth	Head Length	Mean Band Area	Band Number	p_1	p_2	p_3
Tail Length	12.169	22.850	0.976	0.825	0.997	0.954	0.971	0.769	-0.845	-0.502	0.170
Body Depth	1.478	1.951	0.347	0.893	0.985	0.965	0.994	0.862	-0.081	0.108	0.001
Snout Length	0.835	0.690	0.059	0.268	0.854	0.815	0.879	0.927	-0.034	0.143	0.076
Snout Depth	0.383	0.665	0.070	0.028	0.033	0.946	0.974	0.815	-0.025	0.001	0.037
Head Length	1.813	2.385	0.316	0.034	0.061	0.876	0.986	0.737	-0.099	0.083	-0.531
Mean Band Area	0.261	0.328	0.049	0.006	0.012	0.077	0.013	0.826	-0.014	0.018	-0.031
Band Number	2.151	1.921	0.413	0.304	0.106	0.124	0.049	1.590	-0.095	0.460	0.758
FLFD											
SVL	63.068	-0.323	0.253	0.855	0.697	0.906	0.936	-0.613	0.992	-0.067	0.003
Tail Length	-2.446	37.253	0.828	0.209	0.448	0.086	0.028	0.695	-0.078	-0.985	-0.066
Body Depth	2.223	4.255	1.027	0.709	0.854	0.618	0.571	0.317	0.031	-0.119	-0.060
Snout Length	4.604	2.419	0.557	0.852	0.965	0.983	0.981	-0.234	0.070	-0.075	0.152
Snout Depth	1.195	0.971	0.147	0.203	0.100	0.910	0.903	-0.009	0.018	-0.028	0.054
Head Length	3.222	1.296	0.363	0.488	0.074	0.644	0.985	-0.374	0.050	-0.042	-0.005
Mean Band Area	1.165	0.384	0.089	0.132	0.021	0.067	0.061	-0.373	0.018	-0.013	0.019
Band Number	-0.972	2.214	0.129	0.344	0.141	0.014	0.044	2.056	-0.018	-0.060	0.983
FLSI											
SVL	4.410	0.975	0.959	0.554	0.760	0.952	0.971	0.166	-0.505	0.209	0.702
Tail Length	5.611	10.732	0.913	0.400	0.650	0.887	0.968	0.109	-0.849	-0.244	-0.442
Body Depth	0.570	0.623	0.234	0.507	0.685	0.966	0.939	0.118	-0.060	0.041	0.166
Snout Length	0.524	0.239	0.032	0.281	0.619	0.623	0.548	0.690	-0.037	0.191	0.184
Snout Depth	0.093	0.047	-0.014	0.028	0.021	0.734	0.599	-0.056	-0.006	0.001	0.045
Head Length	1.036	1.058	0.220	0.160	0.008	0.571	0.921	0.202	-0.107	0.127	0.336
Mean Band	0.073	0.113	0.023	0.012	-0.002	0.024	0.008	0.311	-0.010	0.011	0.001

	SVL	Tail Length	Body Depth	Snout Length	Snout Depth	Head Length	Mean Band Area	Band Number	p_1	p_2	p_3
Area											
Band Number	0.803	0.662	0.106	0.403	-0.011	0.285	0.037	2.470	-0.086	0.918	-0.369
FLAB											
SVL	17.583	0.981	0.999	0.988	0.988	0.998	0.889	0.831	-0.504	0.789	0.250
Tail Length	23.283	42.789	0.986	0.988	0.969	0.986	0.954	0.902	-0.847	-0.454	-0.260
Body Depth	2.734	3.812	0.611	0.992	0.987	0.999	0.903	0.844	-0.082	0.100	0.079
Snout Length	1.591	2.451	0.333	0.469	0.977	0.995	0.925	0.858	-0.052	0.032	0.062
Snout Depth	0.567	0.794	0.101	0.058	0.070	0.989	0.900	0.771	-0.017	0.030	-0.061
Head Length	3.229	4.515	0.613	0.501	0.133	0.821	0.905	0.838	-0.097	0.122	0.065
Mean Band Area	0.421	1.439	0.130	0.127	0.044	0.177	0.204	0.879	-0.025	-0.077	-0.129
Band Number	1.758	4.844	0.374	0.290	-0.039	0.399	0.084	2.316	-0.091	-0.373	0.914
FLPB											
SVL	48.239	0.943	-0.573	-0.725	0.795	-0.809	-0.616	0.869	0.822	0.557	-0.116
Tail Length	26.826	27.536	-0.572	-0.863	0.877	-0.879	-0.469	0.796	0.563	-0.825	0.027
Body Depth	-0.167	-0.014	0.418	0.771	-0.159	0.873	0.886	-0.107	-0.001	0.000	0.285
Snout Length	-0.185	-0.447	0.268	0.309	-0.592	0.933	0.498	-0.437	-0.006	0.034	0.141
Snout Depth	0.177	0.212	0.089	0.077	0.047	-0.610	-0.100	0.836	0.004	-0.007	0.044
Head Length	-0.550	-0.620	0.258	0.149	0.026	0.271	0.711	-0.452	-0.011	0.029	0.215
Mean Band Area	-0.088	0.042	0.054	0.030	0.012	0.040	0.016	-0.213	-0.001	-0.008	0.050
Band Number	5.117	2.900	0.788	0.336	0.130	0.570	0.139	3.480	0.091	0.084	0.913
FLHB											
SVL	13.312	0.996	0.950	0.995	0.980	0.996	0.994	0.226	-0.635	0.013	0.741
Tail Length	14.546	18.244	0.938	0.992	0.968	0.994	0.987	0.194	-0.748	-0.159	-0.642
Body Depth	2.037	2.235	0.613	0.926	0.986	0.951	0.975	0.511	-0.101	0.175	0.025

	SVL	Tail Length	Body Depth	Snout Length	Snout Depth	Head Length	Mean Band Area	Band Number	p_1	p_2	p_3
Snout Length	1.583	1.715	0.213	0.345	0.966	0.989	0.983	0.172	-0.075	-0.014	0.125
Snout Depth	0.428	0.438	0.080	0.055	0.042	0.976	0.992	0.405	-0.020	0.023	0.033
Head Length	2.182	2.467	0.437	0.255	0.079	0.594	0.990	0.225	-0.107	0.015	0.083
Mean Band Area	0.184	0.196	0.038	0.017	0.004	0.028	0.007	0.317	-0.009	0.005	0.011
Band Number	1.876	1.579	1.083	0.150	0.163	0.362	0.046	4.804	-0.095	0.971	-0.120
FLCC											
SVL	18.415	0.953	0.996	0.992	0.993	0.953	-0.632	-0.670	-0.641	-0.682	0.006
Tail Length	16.370	24.090	0.933	0.918	0.979	0.817	-0.369	-0.676	-0.751	0.644	0.065
Body Depth	2.016	1.675	0.354	0.996	0.986	0.968	-0.670	-0.693	-0.069	-0.097	-0.025
Snout Length	2.684	2.091	0.316	0.534	0.978	0.974	-0.696	-0.714	-0.088	-0.142	-0.101
Snout Depth	0.779	0.827	0.099	0.106	0.055	0.915	-0.546	-0.701	-0.030	-0.012	-0.008
Head Length	3.476	1.900	0.485	0.585	0.150	0.963	-0.832	-0.613	-0.099	-0.296	-0.007
Mean Band Area	-0.090	0.007	-0.003	-0.008	-0.002	-0.020	0.007	0.337	0.001	0.014	0.003
Band Number	-0.819	-1.259	-0.133	-0.313	-0.063	-0.082	0.007	2.277	0.042	-0.057	0.992

APPENDIX VI

Male **P**-matrices. These are the unstandardized variances (diagonal), covariances (lower triangle), and correlations (upper triangle). The columns for $\boldsymbol{p}_1$, $\boldsymbol{p}_2$, and $\boldsymbol{p}_3$ show the three leading eigenvectors for each population.

	SVL	Tail Length	Body Depth	Snout Length	Snout Depth	Head Length	p_1	p_2	p_3
TXSP									
SVL	18.774	0.654	0.869	0.927	0.878	0.897	-0.417	0.900	0.102
Tail Length	12.794	40.826	0.941	0.888	0.936	0.916	-0.901	-0.428	0.054
Body Depth	1.700	2.548	0.308	0.988	0.998	0.995	-0.065	0.037	-0.138
Snout Length	1.609	1.956	0.158	0.233	0.993	0.994	-0.052	0.050	-0.073
Snout Depth	0.657	0.952	0.089	0.089	0.065	0.996	-0.024	0.015	-0.070
Head Length	2.243	3.021	0.292	0.249	0.115	0.576	-0.079	0.060	-0.978
TXCC									
SVL	9.719	0.870	0.958	0.992	0.992	0.985	0.725	-0.674	-0.004
Tail Length	6.215	8.782	0.973	0.914	0.813	0.942	0.671	0.737	-0.032
Body Depth	0.752	0.748	0.115	0.977	0.923	0.993	0.068	0.013	0.470
Snout Length	0.835	0.636	0.062	0.130	0.972	0.994	0.067	-0.034	-0.800
Snout Depth	0.236	0.130	0.031	0.023	0.020	0.958	0.017	-0.022	0.049
Head Length	1.453	1.221	0.139	0.121	0.029	0.266	0.121	-0.030	0.368
TXCB									
SVL	21.096	0.999	0.999	1.000	1.000	1.000	-0.512	0.827	-0.139
Tail Length	33.322	56.188	1.000	0.999	1.000	0.999	-0.848	-0.521	-0.064
Body Depth	2.339	4.031	0.333	0.999	1.000	0.998	-0.061	-0.081	0.624
Snout Length	3.667	5.847	0.428	0.685	1.000	1.000	-0.090	0.122	0.700
Snout Depth	0.871	1.448	0.106	0.151	0.043	0.999	-0.022	-0.003	-0.005
Head Length	3.321	5.211	0.377	0.590	0.135	0.539	-0.080	0.151	0.312
ALST									
SVL	14.178	0.905	0.976	0.995	0.992	0.986	-0.591	0.769	0.236
Tail Length	12.514	21.712	0.973	0.897	0.850	0.956	-0.787	-0.614	0.029
Body Depth	1.142	1.357	0.189	0.966	0.942	0.991	-0.056	0.020	0.010
Snout Length	2.516	2.229	0.203	0.689	0.993	0.987	-0.107	0.146	-0.704
Snout Depth	0.590	0.448	0.046	0.133	0.040	0.965	-0.023	0.042	-0.090

	SVL	Tail Length	Body Depth	Snout Length	Snout Depth	Head Length	p_1	p_2	p_3
Head Length	2.724	2.991	0.242	0.684	0.139	0.771	-0.130	0.086	-0.663
FLSG									
SVL	13.864	0.980	0.991	0.999	0.988	0.992	-0.611	0.767	0.188
Tail Length	14.598	20.780	0.997	0.980	0.998	0.996	-0.771	-0.628	0.068
Body Depth	1.795	2.281	0.320	0.990	0.999	0.999	-0.089	-0.004	-0.159
Snout Length	2.431	2.595	0.329	0.588	0.990	0.993	-0.109	0.134	-0.702
Snout Depth	0.465	0.604	0.079	0.114	0.042	0.999	-0.023	-0.003	-0.186
Head Length	2.312	2.892	0.367	0.494	0.114	0.561	-0.113	0.012	-0.638
FLKB									
SVL	11.820	0.998	0.998	0.993	0.998	1.000	-0.462	0.870	0.077
Tail Length	20.433	39.785	1.000	0.998	1.000	0.999	-0.876	-0.464	0.103
Body Depth	1.976	3.795	0.397	0.998	1.000	0.999	-0.084	-0.022	-0.213
Snout Length	1.181	2.463	0.246	0.252	0.998	0.995	-0.054	-0.108	-0.595
Snout Depth	0.588	1.131	0.109	0.083	0.060	0.999	-0.025	-0.007	-0.266
Head Length	2.420	4.326	0.431	0.265	0.146	0.597	-0.097	0.125	-0.717
FLFD									
SVL	21.653	0.980	0.992	0.994	0.992	0.999	-0.669	0.698	-0.088
Tail Length	20.155	25.398	0.952	0.963	0.971	0.980	-0.730	-0.681	0.023
Body Depth	2.879	2.349	0.610	0.984	0.975	0.992	-0.084	0.167	0.713
Snout Length	2.295	1.962	0.208	0.415	0.994	0.990	-0.068	0.108	-0.621
Snout Depth	0.459	0.418	0.031	0.080	0.047	0.991	-0.014	0.017	-0.116
Head Length	2.902	2.726	0.431	0.268	0.093	0.536	-0.090	0.094	0.290
FLSI									
SVL	8.345	0.937	0.979	0.968	0.997	0.977	-0.592	0.785	0.029
Tail Length	7.917	13.059	0.988	0.917	0.954	0.950	-0.791	-0.608	-0.011
Body Depth	1.099	1.407	0.207	0.955	0.988	0.975	-0.093	0.016	-0.039
Snout Length	1.060	1.062	0.159	0.397	0.975	0.908	-0.078	0.093	-0.772

	SVL	Tail Length	Body Depth	Snout Length	Snout Depth	Head Length	p_1	p_2	p_3
Snout Depth	0.332	0.342	0.056	0.054	0.029	0.970	-0.025	0.025	-0.045
Head Length	1.165	1.276	0.165	0.044	0.038	0.385	-0.090	0.070	0.633
FLAB									
SVL	15.143	0.980	0.994	0.997	0.984	0.995	-0.550	0.813	0.173
Tail Length	18.210	30.420	0.995	0.976	0.995	0.984	-0.825	-0.564	0.026
Body Depth	1.600	2.251	0.271	0.989	0.995	0.994	-0.065	0.030	-0.205
Snout Length	1.417	1.695	0.168	0.292	0.975	0.990	-0.052	0.083	-0.106
Snout Depth	0.485	0.724	0.096	0.042	0.082	0.980	-0.020	0.001	0.014
Head Length	2.669	3.437	0.349	0.272	0.078	0.819	-0.102	0.116	-0.957
FLPB									
SVL	9.530	0.971	0.996	0.987	0.999	0.992	-0.531	0.829	-0.114
Tail Length	11.380	20.136	0.986	0.996	0.976	0.992	-0.831	-0.548	-0.024
Body Depth	1.462	1.972	0.288	0.995	0.998	0.999	-0.089	0.077	0.612
Snout Length	1.408	2.139	0.208	0.305	0.989	0.997	-0.092	0.014	-0.434
Snout Depth	0.681	0.849	0.119	0.086	0.074	0.994	-0.039	0.051	0.141
Head Length	1.518	2.162	0.281	0.246	0.106	0.338	-0.095	0.053	0.635
FLHB									
SVL	10.749	0.989	1.000	0.993	0.994	0.995	-0.536	0.815	-0.060
Tail Length	14.095	23.701	0.988	0.965	0.999	0.998	-0.835	-0.543	-0.052
Body Depth	1.168	1.518	0.169	0.993	0.993	0.994	-0.058	0.095	-0.064
Snout Length	1.224	1.348	0.132	0.175	0.975	0.977	-0.055	0.175	0.079
Snout Depth	0.553	0.857	0.065	0.067	0.055	0.998	-0.031	0.003	-0.230
Head Length	1.535	2.349	0.166	0.165	0.076	0.308	-0.085	0.014	0.964
FLCC									
SVL	11.937	0.978	0.988	0.944	0.984	0.991	-0.536	0.804	0.153
Tail Length	14.687	25.431	0.996	0.859	0.999	0.997	-0.834	-0.536	-0.127
Body Depth	1.362	2.061	0.277	0.884	0.999	0.999	-0.070	0.009	0.505

	SVL	Tail Length	Body Depth	Snout Length	Snout Depth	Head Length	p_1	p_2	p_3
Snout Length	1.543	1.235	0.105	0.410	0.872	0.891	-0.054	0.256	-0.781
Snout Depth	0.472	0.749	0.076	0.032	0.044	0.999	-0.025	-0.004	0.144
Head Length	1.860	2.802	0.260	0.174	0.101	0.396	-0.096	0.018	0.275

APPENDIX VII

Eigen analysis of the female **P**-matrix. The first column contains the population ID for that P-matrix and then the traits associated with each eigenvector ($\boldsymbol{\lambda}_i$) in the same order as the eigenvectors in the following columns. The column labeled "Eigenvalue" contains the eigenvalue associated with each eigenvector associated with the trait in the first column. The remaining columns contain the eigenvectors.

	Eigenvalue	λ_1	λ_2	λ_3	λ_4	λ_5	λ_6	λ_7	λ_8
TXSP									
SVL	11.7276	-0.3205	0.1854	0.9054	0.1443	-0.0364	-0.1261	0.0691	0.0191
Tail Length	1.8072	-0.8993	0.2118	-0.3681	0.0875	0.0429	0.0350	-0.0139	0.0037
Body Depth	1.4789	-0.1063	-0.1068	-0.0419	-0.4482	-0.7442	-0.4603	0.0653	-0.0685
Snout Length	0.1251	-0.1038	-0.0159	0.1777	-0.5566	-0.1193	0.7159	-0.3297	-0.1102
Snout Depth	0.1050	-0.0290	-0.0221	-0.0009	-0.2391	0.0713	0.2564	0.9324	0.0354
Head Length	0.0500	-0.0484	0.0628	0.0411	-0.6277	0.6318	-0.4352	-0.0908	0.0343
Band Area	0.0143	-0.0109	-0.0307	0.0011	-0.0645	-0.0865	0.0559	-0.0640	0.9900
Band Number	0.0013	-0.2514	-0.9506	0.0990	0.0735	0.1310	-0.0136	-0.0171	-0.0165
TXCC									
SVL	58.2662	-0.5044	0.7888	0.2496	-0.1711	-0.0596	-0.1240	0.1055	0.0423
Tail Length	4.2528	-0.8471	-0.4536	-0.2603	-0.0416	-0.0238	0.0723	-0.0323	-0.0163
Body Depth	1.4874	-0.0819	0.1005	0.0793	0.3224	0.7696	0.4921	0.1586	0.1152
Snout Length	0.5397	-0.0517	0.0320	0.0621	0.6748	-0.5507	0.2269	0.2921	0.3115
Snout Depth	0.1517	-0.0169	0.0303	-0.0610	0.0656	0.1201	-0.2285	-0.5679	0.7756
Head Length	0.0815	-0.0970	0.1217	0.0654	0.5679	0.0400	-0.1753	-0.5784	-0.5311
Band Area	0.0517	-0.0254	-0.0771	-0.1294	0.2858	0.2891	-0.7678	0.4693	0.0408
Band Number	0.0315	-0.0907	-0.3732	0.9138	-0.0348	0.0262	-0.1151	-0.0018	0.0482
TXCB									
SVL	38.8109	-0.6410	-0.6816	0.0063	0.3249	-0.1111	0.0752	0.0005	-0.0314
Tail Length	5.2624	-0.7511	0.6437	0.0649	-0.1068	0.0301	-0.0621	-0.0300	0.0130
Body Depth	2.2258	-0.0685	-0.0975	-0.0251	-0.6151	-0.3559	0.6905	-0.0046	0.0577
Snout Length	0.2209	-0.0885	-0.1420	-0.1009	-0.2093	0.9144	0.2479	0.1276	0.0640
Snout Depth	0.1060	-0.0298	-0.0124	-0.0083	-0.0963	-0.1230	-0.1460	0.9761	-0.0189
Head Length	0.0484	-0.0990	-0.2964	-0.0069	-0.6682	-0.0086	-0.6529	-0.1715	0.0030
Band Area	0.0155	0.0014	0.0139	0.0035	-0.0613	0.0452	0.0540	-0.0113	-0.9955
Band Number	0.0046	0.0415	-0.0569	0.9924	-0.0371	0.0814	0.0403	0.0219	0.0106

	Eigenvalue	λ_1	λ_2	λ_3	λ_4	λ_5	λ_6	λ_7	λ_8
ALST									
SVL	63.8758	0.9923	-0.0666	0.0026	-0.0942	0.0105	0.0388	0.0028	0.0211
Tail Length	38.0116	-0.0780	-0.9845	-0.0661	-0.1234	-0.0648	0.0165	-0.0092	0.0215
Body Depth	1.9577	0.0307	-0.1192	-0.0603	0.5641	0.7914	0.1854	0.0314	-0.0371
Snout Length	0.6036	0.0701	-0.0754	0.1516	0.4807	-0.1404	-0.8189	-0.1122	0.1799
Snout Depth	0.3530	0.0177	-0.0285	0.0538	-0.0198	0.0109	-0.2423	0.6981	-0.6704
Head Length	0.1923	0.0497	-0.0421	-0.0051	0.6514	-0.5879	0.4551	0.0712	-0.1165
Band Area	0.0512	0.0179	-0.0127	0.0193	-0.0036	0.0095	-0.0569	-0.7028	-0.7084
Band Number	0.0154	-0.0179	-0.0601	0.9827	-0.0430	0.0620	0.1554	-0.0055	0.0213
FLSG									
SVL	31.6290	-0.6350	0.0132	0.7407	-0.1445	0.1574	-0.0317	-0.0294	0.0191
Tail Length	4.7743	-0.7483	-0.1590	-0.6423	-0.0402	-0.0200	-0.0105	0.0078	-0.0034
Body Depth	0.9975	-0.1010	0.1752	0.0252	0.5251	0.1116	0.8137	0.0711	0.0565
Snout Length	0.2837	-0.0752	-0.0142	0.1247	-0.1168	-0.9603	0.2019	-0.0405	-0.0206
Snout Depth	0.1536	-0.0201	0.0230	0.0327	0.0080	-0.0545	-0.0884	0.9915	-0.0633
Head Length	0.0946	-0.1073	0.0152	0.0834	0.8216	-0.1857	-0.5156	-0.0701	-0.0313
Band Area	0.0251	-0.0087	0.0049	0.0111	0.0037	0.0387	0.0638	-0.0565	-0.9955
Band Number	0.0038	-0.0945	0.9710	-0.1201	-0.1141	-0.0357	-0.1353	-0.0338	-0.0043
FLKB									
SVL	30.9192	-0.5091	0.7045	-0.3262	0.2979	-0.1563	0.1558	-0.0089	0.0259
Tail Length	3.0015	-0.8447	-0.5024	0.1701	-0.0366	0.0551	-0.0038	0.0257	-0.0105
Body Depth	1.0434	-0.0810	0.1081	0.0014	-0.2393	-0.5153	-0.8064	0.0931	0.0091
Snout Length	0.4249	-0.0341	0.1430	0.0758	0.3636	0.7303	-0.5504	0.0190	-0.0611
Snout Depth	0.1687	-0.0252	0.0006	0.0374	-0.0172	-0.0170	-0.0892	-0.9598	0.2613
Head Length	0.0615	-0.0991	0.0833	-0.5307	-0.7373	0.3950	-0.0128	0.0007	0.0414
Band Area	0.0120	-0.0138	0.0183	-0.0312	-0.0517	-0.0442	0.0063	-0.2617	-0.9620
Band Number	0.0034	-0.0947	0.4603	0.7582	-0.4169	0.1238	0.1200	0.0254	-0.0039

	Eigenvalue	λ_1	λ_2	λ_3	λ_4	λ_5	λ_6	λ_7	λ_8
FLFD									
SVL	67.1919	0.8215	0.5565	-0.1162	-0.0311	-0.0216	0.0189	-0.0004	0.0098
Tail Length	9.1925	0.5627	-0.8253	0.0272	-0.0207	-0.0117	-0.0302	-0.0032	-0.0085
Body Depth	3.3605	-0.0012	0.0000	0.2849	-0.5463	-0.1533	0.6860	-0.3494	0.0647
Snout Length	0.4050	-0.0056	0.0336	0.1409	-0.7025	0.4082	-0.5603	-0.0689	-0.0150
Snout Depth	0.1016	0.0041	-0.0069	0.0441	-0.2075	0.2172	0.3277	0.8696	-0.2101
Head Length	0.0423	-0.0112	0.0290	0.2152	-0.2188	-0.8549	-0.3198	0.2452	-0.1077
Band Area	0.0159	-0.0005	-0.0077	0.0499	-0.0317	-0.0252	-0.0216	0.2383	0.9688
Band Number	0.0056	0.0915	0.0841	0.9132	0.3388	0.1748	-0.0636	0.0068	-0.0337
FLSI									
SVL	33.2998	-0.6563	0.0297	-0.6352	-0.1526	0.2116	0.3006	-0.0747	-0.0297
Tail Length	3.5855	-0.7042	-0.2946	0.6244	0.0320	-0.1373	-0.0808	-0.0076	-0.0301
Body Depth	1.2917	-0.1181	0.1062	-0.0166	0.2631	0.6939	-0.5887	0.2779	0.0038
Snout Length	0.3401	-0.0812	-0.0090	-0.2382	-0.5741	-0.4079	-0.6480	0.1441	0.0000
Snout Depth	0.1236	-0.0266	-0.0079	0.0128	-0.0359	0.0664	-0.0851	-0.3324	0.9358
Head Length	0.0832	-0.1377	0.0281	-0.3120	0.7491	-0.5181	-0.1811	0.1117	0.0893
Band Area	0.0321	0.0009	0.0537	-0.0366	0.1098	0.0429	-0.3072	-0.8793	-0.3381
Band Number	0.0102	-0.1822	0.9472	0.2251	-0.0490	-0.1174	0.0474	0.0140	0.0155
FLAB									
SVL	14.3213	-0.5046	0.2085	0.7016	-0.3312	0.2211	0.2113	-0.0786	-0.0153
Tail Length	2.6045	-0.8494	-0.2442	-0.4417	0.0787	-0.0994	-0.0828	0.0254	0.0129
Body Depth	1.2290	-0.0604	0.0414	0.1663	0.4080	0.5903	-0.6409	0.1826	0.0895
Snout Length	0.3089	-0.0371	0.1906	0.1836	-0.2784	-0.6179	-0.6815	-0.0264	0.0640
Snout Depth	0.1640	-0.0061	0.0013	0.0451	-0.1204	-0.1002	0.1036	0.9734	-0.1229
Head Length	0.0841	-0.1066	0.1273	0.3360	0.7898	-0.4393	0.2063	0.0132	-0.0075
Band Area	0.0118	-0.0098	0.0106	0.0014	0.0342	0.0248	-0.1210	-0.1049	-0.9861
Band Number	0.0042	-0.0860	0.9179	-0.3692	0.0258	0.0858	0.0730	0.0199	0.0022

	Eigenvalue	λ_1	λ_2	λ_3	λ_4	λ_5	λ_6	λ_7	λ_8
FLPB									
SVL	47.2551	-0.3419	0.8875	0.1737	-0.2018	0.0213	0.1540	0.0171	0.0073
Tail Length	7.8023	-0.9270	-0.3679	0.0674	-0.0029	0.0201	-0.0210	0.0041	0.0024
Body Depth	1.1777	-0.0329	0.1248	-0.0066	-0.1388	-0.2413	-0.9458	0.1046	0.0202
Snout Length	0.0618	-0.0674	0.1905	0.0141	0.9031	0.2566	-0.1437	0.2347	0.0425
Snout Depth	0.0377	-0.0058	0.0462	0.0171	0.0401	0.4807	-0.2167	-0.8466	-0.0336
Head Length	0.0358	-0.0482	0.0667	0.0197	0.3501	-0.8008	0.1108	-0.4590	-0.0776
Band Area	0.0136	-0.0057	0.0110	-0.0112	0.0054	0.0525	-0.0252	0.0765	-0.9952
Band Number	0.0006	-0.1258	0.1357	-0.9820	-0.0143	0.0021	0.0288	-0.0188	0.0111
FLHB									
SVL	17.3680	0.5862	0.0111	0.7549	-0.0380	0.2546	-0.1168	0.0805	-0.0014
Tail Length	2.2099	0.7918	0.0254	-0.6083	0.0172	-0.0115	-0.0120	-0.0387	-0.0140
Body Depth	1.1834	0.0756	-0.0420	0.1230	0.8011	-0.5368	-0.1547	0.1530	-0.0085
Snout Length	0.1385	0.1306	-0.0031	0.1691	-0.5375	-0.7993	0.1581	-0.0326	-0.0205
Snout Depth	0.0794	0.0119	0.0209	0.0888	0.1137	-0.0378	-0.1357	-0.9500	-0.2374
Head Length	0.0475	0.0761	-0.0229	0.0906	0.2310	0.0675	0.9519	-0.1222	0.0803
Band Area	0.0145	0.0127	-0.0073	0.0110	0.0041	-0.0360	-0.1110	-0.2230	0.9676
Band Number	0.0036	0.0215	-0.9982	-0.0130	-0.0350	0.0255	-0.0195	-0.0219	-0.0139
FLCC									
SVL	27.8262	-0.5737	-0.2537	0.6926	0.2708	0.2245	0.0424	0.0293	-0.0198
Tail Length	5.8228	-0.7852	0.4194	-0.4186	-0.0570	-0.1643	-0.0045	-0.0380	0.0248
Body Depth	0.9661	-0.0866	-0.0285	0.0905	-0.8204	0.3784	0.3984	-0.0323	-0.0869
Snout Length	0.1871	-0.0636	-0.0387	0.0395	-0.3319	0.2328	-0.8808	0.1562	0.1681
Snout Depth	0.1660	-0.0166	0.0022	-0.0089	-0.0291	-0.1413	0.0992	0.9562	-0.2339
Head Length	0.0635	-0.0368	-0.1060	0.3573	-0.3718	-0.8347	-0.0537	-0.0992	0.1101
Band Area	0.0204	-0.0174	-0.0233	0.0052	-0.0273	-0.0663	-0.2241	-0.2191	-0.9464
Band Number	0.0081	-0.2021	-0.8635	-0.4556	-0.0189	-0.0648	0.0246	-0.0124	0.0246

APPENDIX VIII

Eigenvectors and eigenvalues of each population's P-matrix. The first column contains the name of the population and the traits associated with each eigenvector. The second column contains the eigenvalues associated with each trait's eigenvector. The remaining columns contain the eigenvectors.

	Eigenvalue	$\boldsymbol{\lambda}_1$	$\boldsymbol{\lambda}_2$	$\boldsymbol{\lambda}_3$	$\boldsymbol{\lambda}_4$	$\boldsymbol{\lambda}_5$	$\boldsymbol{\lambda}_6$
TXSP							
SVL	32.0189	-0.5910	0.7690	0.2363	-0.0509	0.0151	0.0265
Tail Length	5.0253	-0.7866	-0.6145	0.0292	-0.0339	-0.0366	-0.0158
Body Depth	0.4098	-0.0564	0.0200	0.0103	0.9972	-0.0419	0.0089
Snout Length	0.0856	-0.1067	0.1462	-0.7038	-0.0304	-0.6862	-0.0152
Snout Depth	0.0287	-0.0230	0.0423	-0.0900	0.0129	0.1262	-0.9867
Head Length	0.0108	-0.1297	0.0864	-0.6632	0.0264	0.7141	0.1588
TXCC							
SVL	43.2881	-0.5498	0.8128	0.1730	0.0826	-0.0170	0.0007
Tail Length	3.0951	-0.8246	-0.5639	0.0256	-0.0007	-0.0354	0.0085
Body Depth	0.3484	-0.0647	0.0304	-0.2047	-0.1467	0.7230	-0.6393
Snout Length	0.1567	-0.0516	0.0830	-0.1057	-0.9729	-0.1589	0.0866
Snout Depth	0.1099	-0.0204	0.0005	0.0143	-0.0410	0.6582	0.7513
Head Length	0.0282	-0.1022	0.1161	-0.9572	0.1531	-0.1313	0.1388
TXCB							
SVL	35.4712	-0.5360	0.8043	0.1528	0.2003	0.0491	0.0021
Tail Length	2.6904	-0.8337	-0.5361	-0.1266	0.0094	0.0370	-0.0021
Body Depth	0.1733	-0.0705	0.0090	0.5051	-0.7230	0.4587	0.0818
Snout Length	0.0832	-0.0536	0.2556	-0.7806	-0.5649	-0.0361	-0.0457
Snout Depth	0.0614	-0.0252	-0.0043	0.1443	-0.1101	-0.1633	-0.9694
Head Length	0.0166	-0.0959	0.0175	0.2747	-0.3252	-0.8705	0.2269
ALST							
SVL	44.6552	-0.6686	0.6984	-0.0882	0.1070	0.2130	-0.0247
Tail Length	3.4499	-0.7300	-0.6808	0.0230	0.0078	-0.0540	-0.0033
Body Depth	0.3190	-0.0839	0.1671	0.7132	0.2056	-0.6326	-0.1178
Snout Length	0.1419	-0.0680	0.1081	-0.6207	-0.1274	-0.7390	0.1898
Snout Depth	0.0775	-0.0141	0.0172	-0.1163	-0.3653	-0.0720	-0.9205

	Eigenvalue	λ_1	λ_2	λ_3	λ_4	λ_5	λ_6
Head Length	0.0154	-0.0903	0.0938	0.2901	-0.8925	0.0142	0.3195
FLSG							
SVL	33.2205	-0.5365	0.8155	-0.0600	0.1214	-0.1316	0.1072
Tail Length	1.7837	-0.8352	-0.5434	-0.0521	0.0076	0.0163	-0.0642
Body Depth	0.0701	-0.0580	0.0950	-0.0643	-0.9664	-0.1618	-0.1528
Snout Length	0.0426	-0.0547	0.1746	0.0791	-0.0065	0.7381	-0.6445
Snout Depth	0.0321	-0.0309	0.0026	-0.2303	-0.2010	0.6372	0.7068
Head Length	0.0087	-0.0853	0.0140	0.9645	-0.1039	0.0735	0.2147
FLKB							
SVL	51.5912	-0.4619	0.8701	0.0770	0.1521	0.0149	-0.0189
Tail Length	1.0704	-0.8756	-0.4640	0.1034	-0.0591	0.0554	0.0286
Body Depth	0.1153	-0.0839	-0.0219	-0.2128	0.0186	-0.8946	-0.3827
Snout Length	0.0843	-0.0536	-0.1077	-0.5950	0.7684	0.0868	0.1831
Snout Depth	0.0315	-0.0250	-0.0066	-0.2660	-0.0527	0.4324	-0.8595
Head Length	0.0179	-0.0973	0.1249	-0.7165	-0.6162	0.0426	0.2829
FLFD							
SVL	28.1466	-0.5312	0.8293	-0.1142	-0.0764	0.1010	-0.0312
Tail Length	2.3046	-0.8311	-0.5483	-0.0236	-0.0782	0.0424	-0.0088
Body Depth	0.1104	-0.0885	0.0769	0.6119	-0.0516	-0.5993	-0.5000
Snout Length	0.0723	-0.0924	0.0142	-0.4341	0.7171	-0.5345	0.0540
Snout Depth	0.0242	-0.0390	0.0515	0.1409	-0.3375	-0.4786	0.7956
Head Length	0.0140	-0.0955	0.0529	0.6354	0.5977	0.3378	0.3361
FLSI							
SVL	33.4236	-0.6108	0.7666	0.1877	0.0314	0.0472	-0.0300
Tail Length	2.3603	-0.7706	-0.6278	0.0683	-0.0847	0.0124	0.0047
Body Depth	0.2393	-0.0886	-0.0036	-0.1586	0.6023	-0.7624	0.1516
Snout Length	0.0767	-0.1088	0.1344	-0.7024	-0.6044	-0.2849	0.1736

	Eigenvalue	λ_1	λ_2	λ_3	λ_4	λ_5	λ_6
Snout Depth	0.0396	-0.0234	-0.0027	-0.1855	0.0085	-0.1451	-0.9715
Head Length	0.0153	-0.1135	0.0120	-0.6381	0.5134	0.5605	0.0453
FLAB							
SVL	19.4177	-0.5924	0.7849	0.0286	0.1683	-0.0603	-0.0119
Tail Length	2.4759	-0.7908	-0.6078	-0.0114	0.0326	-0.0603	0.0172
Body Depth	0.3480	-0.0933	0.0156	-0.0389	-0.0870	0.9277	-0.3485
Snout Length	0.1292	-0.0782	0.0932	-0.7715	-0.6160	-0.1024	-0.0077
Snout Depth	0.0405	-0.0248	0.0250	-0.0453	-0.0057	0.3464	0.9363
Head Length	0.0115	-0.0903	0.0699	0.6326	-0.7640	-0.0414	0.0370
FLPB							
SVL	77.7486	-0.5121	0.8273	-0.1395	-0.1232	-0.1245	0.0562
Tail Length	1.0274	-0.8480	-0.5210	-0.0638	0.0640	0.0361	0.0041
Body Depth	0.0650	-0.0605	-0.0805	0.6238	-0.7375	-0.1911	0.1428
Snout Length	0.0278	-0.0897	0.1218	0.6999	0.6479	-0.2586	-0.0266
Snout Depth	0.0098	-0.0219	-0.0032	-0.0054	-0.1288	-0.2324	-0.9638
Head Length	0.0049	-0.0803	0.1509	0.3123	-0.0231	0.9088	-0.2165
FLHB							
SVL	15.8637	0.7252	-0.6741	-0.0036	-0.0797	0.1097	0.0348
Tail Length	3.0262	0.6708	0.7368	-0.0316	-0.0515	0.0578	-0.0101
Body Depth	0.0653	0.0678	0.0126	0.4700	0.7668	0.0664	0.4265
Snout Length	0.0434	0.0668	-0.0337	-0.8003	0.4824	-0.3431	0.0585
Snout Depth	0.0280	0.0168	-0.0216	0.0488	0.4125	0.3269	-0.8484
Head Length	0.0056	0.1212	-0.0299	0.3676	0.0098	-0.8693	-0.3058
FLCC							
SVL	47.3358	-0.4172	0.8997	0.1023	0.0011	0.0741	-0.0242
Tail Length	13.0105	-0.9012	-0.4277	0.0544	0.0145	0.0404	-0.0090
Body Depth	0.2413	-0.0646	0.0367	-0.1381	-0.7988	-0.5265	0.2450

	Eigenvalue	$\boldsymbol{\lambda}_1$	$\boldsymbol{\lambda}_2$	$\boldsymbol{\lambda}_3$	$\boldsymbol{\lambda}_4$	$\boldsymbol{\lambda}_5$	$\boldsymbol{\lambda}_6$
Snout Length	0.1095	-0.0524	0.0495	-0.0728	0.5916	-0.6554	0.4582
Snout Depth	0.0624	-0.0244	0.0153	-0.0699	0.0873	-0.5073	-0.8540
Head Length	0.0215	-0.0790	0.06034	-0.9784	0.06334	0.1693	-0.0107